MARTIN MARIETTA ENERGY SYSTEMS LIBRARIES

3 4456 0050329 3

CENTRAL RESEARCH LIBRARY
DOCUMENT COLLECTION

ORNL-3714, Vol. I
UC-34 – Physics
TID-4500 (35th ed.)

NEUTRON PHYSICS DIVISION
ANNUAL PROGRESS REPORT
FOR PERIOD ENDING AUGUST 1, 1964

CENTRAL RESEARCH LIBRARY
DOCUMENT COLLECTION
LIBRARY LOAN COPY
DO NOT TRANSFER TO ANOTHER PERSON
If you wish someone else to see this document, send in name with document and the library will arrange a loan.

OAK RIDGE NATIONAL LABORATORY
operated by
UNION CARBIDE CORPORATION
for the
U.S. ATOMIC ENERGY COMMISSION

Printed in USA. Price $4.00. Available from the Clearinghouse for Federal Scientific and Technical Information, National Bureau of Standards, U.S. Department of Commerce, Springfield, Virginia

LEGAL NOTICE

This report was prepared as an account of Government sponsored work. Neither the United States, nor the Commission, nor any person acting on behalf of the Commission:

A. Makes any warranty or representation, expressed or implied, with respect to the accuracy, completeness, or usefulness of the information contained in this report, or that the use of any information, apparatus, method, or process disclosed in this report may not infringe privately owned rights; or

B. Assumes any liabilities with respect to the use of, or for damages resulting from the use of any information, apparatus, method, or process disclosed in this report.

As used in the above, "person acting on behalf of the Commission" includes any employee or contractor of the Commission, or employee of such contractor, to the extent that such employee or contractor of the Commission, or employee of such contractor prepares, disseminates, or provides access to, any information pursuant to his employment or contract with the Commission, or his employment with such contractor.

ORNL-3714, Vol.I
UC-34 – Physics
TID-4500 (35th ed.)

Contract No. W-7405-eng-26

NEUTRON PHYSICS DIVISION
ANNUAL PROGRESS REPORT
For Period Ending August 1, 1964

E. P. Blizard, Director
A. D. Callihan, Associate Director
F. C. Maienschein, Associate Director

DECEMBER 1964

OAK RIDGE NATIONAL LABORATORY
Oak Ridge, Tennessee
operated by
UNION CARBIDE CORPORATION
for the
U. S. ATOMIC ENERGY COMMISSION

MARTIN MARIETTA ENERGY SYSTEMS LIBRARIES
3 4456 0050329 3

Preface

For the second consecutive year the Neutron Physics Division is issuing its annual progress report in two volumes, with the papers describing research performed in the high-energy radiation shielding program collected in Volume II. Again this separation is made primarily to aid our readers, most of whom we believe to be interested in the work reported in one volume only. It is not prompted by the size of the report, for, as you have already realized, the number of pages in this year's report has decreased considerably below that in our previous reports. This decrease reflects a change in the Division's procedure for reporting research performed during the year. It has become increasingly apparent that emphasis on the annual progress report has resulted in some of our research not being reported elsewhere, an effect which we deplore. The lack of other publications is made even less desirable by the fact that the individual papers of progress reports are not treated specifically by information centers or otherwise collated into the organized scientific literature. Therefore, in planning our report this year, we decided to limit each paper to the length of either an abstract or a summary in order to give the authors more time to spend on "topical" reports. In fact, we had hoped that for each abstract included in the annual report a separate detailed report or journal article would have already been published, but unfortunately the attractiveness of not duplicating writing efforts resulted in so great an influx of topical reports to our publications staff that it became impossible to handle all of them prior to the publication of the annual report. It can be presumed, however, that for each abstract included in the annual report the publication of a topical report is imminent. Those papers which are not identified as abstracts are summaries that describe work which is still in progress and thus is not yet ready for publication in a topical report.

In a few cases, the reader will notice that abstracts are included which report work that was described in last year's annual report. We have allowed this duplication intentionally so that we might call your attention to the fact that topical reports on these particular subjects have now been issued. This is a practice we will not repeat next year, however, since we assume that the abstract in this year's report will be sufficient notice of the forthcoming document.

Contents

1. NUCLEAR AND REACTOR PHYSICS 1

1.1. Elastic and Inelastic Scattering of 11-Mev Protons from Medium Weight Nuclei – J. K. Dickens, F. G. Perey, and R. J. Silva 1

1.2. The Local Energy Approximation to Nonlocality and Finite Range Effects – F. G. Perey and D. S. Saxon 3

1.3. Inelastic Effects in Stripping and Other Direct Reactions – S. K. Penny and G. R. Satchler 3

1.4. Distorted-Wave Analysis of the $^{90}Zr(d,p)^{91}Zr$ Reaction Using Nonlocal Optical-Model Wave Functions – J. K. Dickens, F. G. Perey, and R. J. Silva 3

1.5. Elastic and Inelastic Scattering of 5- to 13.5-Mev Deuterons from ^{60}Ni: Tabulated Differential Cross Sections – J. K. Dickens and F. G. Perey 4

1.6. Elastic and Inelastic Scattering of 8- to 15-Mev Deuterons from ^{114}Cd: Tabulated Differential Cross Sections – J. K. Dickens and F. G. Perey 7

1.7. The Effect of Data Normalization upon Deuteron Optical-Model Parameters – J. K. Dickens and F. G. Perey 7

1.8. Elastic Scattering of Low-Energy Deuterons from ^{60}Ni and ^{114}Cd and the Effect of the Deuteron Electric Polarizability in the Optical-Model Potential – J. K. Dickens and F. G. Perey 7

1.9. Effects of Nonlocality in Off-Diagonal Potentials – F. G. Perey and A. M. Saruis 7

1.10. Wide-Angle Scattering of 43-Mev Alpha Particles by ^{58}Ni – H. W. Broek, J. L. Yntema, B. Buck, and G. R. Satchler 8

1.11. Kinematics Nomogram for Low-Energy Nuclear Reactions – J. K. Dickens 8

1.12. The Use of Elastic Scattering Parameters in (d,p) Stripping Calculations – W. R. Smith 8

1.13. Distorted-Wave Calculations of $^{28}Si(d,p)^{29}Si$ Angular Distributions – W. R. Smith 10

1.14. Optical-Model Parameters for $^{90}Zr(d,p)^{91}Zr$ Below 4 Mev – C. E. Brient, E. L. Hudspeth, E. M. Bernstein, and W. R. Smith 10

1.15. Use of the Neutron Die-Away Technique to Test Control Rod Effectiveness Theories – R. B. Perez, G. de Saussure, and E. G. Silver 13

1.16. On the Extension of Weinberg's Second Fundamental Theorem to Nonhomogeneous Nuclear Systems – F. G. Perey and R. B. Perez 13

1.17. Differential and Total Cross Sections for the $^{9}Be(\alpha,n)$ Reactions from 6 to ~10 Mev – V. V. Verbinski, W. R. Burrus, J. K. Dickens, J. Gibbons, W. E. Kinney, R. L. Macklin, and F. G. Perey 15

1.18. Photoneutron Spectra from ^{16}O, ^{12}C, and ^{27}Al – V. V. Verbinski and J. C. Courtney 17

1.19. Spectra of Bremsstrahlung-Produced Neutrons Emitted from ^{206}Pb, ^{208}Pb, and ^{209}Bi at 90 and 141° – V. V. Verbinski and J. C. Courtney 20

1.20. Polarization of Deuterons in the ^{9}Be$(p,d)^{8}$Be Reaction at 3 to 5 Mev – V. V. Verbinski and M. S. Bokhari 23

1.21. Measurements of the Variation of the Ratio of the Capture and Fission Cross Sections of ^{235}U – L. W. Weston, G. de Saussure, R. Gwin, J. E. Russell, and R. W. Hockenbury 25

1.22. Measurement of the Slow Neutron Fission Cross Section of ^{239}Pu – G. de Saussure, J. Blons, C. Jousseaume, A. Michaudon, and Y. Pranal 26

1.23. Status of Pulsed-Neutron Measurements of the Temperature Dependence of Neutron Diffusion Parameters for Light-Water Ice – E. G. Silver 28

2. CRITICAL EXPERIMENTS 31

2.1. Critical Three-Dimensional Arrays of Neutron-Interacting Units. Part II. U(93.2) Metal – J. T. Thomas 31

2.2. Critical Dimensions of Aqueous UO_2F_2 Solutions Containing 4.9% ^{235}U-Enriched Uranium – E. B. Johnson and D. F. Cronin 31

2.3. Geometrically Complicated Critical Assemblies of 93.2% ^{235}U-Enriched Uranium Metal – J. T. Mihalczo 33

2.4. Critical Experiments and Calculations with Reflected Annular Cylinders of U(93.2) Metal – J. T. Mihalczo 36

2.5. Prompt-Neutron Lifetime in Critical Enriched-Uranium Metal Cylinders and Annuli – J. T. Mihalczo 37

2.6. High Flux Isotope Reactor Critical Experiment No. 3 – J. T. Thomas 37

2.7. Experimental and Calculational Determinations of the Reactivity Effects of Perturbations in a One-Dimensional Critical Experiment – E. G. Silver and E. B. Johnson 38

2.8. Calculated Neutron Multiplication Factors of a Spherical Volume of Fissile Material in Aqueous Solution Enclosed in Combinations of Absorbers and Reflectors – D. W. Magnuson 41

2.9. Critical Dimensions of Systems Containing ^{235}U, ^{239}Pu, and ^{233}U – H. C. Paxton, J. T. Thomas, D. Callihan, and E. B. Johnson 42

3. REACTOR SHIELDING 43

3.1. Measurements and Calculations of Neutron Spectral Intensities Throughout a Reactor Water Shield – M. S. Bokhari and V. V. Verbinski 43

3.2. Power Calibration of the Bulk Shielding Reactor I – M. S. Bokhari, V. V. Verbinski, T. V. Blosser, G. T. Chapman, and A. Bakeshloo 44

3.3. Pulse-Height Spectra of Gamma Rays Emitted by the Stainless-Steel-Clad Bulk Shielding Reactor II (BSR-II) – G. T. Chapman, K. M. Henry, and J. D. Jarrard 45

3.4. Determination of Thermal-Neutron Flux Distributions in the Bulk Shielding Reactor II by Copper Wire Activation Techniques – G. T. Chapman 46

3.5. An Experimental Verification of a Source Geometry Transformation for Shielding Calculations – L. Jung 46

3.6. A Comparison of First- and Last-Flight Expectation Values Used in an O5R Monte Carlo Calculation of the Neutron Distribution in Water – D. K. Trubey and M. B. Emmett 52

3.7. Calculation of Fission-Source Thermal-Neutron Distribution in Water by the Transfusion Method – D. K. Trubey 54

3.8. Some Calculations of the Fast-Neutron Distribution in Ordinary Concrete from Point and Plane Isotropic Fission Sources – D. K. Trubey and M. B. Emmett 54

3.9. A Calculation of the Neutron Dose in Ordinary Concrete Due to Air-Scattered Neutrons from a Point Fission Source – D. K. Trubey 54

3.10. Measurements of the Angular Dependence of Fast-Neutron Dose Reflected from Concrete – F. J. Muckenthaler, K. M. Henry, L. B. Holland, J. L. Hull, J. J. Manning, and D. R. Ward 55

3.11. A Calculation of the Fast-Neutron Differential Dose Albedo for Concrete – R. E. Maerker 57

3.12. An Angle-Dependent Albedo for Fast-Neutron Reflection Calculations – R. L. French and M. B. Wells 58

3.13. A First-Last Collision Model of the Air-Ground Interface Effects on Fission Neutron Distributions – R. L. French 58

3.14. Angular Distribution of the Air-Scattered Fast-Neutron Dose Rate at the Air-Ground Interface – M. B. Wells 58

3.15. Reflection of Thermal Neutrons and Neutron-Capture Gamma Rays from Concrete – M. B. Wells 59

3.16. A Study of the Radiation Shielding Characteristics of Basic Concrete Structures at the Tower Shielding Facility – V. R. Cain 59

3.17. Measurements of Radiation Intensities in Vertical Concrete-Lined Holes and an Adjoining Tunnel at the Tower Shielding Facility – V. R. Cain, C. E. Clifford, and L. B. Holland 60

3.18. Calculations of Thermal-Neutron Flux Distributions in Concrete-Walled Ducts Using an Albedo Model with Monte Carlo Techniques – V. R. Cain 60

3.19. Penetration of Neutrons and Gamma Radiation Through the Openings of Underground Structures – R. L. French, M. B. Wells, and N. M. Schaeffer 61

3.20. Measurement of Fast-Neutron Transmission Through an "Infinite" Slab of LiH – F. J. Muckenthaler, K. M. Henry, L. B. Holland, J. L. Hull, J. J. Manning, and D. R. Ward 61

3.21. Monte Carlo Calculations of Neutron Transmission Through Lithium Hydride – F. H. Clark and F. B. K. Kam 62

3.22. A Lithium Hydride Conical-Shell Neutron Shadow Shield – F. H. Clark and N. A. Betz 64

3.23. Scattering of Fast Neutrons from Cylinders of Lithium Hydride, Graphite, Concrete, Aluminum, and Steel – J. C. Courtney and V. V. Verbinski 64

4. RADIATION SHIELDING INFORMATION CENTER 68

4.1. Program of the Radiation Shielding Information Center (RSIC) – S. K. Penny, D. K. Trubey, and B. F. Maskewitz 68

4.2. RSIC Information Retrieval System – S. K. Penny, D. K. Trubey, M. B. Emmett, and L. Jung 68

4.3. Collection of Shielding Computer Codes – B. F. Maskewitz, S. K. Penny, and D. K. Trubey 69

5. MATHEMATICS AND COMPUTER PROGRAMS 70

5.1. Hauser-Feshbach Computer Programs – W. R. Smith 70

5.2. O5R: A General-Purpose Monte Carlo Neutron Transport Code – R. R. Coveyou, D. C. Irving, F. B. K. Kam, and J. G. Sullivan 70

5.3. An O5R Analysis Routine to Estimate Neutron Fluxes in Anisotropic Scattering Media – W. E. Kinney 71

5.4. A Monte Carlo Technique for Selecting Neutron Scattering Angles from Anisotropic Distributions – R. R. Coveyou 72

5.5. Some Tests of the Technique Used by the O5R Neutron Transport Code for Selecting from Anisotropic Angular Scattering Distributions – W. E. Kinney 72

5.6. An Improved Method for Handling Angular Distributions in the O5R Code – R. MacPherson and R. R. Coveyou 73

5.7. A CDC-1604A Code to Process O5R Collision Tapes – F. B. K. Kam and K. Franz 73

5.8. Derivation of First- and Last-Flight Estimators for Monte Carlo Computations of Scattered Particle Fluxes in Attenuating Media with Spherical or Plane Symmetry – S. K. Penny 74

5.9. OGREISH-P1 – A Monte Carlo Code Utilizing Importance Sampling for the Computation of Gamma-Ray Transmission Through Laminated Slabs – T. W. Armstrong and S. K. Penny 74

5.10. An Algorithm for the Working Inverse of a Matrix – W. R. Burrus, C. Schneeberger, and B. Rust 74

5.11. The Utilization of *a Priori* Information by Means of Mathematical Programming in the Statistical Interpretation of Measured Distributions – W. R. Burrus 77

5.12. A Generalized One-Constraint Lagrange Multiplier Numerical Formulation – F. S. Clark and F. B. K. Kam 77

6. RADIATION DETECTOR STUDIES (I) 78

6.1. Recent Developments in the Proton-Recoil Scintillation Neutron Spectrometer – W. R. Burrus and V. V. Verbinski 78

6.2. Response Functions of an Organic Scintillator to Fast Neutrons – V. V. Verbinski, J. C. Courtney, W. R. Burrus, T. A. Love, and J. G. Sullivan 79

6.3. Modifications of Bonner Sphere Spectrometer to Measure Spectra of Low-Energy Neutrons from (α,n) Sources – S. K. Mehta 80

6.4. Design of Two Neutron-Responding Instruments: An Isotropically Responding Fast-Neutron Dosimeter and a Spectrometer for the Energy Range from Thermal to 10 kev – T. V. Blosser 84

7. WATER DESALINATION STUDIES – THEORETICAL 87

7.1. Boundary Layer Buildup in the Demineralization of Salt Water by Reverse Osmosis – L. Dresner 87

7.2. Salt Concentration at Phase Boundaries in Desalination Processes – T. K. Sherwood, P. L. T. Brian, R. E. Fisher, and L. Dresner 87

7.3. A Concentration Polarization Method for Determining Salt Rejection by Hyperfiltration Membranes – K. A. Kraus, R. J. Raridon, and L. Dresner 87

PUBLICATIONS 90

1. Nuclear and Reactor Physics

1.1. ELASTIC AND INELASTIC SCATTERING OF 11-Mev PROTONS FROM MEDIUM-WEIGHT NUCLEI

J. K. Dickens F. G. Perey
R. J. Silva[1]

A better understanding of nuclear mechanisms is needed to predict nuclear cross sections or to allow interpolation between energies where nuclear data are available. The elastic scattering of nucleons from nuclei can be fairly successfully reproduced by using a complex optical-model potential.[2,3] Above incident energies of a few Mev the inelastic nucleon scattering cross section for exciting certain states of nuclei is very large; it is believed that these states represent some form of collective motion of the nucleons in the nucleus. Therefore an extension of the optical model such as that suggested by Buck[4] might successfully describe the inelastic scattering exciting these states.

To test such a model we have performed a series of measurements of inelastic, as well as elastic, proton scattering from several nuclei in the intermediate-mass region. The 11-Mev proton beam of the ORNL tandem Van de Graaff was used; other details of the experimental technique were reported previously.[5] Nuclei which were studied[6] are ^{48}Ti, ^{51}V, ^{54,56}Fe, ^{60,62,64}Ni, ^{63,65}Cu, ^{64,66,68}Zn, and ^{70,72,74,76}Ge. Angular distributions were obtained for elastic scattering and for inelastic scattering to the 2^+ and 3^- collective states as well as to several other low-lying levels in the even-even nuclei; angular distributions for the odd-mass targets were obtained for elastic scattering and for inelastic scattering to several low-lying levels.

Analysis of the elastic angular distributions by means of an optical model is complete. Table 1.1.1 presents the real- and imaginary-well depths (V_S and W_D) obtained for several nuclei. The other parameters are the same as those used in ref. 3. The real-well depths are within ±0.6 Mev of the value predicted by using a formula[3] that includes Coulomb effects and a nuclear symmetry dependence. They tend, however, to be smaller than the values predicted by the formula. Possibly the fluctuations in the potential parameters can be correlated with the known nuclear properties of these nuclei.

Table 1.1.1. Real- and Imaginary-Well Depths (V_S and W_D) for the Optical-Model Analysis of Elastic Scattering

Nuclei	V_S (Mev)	W_D (Mev)
^{48}Ti	49.3	10.7
^{51}V	50.4	12.5
^{54}Fe	50.6	7.8
^{56}Fe	50.8	13.3
^{60}Ni	51.6	12.9
^{62}Ni	52.4	12.7
^{64}Ni	52.7	13.1
^{63}Cu	52.0	11.7
^{65}Cu	52.4	10.4
^{64}Zn	52.0	11.9
^{66}Zn	52.3	12.1
^{68}Zn	52.6	13.1
^{70}Ge	52.8	12.8
^{72}Ge	52.3	14.7
^{74}Ge	51.6	17.9
^{76}Ge	52.4	16.4

The analysis for the inelastic scattering assumed that the optical model describing the elastic scattering is capable of vibration. In a preliminary survey only the real part of the potential was assumed to have quadrupole and octupole vibrations. The distorted-wave Born approximation was used to analyze all the 2^+ and 3^- angular distributions; the coupled-channel code of Buck[4] was used to fit all the 2^+ cross sections coupled to the ground state. In two of the latter cases both the 2^+ and 3^- states were coupled to the ground state. Table 1.1.2 gives the values of the deformation parameters (β) obtained. For most cases the β values obtained are in good agreement and are comparable to those obtained from Coulomb excitation studies.[7] A typical fit to the data is shown in Fig. 1.1.1; in the coupled-channel calculation (CC), the 2^+ and 3^- states were coupled to the ground state.

The analysis using only the real part of the optical potential as vibrating is in fair agreement with the data; however, several other factors remain to be investigated. Vibration of the nuclear charge due to Coulomb excitation is certainly taking place and should be included in the calculation. Furthermore, if only a few channels are coupled explicitly, then the coupling potential should be complex. A calculation using a complex coupling potential and including the effect of Coulomb excitation is shown in Fig. 1.1.2. The calculated angular distribution is compared in this figure with that obtained by using the same optical potential but allowing only the real part of the potential to give rise to the coupling.

The difference between the two calculations is sufficiently great to warrant further analyses of these data.

Table 1.1.2. Deformation Parameters β_{2^+} and β_{3^-} for Coulomb Excitation (CE), Coupled-Channel (CC), and Distorted-Wave (DW) Calculations

	β_{2^+} for			β_{3^-} for DW
	CE	CC	DW	
^{48}Ti	0.26	0.24	0.25	0.14
^{56}Fe	0.23	0.25	0.32	0.23
^{62}Ni	0.19	0.24	0.26	0.21
^{64}Ni	0.19	0.21	0.20	0.22
^{64}Zn	0.25	0.26	0.28	0.28
^{66}Zn	0.23	0.25	0.23	0.25
^{68}Zn	0.20	0.19	0.19	0.21
^{70}Ge	0.22	0.20	0.20	0.25
^{72}Ge	0.25	0.19	0.20	0.23

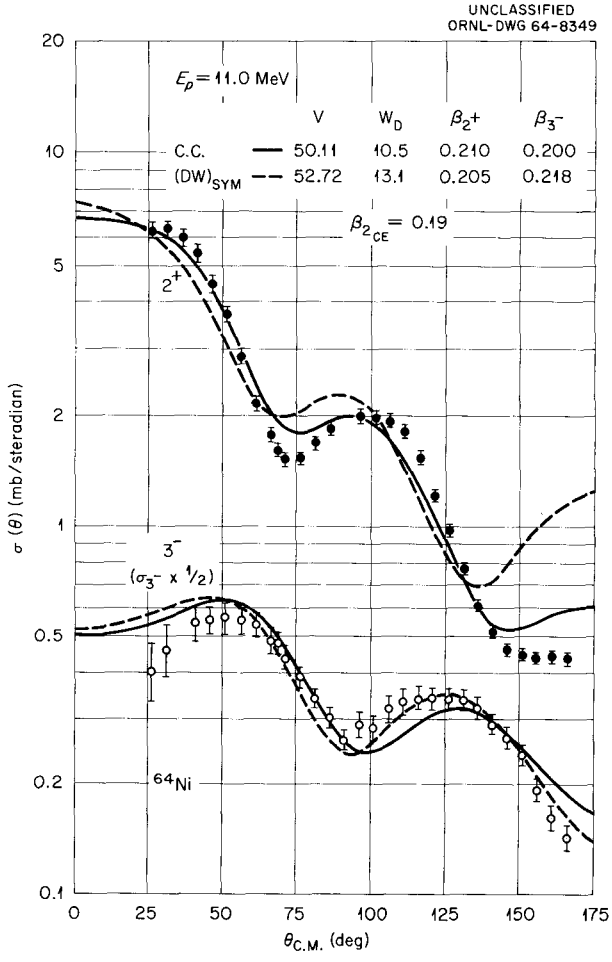

Fig. 1.1.1. Comparison of Calculated Angular Distributions with Experimental Data Points for Inelastic Scattering of Protons from ^{64}Ni. Both theoretical curves were obtained by assuming that the coupling potential is real. The solid curve is the result of the coupled-channel calculation, and the dashed curve results from the distorted-wave calculation.

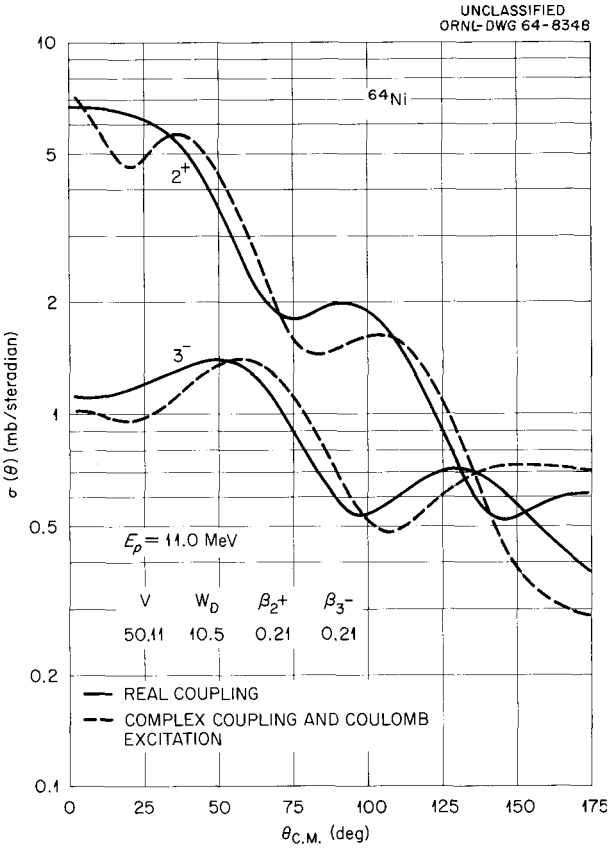

Fig. 1.1.2. Comparison of Two Sets of Calculated Angular Distributions for Inelastic Scattering of Protons from ^{64}Ni.

References

[1]Chemistry Division.

[2]F. G. Perey and B. Buck, *Nucl. Phys.* **32**, 353 (1962).

[3]F. G. Perey, *Phys. Rev.* **131**, 745 (1963).

[4]B. Buck, *Phys. Rev.* **130**, 712 (1963).

[5]J. K. Dickens, F. G. Perey, and R. J. Silva, *Neutron Phys. Div. Ann. Progr. Rept. Aug. 1, 1963*, ORNL-3499, Vol. I, p. 20. R. J. Silva and G. Gordon, "Nuclear Levels of ^{115}Cd and ^{117}Cd from (*d,p*)-Reaction Studies," *Phys. Rev.* (in press).

[6]Some of the data have been published. See: F. G. Perey, R. J. Silva, and G. R. Satchler, *Phys. Letters* **4**, 25 (1963); J. K. Dickens *et al.*, *Phys. Letters* **6**, 53 (1963); J. K. Dickens, F. G. Perey, and R. J. Silva, *Phys. Rev.* **132**, 1190 (1963).

[7]P. H. Stelson and F. K. McGowan, *Annual Review of Nuclear Science*, Vol. 13, pp. 163–90, George Banta Co., Palo Alto, Calif., 1963.

1.2. THE LOCAL ENERGY APPROXIMATION TO NONLOCALITY AND FINITE RANGE EFFECTS[1]

F. G. Perey D. S. Saxon[2]

The application of the local energy approximation to calculations of the nonlocal optical and shell model potentials and to the finite range effects in the distorted theory of transfer reactions is discussed.

References

[1]Abstract of *Phys. Letters* **10**, 107 (1964) as presented in *Nucl. Sci. Abstr.* **18**, 3867 (1964).

[2]University of California, Los Angeles.

1.3. INELASTIC EFFECTS IN STRIPPING AND OTHER DIRECT REACTIONS[1]

S. K. Penny G. R. Satchler[2]

The distorted-wave theory of direct nuclear reactions, such as deuteron stripping, is generalized to include in the distorted waves the effects of the strong inelastic scattering which may be present when the nuclei show collective behavior. The possible changes in parity and angular momentum selection rules are discussed in detail. Formulas are given for the general case and also for a simple model in which only one level of the target nucleus (assumed even) can be excited.

References

[1]Abstract of published paper: *Nucl. Phys.* **53**, 145–58 (1964).

[2]Physics Division.

1.4. DISTORTED-WAVE ANALYSIS OF THE ^{90}Zr(*d,p*)^{91}Zr REACTION USING NONLOCAL OPTICAL-MODEL WAVE FUNCTIONS

J. K. Dickens F. G. Perey
R. J. Silva[1]

The elastic scattering of nucleons from nuclei can be described by an energy-independent non-

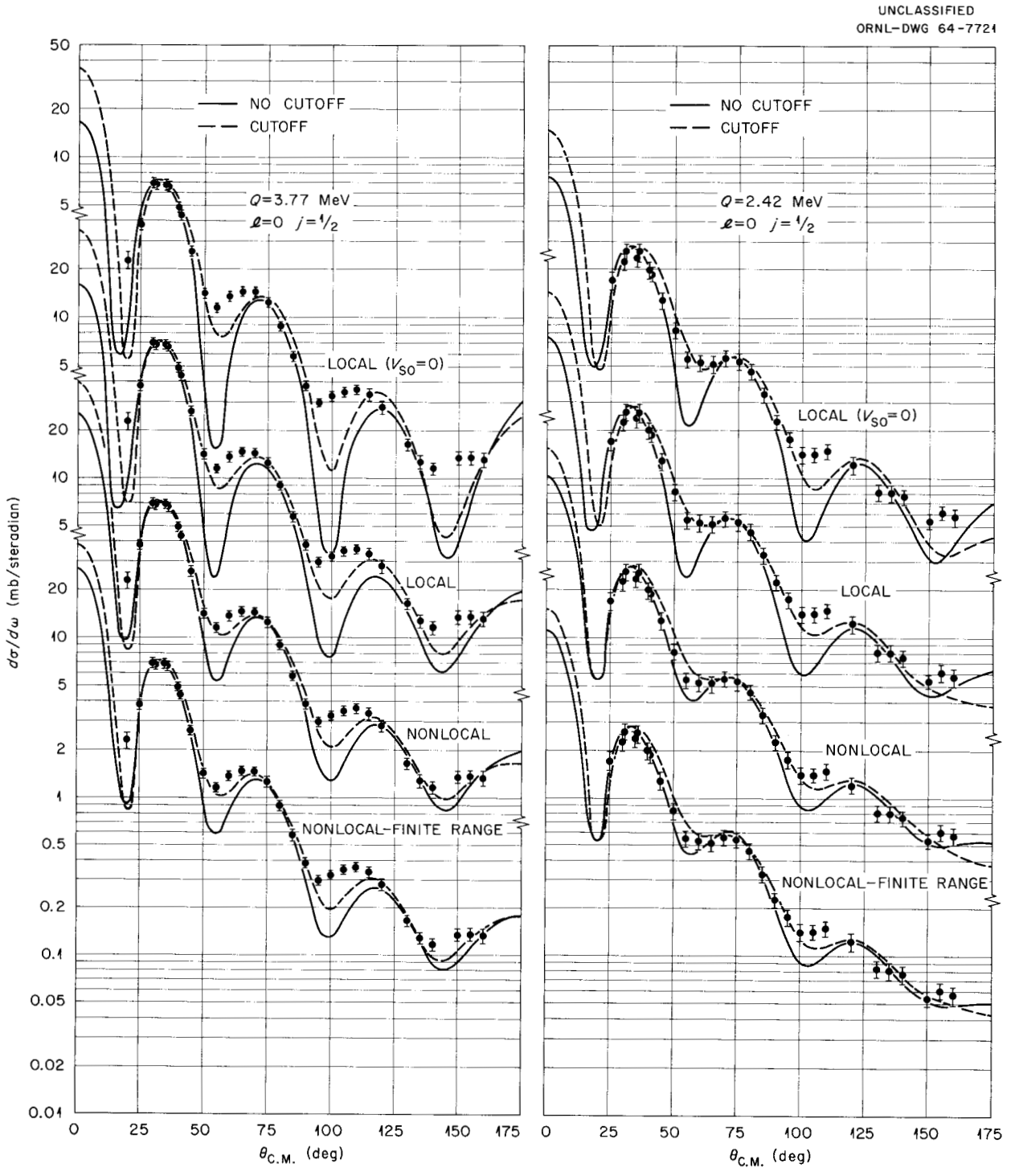

Fig. 1.4.1. Comparison of Calculated Angular Distributions with Experimental Data for Two $l = 0$ Transitions of the $^{90}Zr(d,p)^{91}Zr$ Reaction. The cutoff radius was 4.25 *F*.

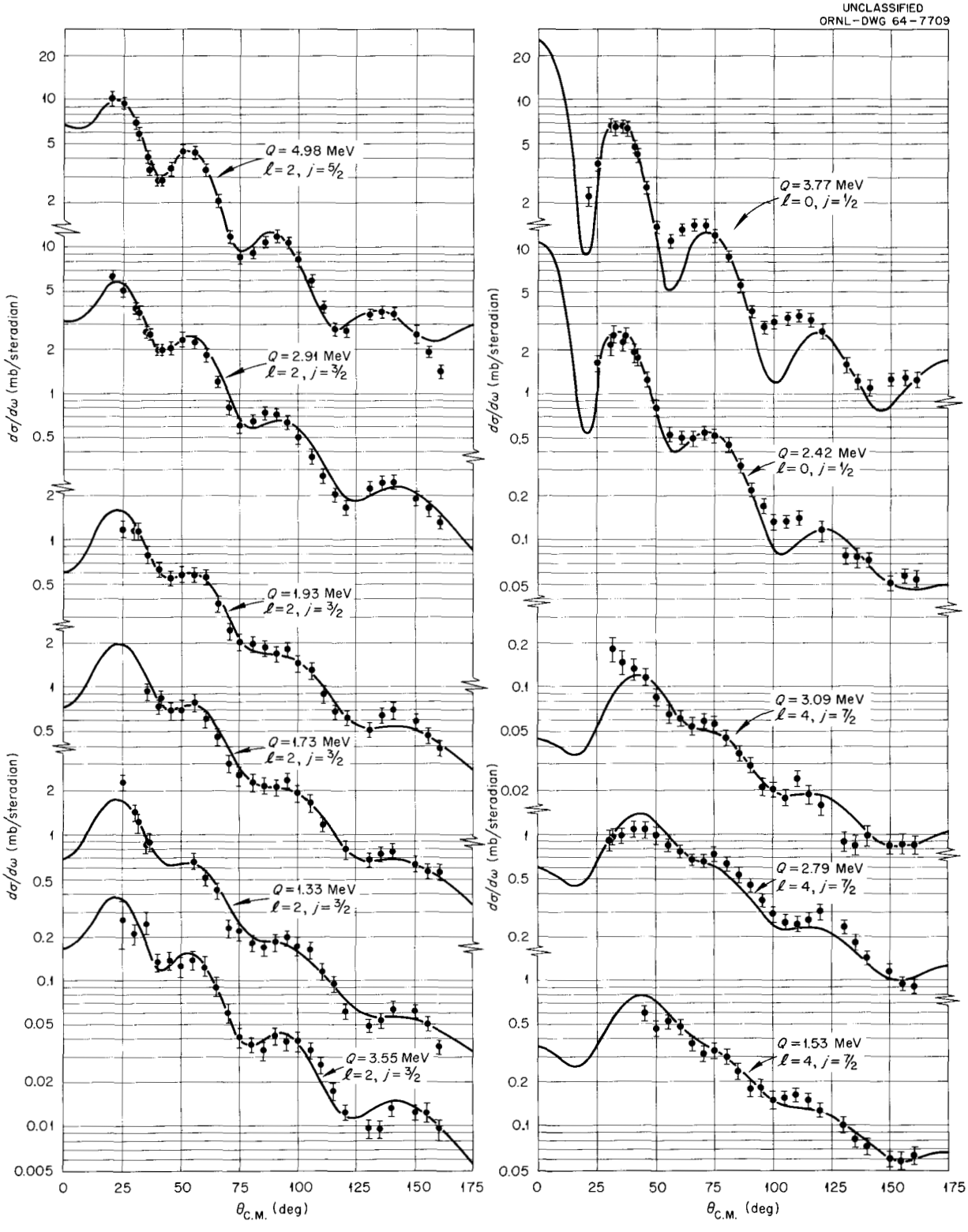

Fig. 1.4.2. Experimental Differential Cross Sections for Protons from the $^{90}Zr(d,p)^{91}Zr$ Reactions Corresponding to Eleven ^{91}Zr Nuclear States, $E_d = 12$ Mev. The solid lines represent theoretical calculations using distorted-wave theory and wave functions given by the nonlocal optical-model potential.

local optical-model potential[2] as well as an equivalent energy-dependent local optical-model potential.[3] Both models adequately reproduce elastic-scattering angular distributions; however, wave functions generated by the first method are smaller in the region of the potential (i.e., inside the nucleus) than those obtained by the second method.[4] Further insight on the nature of these wave functions should be provided by study of a reaction such as (d,p) stripping.

The distorted-wave theory[5] of (d,p) stripping reactions makes use of appropriate optical-model wave functions; the calculated angular distributions are sensitive to the amplitudes of the wave functions in the region of the potential. Experimental angular distributions for stripping are usually much better reproduced if the wave functions inside the nucleus are assumed to be zero. This suggests that calculations using wave functions obtained from nonlocal potentials may be more consistent with stripping data.

Experimental data on the $^{90}Zr(d,p)^{91}Zr$ reaction have been obtained by measuring techniques described previously.[6] An isotopically enriched ^{90}Zr target $\sim$1.5 mg/cm^2 thick was bombarded by 12- and 14-Mev deuteron beams from the tandem Van de Graaff, and outgoing charged particles were detected by solid-state detectors. Angular distributions for protons corresponding to the ground state and ten excited states of the ^{91}Zr nucleus were obtained; in addition, differential cross sections for deuteron elastic scattering were measured.

Calculations for the stripping angular distributions were performed with the code JULIE; input to this code included optical-model potentials which reproduced the elastic scattering data. Many calculated angular distributions for (d,p) reactions are obtained by using a local optical-model potential which neglects spin-orbit coupling. This model served as a starting point. Calculated angular distributions for several proton groups were obtained for four cases: local optical-model potential with no spin-orbit coupling; local optical-model potential with spin-orbit coupling; nonlocal optical-model potential with spin-orbit coupling; and nonlocal optical-model potential, spin-orbit coupling, and a finite range for the nucleon-nucleon force. Angular distributions for two $l = 0$ transitions are shown in Fig. 1.4.1. The data are reproduced much better if a cutoff is used, that is, if the wave function is assumed to be zero inside the nucleus. The effect of the nonlocality of the potential is that of simulating a cutoff such that the nonlocal, no-cutoff calculations give acceptable fits. The effect of the finite range – small for these cases – was calculated with the code FANNY.

All 11 angular distributions were analyzed by using wave functions from the nonlocal optical model potential. The results at 12 Mev are shown in Fig. 1.4.2. This analysis suggests that with the present theories of (d,p) stripping the data favor the reduction of the wave functions given by the nonlocal potential.

References

[1] Chemistry Division.

[2] F. G. Perey and B. Buck, *Nucl. Phys.* **32**, 353 (1962).

[3] F. G. Perey, *Phys. Rev.* **131**, 745 (1963).

[4] F. G. Perey, p. 125 in *Proceedings of the Conference on Direct Interactions and Nuclear Reaction Mechanisms, University of Padua, September 3–8, 1962* (eds., E. Clementel and C. Villi), Gordon and Breach, Science Publishers, New York, 1963.

[5] G. R. Satchler, *Nucl. Phys.* **55**, 1 (1964).

[6] J. K. Dickens, F. G. Perey, and R. J. Silva, *Neutron Phys. Div. Ann. Progr. Rept. Aug. 1, 1963,* ORNL-3499, Vol. I, p. 20; R. J. Silva and G. E. Gordon, "Nuclear Levels of ^{115}Cd and ^{117}Cd from (d,p)-Reaction Studies," *Phys. Rev.* (in press).

1.5. ELASTIC AND INELASTIC SCATTERING OF 5- TO 13.5-Mev DEUTERONS FROM ^{60}Ni: TABULATED DIFFERENTIAL CROSS SECTIONS[1]

J. K. Dickens F. G. Perey

Angular distributions for elastic scattering of deuterons from ^{60}Ni have been measured for incident deuteron energies of 4.86, 5.86, 6.87, 7.88, 8.88, 9.89, 10.86, 11.92, and 13.56 Mev. Differential cross sections were obtained at 5° intervals between laboratory angles of 30 and 160°. Cross sections for deuterons inelastically scattered from the first excited state of ^{60}Ni ($Q = -1.33$ Mev) were obtained for the four incident deuteron energies between 9.89 and 13.56 Mev listed above. Numerical values for all measured cross sections are tabulated.

References

[1] Abstract of ORNL-3637 (June 1964).

1.6. ELASTIC AND INELASTIC SCATTERING OF 8- TO 15-Mev DEUTERONS FROM ^{114}Cd: TABULATED DIFFERENTIAL CROSS SECTIONS[1]

J. K. Dickens F. G. Perey

This report consists of a tabulation of numerical values of differential cross sections of deuterons that were elastically and inelastically scattered from ^{114}Cd. The cross sections were determined at 5° intervals between laboratory angles of 20 and 160° for incident energies of 7.96, 8.97, 9.97, 10.99, 12.0, 13.0, 14.0, and 15.0 Mev. The inelastic-scattering data are for deuterons that were inelastically scattered from the first excited state of ^{114}Cd ($Q = -0.554$ Mev).

References

[1]Abstract of ORNL-3727 (in press).

1.7. THE EFFECT OF DATA NORMALIZATION UPON DEUTERON OPTICAL-MODEL PARAMETERS[1]

J. K. Dickens F. G. Perey

The sensitivity of optical-model parameters to the absolute normalization of 12-Mev deuteron elastic-scattering angular distributions from ^{60}Ni, ^{90}Zr, and ^{114}Cd was studied. Very large variations in parameters were found, particularly when the diffraction pattern of the angular distribution is not pronounced. It is concluded that very accurate absolute normalization of the data is necessary to make a meaningful optical-model analysis. Large parameter fluctuations from element to element observed in previous deuteron optical-model analyses are probably due to differences in normalization of the data.

References

[1]Abstract of article submitted for publication in the *Physical Review*.

1.8. ELASTIC SCATTERING OF LOW-ENERGY DEUTERONS FROM ^{60}Ni AND ^{114}Cd AND THE EFFECT OF THE DEUTERON ELECTRIC POLARIZABILITY IN THE OPTICAL-MODEL POTENTIAL[1]

J. K. Dickens F. G. Perey

Differential cross sections for elastic scattering of deuterons from ^{60}Ni and ^{114}Cd were measured for deuteron bombarding energies of between 5 and 15 Mev. The data were analyzed by means of an optical model that includes a potential due to the deuteron electric polarizability. We conclude that the effects of the polarizability are small, although not negligible, and that nuclear interactions still dominate the elastic scattering at these energies.

References

[1]Abstract of article submitted for publication in the *Physical Review*.

1.9. EFFECTS OF NONLOCALITY IN OFF-DIAGONAL POTENTIALS[1]

F. G. Perey A. M. Saruis[2]

The effects of nonlocality in the off-diagonal parts of the optical potential are studied in distorted-wave Born approximation by using a local energy approximation. The effects are found to be very small in the case of inelastic scattering to low-lying collective states because of the small Q value and the approximate equality usually assumed for the distorting potentials in the initial and final channels. For (p,n) reactions to isobaric analog states, the effects are appreciable because of the large Q value and the differences between distorting potentials, but they largely affect the magnitude of the cross section and not its shape.

References

[1]Abstract of paper submitted for publication in *Nuclear Physics*.

[2]Fulbright Fellow on leave of absence from Centro di Calcolo, CNEN, Bologna, Italy.

1.10. WIDE-ANGLE SCATTERING OF 43-Mev ALPHA PARTICLES BY ^{58}Ni[1]

H. W. Broek[2,3] B. Buck[4]
J. L. Yntema[3] G. R. Satchler[5]

Elastic and inelastic scattering of 43-Mev alpha particles by ^{58}Ni has been observed over the angular range from 15 to 142° (c.m.). Angular distributions were derived for elastic scattering and for inelastic scattering to the 2^+ first excited level at 1.45 Mev, to the two-phonon group at 2.47 Mev, and to the strong 3^- level at 4.45 Mev. The angular distributions showed strong oscillations (with a period of 10°) at angles less than about 70°, but the oscillations became less pronounced for angles greater than 70°. The oscillation period tended to increase with increasing angle to a value of about 15° at the largest angles observed. Optical-model analysis of the elastic scattering was made, and the inelastic scattering to the 2^+ and 3^- levels was calculated by the distorted-wave method. A coupled-channel analysis of the elastic scattering and of the inelastic scattering to the 2^+ and 4^+ levels was also undertaken. Good agreement with experiment was found in all cases. It was found to be necessary to use an optical potential in which the absorptive potential has a somewhat different shape than the real potential. Also, there was some indication that better results could be obtained by using a complex coupling in the distorted-wave calculations.

References

[1]Abstract of paper submitted for publication in *Nuclear Physics*.
[2]Present address: Bell Telephone Laboratories, Whippany, N.J.
[3]Argonne National Laboratory.
[4]Present address: Nuclear Physics Laboratory, Oxford University.
[5]Physics Division.

1.11. KINEMATICS NOMOGRAM FOR LOW-ENERGY NUCLEAR REACTIONS[1]

J. K. Dickens

For given particles *a*, *b* in the nuclear two-body reaction $X(a,b)Y$, the nomogram described in this report solves the nonrelativistic kinematics reaction

$$Q = E_b(1 + M_b/M_Y) - E_a(1 - M_a/M_Y) - 2\cos\theta\,(M_a M_b E_a E_b)^{1/2}/M_Y$$

for any one of the variables Q, E_a, E_b, θ, and M_Y in terms of the others. Nomograms are presented for the reactions (p,p'), (p,d), (p,t), (p,α), (d,d), (d,p), $(^3\mathrm{He},d)$, (α,α), (α,p), $(^{16}\mathrm{O},^{16}\mathrm{O})$, and $(^{16}\mathrm{O},\alpha)$, and the FORTRAN program used to plot them is included.

References

[1]Abstract of ORNL-3636 (June 1964).

1.12. THE USE OF ELASTIC SCATTERING PARAMETERS IN (d,p) STRIPPING CALCULATIONS

W. R. Smith

Several investigations[1-3] have shown that distorted-wave Born approximation (DWBA) calculations[4] of (d,p) angular distributions give results in substantial agreement with experiment when medium or heavy targets are used. In principle, the optical-model parameters to use in such calculations should resemble those which yield agreement with the appropriate experimental deuteron and proton elastic-scattering data. However, it is well known that a given elastic-scattering angular distribution can usually be fitted by any one of many different sets of parameters.[5] It is therefore of interest to determine how sensitive the stripping results are to different choices of acceptable elastic-scattering parameters. Table 1.12.1 summarizes the elastic-scattering and stripping data used in this investigation.

The E_d = 10.85 Mev $^{90}\mathrm{Zr}(d,p)^{91}\mathrm{Zr}$ reactions were the most intensively studied, and the remaining reactions were then used to check and extend the zirconium results. This research is subsequent to a similar study of the $^{90}\mathrm{Zr}(d,p)^{91}\mathrm{Zr}$ reaction already reported.[6] The present work began with a search of the parameter space for regions which yielded fits to the $\mathrm{Zr}(d,p)\mathrm{Zr}$ and $\mathrm{Nb}(p,p)\mathrm{Nb}$ data. Such regions were found by using volume absorption, surface absorption, and half-volume half-

surface absorption potentials. Introducing these various types of potentials into $^{90}Zr(d,p)^{91}Zr$ calculations yielded almost identical results. It was further determined that two types of surface-peaked imaginary potentials could be found which produced fits to the $Zr(d,d)Zr$ data: one which was narrow and deep and one which was wide and shallow. Their use in the stripping calculations yielded angular distributions that differed somewhat from one another, but not so much that a comparison with the experimental data would definitely show one potential to be preferred over the other.

Table 1.12.1. List of Reactions

Reaction	E (Mev)	Q (Mev)	l	j	Reference
$^{90}Zr(d,p)^{91}Zr$	10.85	5.02	2	5/2	a
	15				b
	10.85	3.8	0	1/2	a
	15				b
	10.85	2.8	4	7/2	a
	15				b
$Zr(d,d)Zr$	11.8				c
	15				c
$Nb(p,p)Nb$	16.2				e
$^{91}Zr(p,p)^{91}Zr$	22.5				f
$^{52}Cr(d,p)^{53}Cr$	3.29	5.72	1	3/2	g
	4.07				
	5.72				h
	7.0				i
	7.0	5.15	1	1/2	
	7.0	4.72	3	7/2	
$^{52}Cr(d,d)^{52}Cr$	7.0				i
$^{53}Cr(p,p)^{53}Cr$	10.0				i
$^{206}Pb(d,p)^{207}Pb$	14.0	4.51	1	1/2	j
$^{206}Pb(d,d)^{206}Pb$	14.0				j
$Bi(p,p)Bi$	17.0				k
$Zn(d,p)$	11.8	5.2	1	1/2	
	11.8		4	9/2	
	11.8		2	5/2	
$Zn(d,d)Zn$	11.8				c
$Zn(p,p)Zn$	17.0				l

[a] R. L. Preston, H. J. Martin, and M. B. Sampson, *Phys. Rev.* **121**, 1741 (1961).

[b] B. L. Cohen and O. V. Chubinsky, *Phys. Rev.* **131**, 2184 (1963).

[c] G. Igo, W. Lorenz, and U. Schmidt-Rohr, *Phys. Rev.* **124**, 832 (1961).

[d] R. K. Jolly, E. K. Lin, and B. L. Cohen, *Phys. Rev.* **130**, 2391 (1963).

[e] C. B. Fulmer, *Phys. Rev.* **125**, 631 (1962).

[f] J. B. Ball, C. B. Fulmer, and R. H. Bassel (to be published).

[g] I. Slaus, *Nucl. Phys.* **10**, 457 (1959).

[h] J. C. Legg, H. D. Scott, and M. K. Mehta, *Nuclear Spectroscopy with Direct Reactions, I. Contributed Papers*, ANL-6848.

[i] P. T. Andrews, R. W. Clifft, L. L. Green, and J. F. Scharpey-Schafer, *Phys. Letters* **3**, 97 (1963).

[j] D. W. Miller, H. E. Wegner, and W. S. Hall, *Phys. Rev.* **125**, 2054 (1962).

[k] G. Schrank and R. E. Pollock, *Phys. Rev.* **132**, 2200 (1963).

[l] I. E. Dayton and G. Schrank, *Phys. Rev.* **101**, 1358 (1956).

In further investigations a set of optimum proton and deuteron parameters was chosen as a central set and then parameter variations about this set were made. In one case the real potential radii were displaced from the central values and then the remaining parameters were varied (subject to the constraint of fixed radii) so as to optimize the fit to the elastic-scattering data. In the other two investigations the real potential radii were kept fixed at the central values; then in one case one additional parameter at a time was displaced and the remaining parameters were then optimized, and in the other case the absolute cross section of the data was changed by ±5% and the parameters were reoptimized. Of these various procedures, only the changes in the real potential radius produced significant variations in the stripping results. Indeed, the resulting spectroscopic factors varied by more than a factor of 2 when the radii were varied by a factor of 1.18. This result implies that DWBA determinations of spectroscopic factors are subject to considerable uncertainty.

The investigations of the other stripping reactions confirmed that the stripping results are sensitive to the choice of radius. In addition, it was shown that for the reaction $^{52}Cr(d,p)^{53}Cr$ a set of potentials could be found which simultaneously fitted the elastic-scattering data, and also the stripping data over the range of bombarding energies from 3.3 to 7 Mev. The $^{90}Zr(d,p)^{91}Zr$ data were also reasonably well fitted at both energies studied; furthermore, the variations in the results generated by different choices of radii were not so large as to destroy the qualitative nature of the fits in the case of both zirconium and chromium, thus indicating that despite ambiguities in the potentials the DWBA stripping theory is a good first approximation for medium-weight targets.

The study of the $^{206}Pb(d,p)^{207}Pb$ reaction differed somewhat from the other cases in that the stripping results were highly sensitive to the choice of parameters. This sensitivity was traced to the comparatively small values of the absorption potentials yielded by the elastic-scattering analysis.

The small absorption enhanced the amount of stripping occurring in the nuclear interior where the various nuclear wave functions yielded by potentials which fit the elastic scattering may be a great deal less alike than they are in the region exterior to the nucleus.

References

[1]W. Tobocman, *Phys. Rev.* **115**, 99 (1959); R. Middleton and D. J. Pullen, *Phys. Letters* **1**, 12 (1962); W. R. Smith and E. V. Ivash, *Phys. Rev.* **128**, 1175 (1962).

[2]D. W. Miller, H. E. Wegner, and W. S. Hall, *Phys. Rev.* **125**, 2054 (1962).

[3]P. T. Andrews *et al.*, *Phys. Letters* **3**, 97 (1963).

[4]W. Tobocman, *Theory of Direct Nuclear Reactions*, Oxford University Press, New York, 1961.

[5]F. G. Perey, *Phys. Rev.* **131**, 745 (1963); C. M. Perey and F. G. Perey, *Phys. Rev.* **132**, 755 (1963); E. C. Halbert, *Nucl. Phys.* **50**, 353 (1964).

[6]W. R. Smith, *Nuclear Spectroscopy with Direction Reactions, I. Contributed Papers*, ANL-6848.

1.13. DISTORTED-WAVE CALCULATIONS OF $^{28}Si(d,p)^{29}Si$ ANGULAR DISTRIBUTIONS

W. R. Smith

A previous analysis[1] indicated that the distorted-wave Born approximation[2] for (d,p) stripping reactions is not a good approximation when light targets are involved but that its success improves markedly when the atomic weight of the target increases from about 30 to around 50. It does not seem plausible for the validity of the theory to change so completely over this mass range, and it is suspected that the light-nuclei reactions may not have been studied carefully enough. The $^{28}Si(d,p)^{29}Si$ reaction involves one of the heavier nuclei for which the theory proved inadequate, and since experimental angular distributions for this reaction exist for bombarding energies ranging from 2 to 15 Mev and since $Al(p,p)Al$, $Al(d,d)Al$, and $Si(d,d)Si$ data are available at several energies, an attempt at reconciling experiment and theory in this case is believed to be worthwhile.

The approach involves finding the parameters which best fit the elastic-scattering data at each energy and each radius – for a wide range of real potential radii – and then attempting to modify these parameters so that they vary smoothly with energy while still yielding satisfactory fits to the elastic-scattering data. Then, including the known energy variation, the parameters would be used in $^{28}Si(d,p)^{29}Si$ stripping calculations throughout the energy range of available data so that a decision can be made as to whether the theory is truly deficient or whether the correct parameters have not yet been tried. At this time, the fitting of the elastic-scattering data is in an advanced state of progress.

References

[1]W. R. Smith and E. V. Ivash, *Phys. Rev.* **131**, 304 (1963).

[2]W. Tobocman, *Theory of Direct Nuclear Reactions*, Oxford University Press, New York, 1961.

1.14. OPTICAL-MODEL PARAMETERS FOR $^{90}Zr(d,p)^{91}Zr$ BELOW 4 Mev

C. E. Brient[1] E. M. Bernstein[1]
E. L. Hudspeth[1] W. R. Smith

The distorted-wave Born approximation (DWBA)[2] provides a suitable description of (d,p) stripping angular distributions when medium-weight targets are employed.[3] However, there is very little experimental information on such reactions at bombarding energies less than half the Coulomb barrier height. There are reasons for believing that the DWBA theory may be even more valid at such energies than at the more usual higher energies. For example, the weak coupling approximation employed is well satisfied because of the relative increase in the deuteron elastic scattering and the decrease in the (d,p) intensity and also because the enhanced Coulomb repulsion of the deuterons and protons favors the occurrence of stripping from the exterior region of the nucleus, for which the theory is considered to be more accurate.

The $^{90}Zr(d,p)^{91}Zr$ reaction in particular was selected for study both because of the availability of deuteron and proton elastic-scattering data

appropriate to this reaction and because the higher energy $^{90}Zr(d,p)^{91}Zr$ stripping data have already proved amenable to DWBA analysis.[3] In the present study angular distributions corresponding to the ground and first excited states of ^{91}Zr have been obtained[4] at bombarding energies of 2.713, 3.017, 3.213, 3.414, and 3.518 Mev, together with a fourth-excited-state angular distribution at 3.518 Mev. The basic deuteron and proton parameters used in the DWBA calculations were obtained from the published deuteron[5] and proton[6] elastic-scattering analyses of Perey. These parameters, for a derivative-type surface absorption, are as follows:

$R_{op} = 1.25$ F	$a'_d = 0.679$ F
$a_p = 0.65$ F	$R'_{od} = 1.236$ F
$R'_{op} = 1.25$ F	$a'_d = 0.677$ F
$a'_p = 0.47$ F	$V_d = 85.4$ Mev
$V_p = 53$ Mev	$W_d = 18.39$ Mev
$W_p = 12$ Mev	$R_{on} = 1.25$ F
$R'_{od} = 1.272$ F	$a_n = 0.65$ F

The primes denote the imaginary potential parameters, and the subscripts p, d, and n denote, respectively, proton, deuteron, and neutron. Only the parameters V_d and W_d were varied in obtaining the agreement with experiment shown in Fig. 1.14.1. The values of V_d, W_d and the spectroscopic factors S corresponding to the calculations of Fig. 1.14.1 are listed in Table 1.14.1.

Three discrepancies appear in the comparisons between experiment and theory: W_d decreases sharply between 3.2 and 2.7 Mev, the lowest energy first-excited-state data are not well fitted, and the spectroscopic factors are larger in all cases than those similarly obtained (see Sect. 1.12) at bombarding energies of 10.85 (ref. 7) and 15 Mev.[8] Attempts to remove these difficulties by an appropriate selection of parameters were not successful. The nature of the fit to the 2.713-Mev first-excited-state data suggests the presence of a sizable compound-nucleus contribution. Calculations made with the Hauser-Feshbach statistical theory[9] yielded an angular distribution for this case which was symmetric about 90° and had a 0–90° intensity ratio of 1.307. When added in the correct proportion to the DWBA angular distribution, this produced a much better fit, but the "horns" on either end of the experimental distribution were still not reproduced.

The effects of including spin-orbit coupling,[10] deuteron polarizability,[11] and a finite-range neutron-proton interaction[12] were also calculated and found to be negligible. The results of this investigation indicate that (d,p) angular distributions obtained at bombarding energies half the Coulomb barrier height with medium-weight targets can be useful sources of spectroscopic and optical-model information when interpreted by means of DWBA calculations, provided that the Q value and the bombarding energies are not excessively low.

Table 1.14.1. Optical-Model Parameters and Spectroscopic Factors

Level	E_d (Mev)	V_d (Mev)	W_d (Mev)	S
0	3.518	89.17	11.28	1.55
	3.414	87.49	10.89	1.54
	3.213	89.15	7.381	1.77
	3.017	88.72	5.796	2.44
	2.713	88.47	2.464	3.51
1	3.518	86.85	16.16	1.50
	3.414	84.26	17.22	1.33
	3.213	84.39	13.19	1.48
	3.017	84.82	7.700	1.34
	2.713	84.65	4.550	2.42
4	3.518	87.39	5.442	1.60

References

[1]University of Texas, Austin.

[2]W. Tobocman, *Theory of Direct Nuclear Reactions*, Oxford University Press, New York, 1961.

[3]W. R. Smith and E. V. Ivash, *Phys. Rev.* **128**, 1175 (1962).

[4]C. E. Brient *et al.*, *Bull. Am. Phys. Soc.* **9**, 483 (1964).

[5]C. M. Perey and F. G. Perey, *Phys. Rev.* **132**, 755 (1963).

[6]F. G. Perey, *Phys. Rev.* **131**, 745 (1963).

[7]R. L. Preston, H. J. Martin, and M. B. Sampson, *Phys. Rev.* **121**, 1741 (1961).

[8]B. L. Cohen and O. V. Chubinsky, *Phys. Rev.* **131**, 2184 (1963).

[9]W. Hauser and H. Feshbach, *Phys. Rev.* **87**, 366 (1952).

[10]D. Robson, *Nucl. Phys.* **22**, 34 (1961).

[11]C. F. Clement, *Phys. Rev.* **128**, 2724 (1962).

[12]G. Bencze and J. Zimanyi, *Phys. Letters* **9**, 246 (1964).

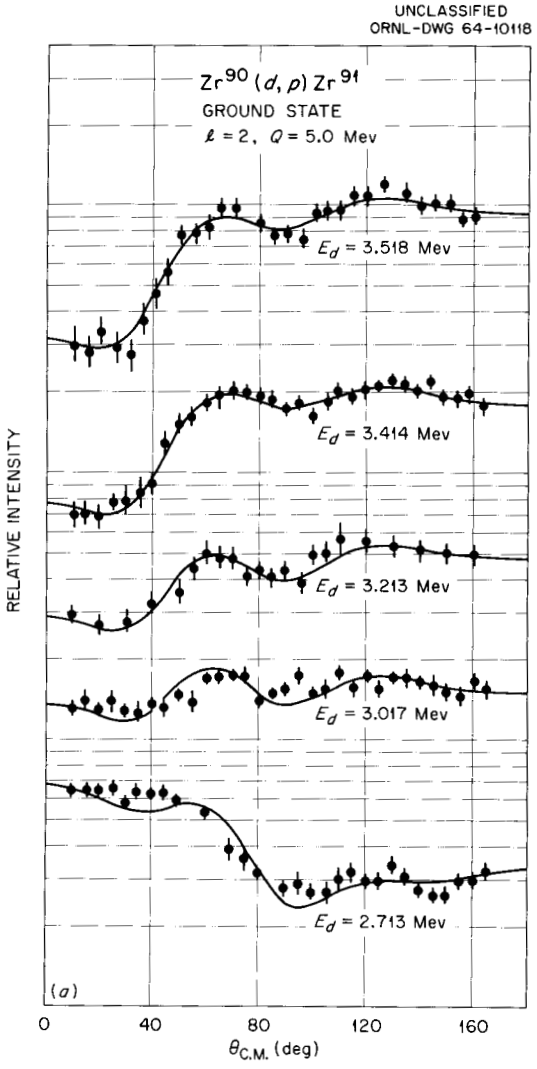

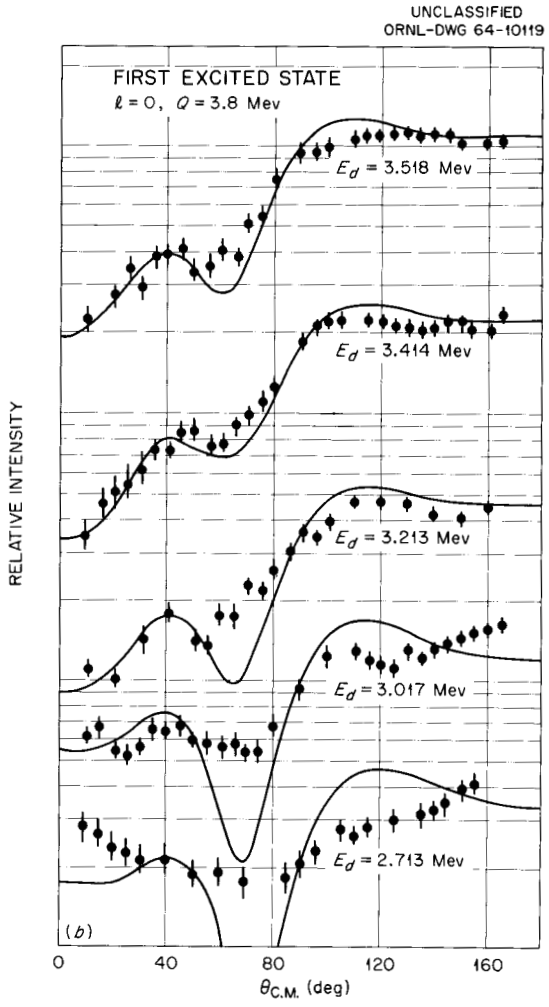

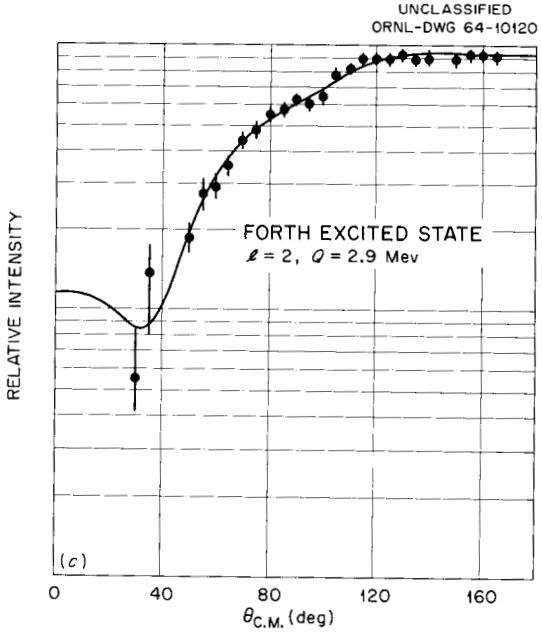

Fig. 1.14.1. Comparisons Between Experimental and Theoretical Angular Distributions for $^{90}Zr(d,p)^{91}Zr$ Transitions to the (a) Ground ($l = 2$), (b) 1.21-Mev ($l = 0$), and (c) 2.07-Mev Levels of ^{91}Zr. The parameters are listed in Table 1.14.1.

1.15. USE OF THE NEUTRON DIE-AWAY TECHNIQUE TO TEST CONTROL ROD EFFECTIVENESS THEORIES[1]

R. B. Perez[2] G. de Saussure
E. G. Silver

The calculation of control rod effectiveness is complicated by its dependence on both the neutron energy distribution and the geometry of the assembly. Comparisons of the theory with experimental results obtained from either reactors or subcritical systems are difficult because of the intrinsic complexity of such systems.

The neutron die-away technique affords the possibility of having an all-thermal neutron model, in which the neutron energy distribution can be separated from spatial effects. Hence, the geometrical factor of the control rod effectiveness can be studied without regard to the details of the neutron spectrum, and the results compared with a clean, simple experimental setup. The method is based on the fact that in a neutron die-away experiment of the type described here, the buckling of the assembly is related to the decay constant of the fundamental mode by

$$B^2 = (\lambda - \lambda_a)/D ,$$

where λ_a = inverse lifetime of the neutrons in moderator (s^{-1}), D = diffusion constant (cm^2/s).

The moderating assemblies used for these experiments were rectangular prisms of beryllium, built in several sizes from small blocks (2.54 cm high, 7.3 cm square). Three types of cadmium control rods were used: thin 0.476-cm-diam rods; a cruciform-section rod; and hollow "thick" rods 7.3 cm × 7.3 cm in cross section.

The theoretical schemes tested were (1) Nordheim-Scalettar, (2) Hurwitz-Roe, and (3) the numerical diffusion code. The effect of a cruciform absorber was computed by using the Hurwitz-Roe conformal transformation technique, and a value of 0.0188 cm^{-2} was found for the buckling which compares with the experimental results of 0.0187 ± 0.0006 cm^{-2}. For the thick rods, both the Nordheim-Scalettar scheme and the diffusion code overestimated the experimental results by about 10%. However, the interaction between thick rods was correctly predicted by both methods. For thin rods, the Nordheim-Scalettar technique was extremely accurate. The disagreement found for the thick rods is to be expected when diffusion theory is used to describe the effect of absorbers with cross-sectional dimensions comparable to the neutron mean free path in the moderator.

Measurements with rods of intermediate sizes are being carried out to determine the point at which diffusion theory becomes inadequate.

References

[1]Abstract of paper published in *Exponential and Critical Experiments*, Proceedings of the Symposium on Exponential and Critical Experiments Held by the International Atomic Energy Agency in Amsterdam, Netherlands, 2–6 September, 1963, Vol. III, p. 241, International Atomic Energy Agency, Vienna, 1964.

[2]University of Florida, Gainsville.

1.16. ON THE EXTENSION OF WEINBERG'S SECOND FUNDAMENTAL THEOREM TO NONHOMOGENEOUS NUCLEAR SYSTEMS

F. G. Perey R. B. Perez[1]

A convenient and elegant way of dealing with reactor physics problems is to include all the details of the neutron slowing-down processes in the so-called synthetic kernels[2] which can be generated so that the computed slowing-down density agrees with the one measured in the media under study.[3] This technique effectively converts a set of coupled partial differential equations (Fermi age theory coupled with thermal-neutron diffusion, or multigroup, theories) into a single integrodifferential equation for the thermal-neutron population in the assembly.

The interest in Weinberg's second fundamental theorem lies in the fact that when a homogeneous reactor loading is assumed and infinite media kernels are used, the integrodifferential equation can be converted into a differential equation, a fact which greatly simplifies the theory.

We present here the extension of Weinberg's theorem to nonhomogeneous loadings using a method developed[4] in connection with some quantum mechanical studies which lead to similar integro-differential equations.

Let us call $P(\vec{r},\vec{r}_0)$ the probability that a neutron born by fission in the unit volume at $\vec{r}_0$ becomes thermalized at $\vec{r}$. To illustrate the method, we assume that the kernel is a displacement kernel; in other words, that it is only a function of the modulus of the displacement vector $\vec{r}-\vec{r}_0$:

$$P(\vec{r},\vec{r}_0) = P(|\vec{r}-\vec{r}_0|) . \tag{1}$$

The diffusion equation for the thermal neutrons becomes

$$D\nabla^2 \phi(\vec{r}) - \Sigma_a(\vec{r})\,\phi(\vec{r}) + \Lambda g(\vec{r}) = 0 , \tag{2}$$

where the slowing-down density $g(\vec{r})$ is

$$g(\vec{r}) = \int d\vec{r}_0\, P|\vec{r}-\vec{r}_0|)\, \nu\, \Sigma_f(\vec{r}_0)\, \phi(\vec{r}_0) . \tag{3}$$

The nonhomogeneous fuel distribution is introduced through the space-dependent macroscopic fission cross section $\Sigma_f(\vec{r}_0)$, and Λ is the reactivity eigenvalue.

In order to convert Eq. (1) into a differential equation, we make the following change of variable in Eq. (3):

$$\vec{s} = \vec{r}_0 - \vec{r}. \tag{4}$$

Then,

$$g(\vec{r}) = \int d\vec{s}\, \overline{P}(s)\, \nu\, \Sigma_f(\vec{r}+\vec{s})\, \phi(\vec{r}+\vec{s}) . \tag{5}$$

Introducing $\overline{P}$, the Fourier transform of P, we have

$$g(\vec{r}) = \iint d\vec{r}\, d\vec{\lambda}\, e^{-i\vec{\lambda}\cdot\vec{s}}\, \overline{P}(\lambda)\, \nu\, \Sigma_f(\vec{r}+\vec{s})\, \phi(\vec{r}+\vec{s}) . \tag{6}$$

Since P is an even function of s, it is possible to expand $\overline{P}$ in a Taylor series in λ^2 about a value $\lambda^2 = B^2$; that is,

$$\overline{P}(\lambda^2) = \overline{P}(B^2) + (\lambda^2 - B^2)\, \overline{P}'(B^2) + \dots . \tag{7}$$

By keeping only two terms in the Taylor expansion in Eq. (6) and by using well-known properties of delta functions, the integration, first over λ and then over s, easily yields

$$\begin{aligned} g(\vec{r}) = {} & \nu\, \Sigma_f(\vec{r})\, \overline{P}(B^2)\, \phi(\vec{r}) \\ & - \nu\, \overline{P}'(B^2)\, \Sigma_f(\vec{r})\, (\nabla^2 + B^2)\, \phi(\vec{r}) \\ & - \nu\, \overline{P}'(B^2)\, \phi(\vec{r})\, \nabla^2\, \Sigma_f(\vec{r}) \\ & - 2\nu\, \overline{P}'(B^2)\, \nabla\, \Sigma_f(\vec{r}) \cdot \nabla\, \phi(\vec{r}) . \end{aligned} \tag{8}$$

If one now chooses

$$B^2(\vec{r}) = \frac{\Lambda\, \nu\, \Sigma_f(\vec{r})\, \overline{P}(B^2) - \Sigma_a(\vec{r})}{D} - \frac{\nabla^2\, \Sigma_f(\vec{r})}{\Sigma_f(\vec{r})} , \tag{9}$$

the substitution of Eq. (8) in Eq. (2) gives

$$D\, \nabla^2\, \phi(\vec{r}) - \Sigma_a(\vec{r})\, \phi(\vec{r}) + \Lambda\, \nu\, \Sigma_f(\vec{r})\, \overline{P}(B^2)\, \phi(\vec{r}) = \frac{2\lambda\, \nu\, \overline{P}'(B^2)\, \nabla \Sigma_f(\vec{r}) \cdot \nabla \phi(\vec{r})}{1 - \Lambda\, \nu\, \overline{P}'(B^2)\, \Sigma_f(\vec{r})/D} . \tag{10}$$

The above choice of $B^2(\vec{r})$ is made in order to optimize the convergence of the Taylor series [Eq. (7)] and is seen to be a "local buckling." The final result [Eq. (10)] reduces to the second fundamental theorem when Σ_f is constant. The effect of the spatial variation of Σ_f is to introduce the term on the right-hand side of Eq. (10) and the need to evaluate $\overline{P}$ at the "local buckling" value. The term in $\nabla\Sigma_f \cdot \nabla\, \phi$ can be eliminated from Eq. (10) by a suitable transformation of ϕ.

Since we have kept only two terms in the Taylor expansion of $\overline{P}$, our final result is an approximation. It is easy to see that the approximation is good when the "local buckling" changes slowly over the range of the slowing-down kernel $\overline{P}(|\vec{r}-\vec{r}_0|)$. In the limit where the "local buckling" is constant – the infinite homogeneous medium – the approximation becomes exact; that is, it is the second fundamental theorem.

The above treatment can be extended to a finite-medium kernel, where the slowing-down kernel is no longer a function of only $|\vec{r}-\vec{r}_0|$, provided that the dependence of the kernel on $\vec{r}-\vec{r}_0$ is symmetric in $\vec{r}$ and $\vec{r}_0$.

References

[1]University of Florida, Gainesville.

[2]A. M. Weinberg and E. P. Wigner, *The Physical Theory of Neutron Chain Reactors*, p. 373, University of Chicago Press, Chicago, 1958.

[3]S. Glasstone and M. C. Edlund, *The Elements of Nuclear Reactor Theory*, p. 368, Van Nostrand, Princeton, N.J., 1954.

[4]F. G. Perey and D. S. Saxon, *Phys. Letters* **10**, 107 (1964).

1.17. DIFFERENTIAL AND TOTAL CROSS SECTIONS FOR THE ^{9}Be(α,n) REACTIONS FROM 6 TO ~10 Mev

V. V. Verbinski — J. Gibbons[1]
W. R. Burrus — W. E. Kinney
J. K. Dickens — R. L. Macklin[1]
F. G. Perey

Measurements of total and differential cross sections for the ^{9}Be(α,n) reactions have been made for alpha-particle energies up to 10 Mev. The beam of α^{2+} particles was obtained from the ORNL 5.5-Mev Van de Graaff accelerator. The total cross sections were measured with the ORNL graphite-sphere long counter, but because the sphere efficiency drops off above 8 Mev, the neutron spectral intensities were obtained with a 2- by 2-in.-diam NE-213 liquid scintillator[2] spectrometer having a low-energy bias of 0.5 Mev. The differential data for energies above 8 Mev were then employed to correct the total cross-section data for the "nonflat" response of the long counter.

Angular and spectral measurements, in addition to being useful to the measurement of total cross sections, are of significant interest to the study of nuclear reaction mechanisms. This is especially true when the incident particle is an alpha particle, for which calculations and interpretation of experimental results are simplified by virtue of the alpha particle being a tightly bound spin-zero particle.

Figure 1.17.1 shows the total ^{9}Be(α,n) cross section and the 0° (c.m.) excitation functions (in mb/steradian) for the n_0, n_1, and n_2 neutron groups from the ^{9}Be(α,n)^{12}C, ^{12}C* reactions, leaving ^{12}C in the ground, first, and second excited states respectively. Both the total and the differential cross sections show a significant amount of structure, which is characteristic of compound nucleus effects. Because of this structure, the falloff of σ_T above 9.1 Mev is likely to be local and may not continue to decrease above 10.5 Mev.

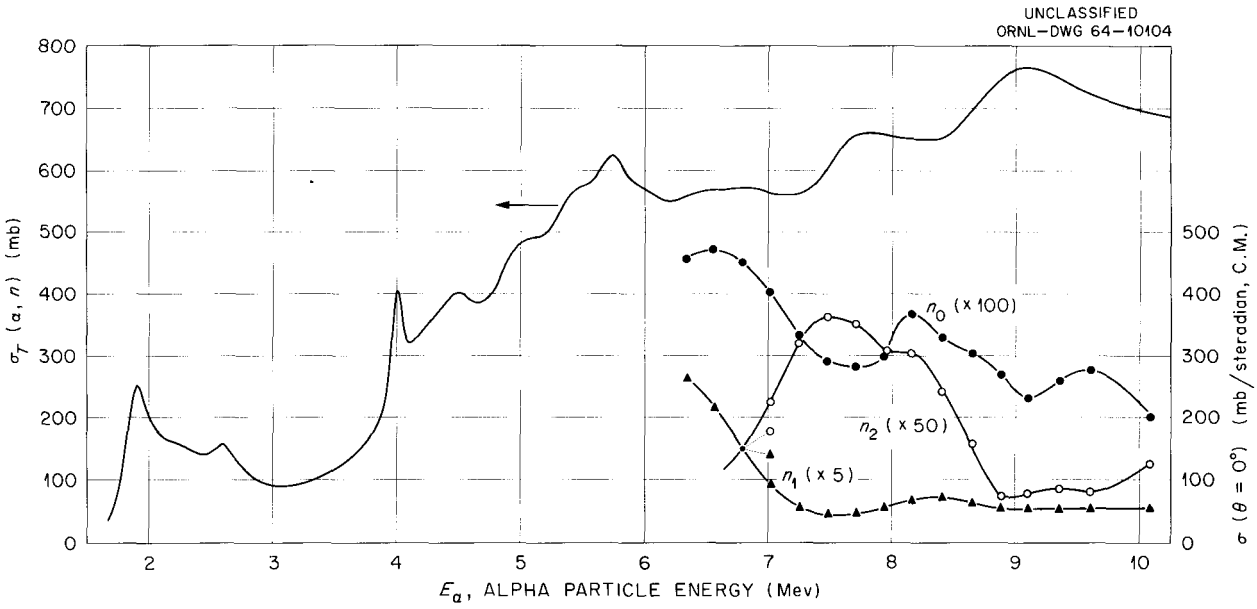

Fig. 1.17.1. Total Neutron Yield from ^{9}Be(α,n) Reactions and 0° Excitation Functions for n_0, n_1, and n_2 Neutrons.

In other measurements[3] of n_0 and n_1 neutron angular distributions from $^9Be(\alpha,n)^{12}C, ^{12}C^*$ reactions, the structure was observed to vanish above 17 Mev (a strong forward peaking sets in, indicative of direct interaction); therefore the total cross section above 17 Mev should be smoother and more reliably extrapolated. Measurements above 17 Mev should be made since the $^9Be(\alpha,n)$ cross section is of particular concern to spacecraft designers considering beryllium alloys (see Chaps. 8–10) because of the alpha particles in solar flares.

In obtaining the differential data a pulse-shape discrimination[4] was used to reject gamma-ray counts. A few samples of the spectra unfolded with the SLOP code (see Sect. 6.1) are shown in Fig. 1.17.2. The data for a 10.1-Mev alpha bombarding energy yield four distinct peaks: n_0, n_1, n_2, and n_3 neutrons from the $^9Be(\alpha,n)^{12}C, ^{12}C^*$ reactions.

Analysis of the data was delayed because the scintillator response to monoenergetic neutrons, which is a required input to the SLOP unfolding code, was accurately calculable to only 11 Mev (see Sect. 6.2). However, Monte Carlo calculations of the response functions for organic scintillators have been modified to include $(n,n',3\alpha)$, (n,α), (n,p), and (n,pn) reactions on the ^{12}C of the scintillator, and reliable calculations of scintillator response were made possible for energies up to 25–30 Mev. These have satisfactorily reproduced the pulse-height distribution obtained for 14.4-Mev incident neutrons with an NE-213 scintillator.

The scintillator resolution has recently been improved by a factor of about 2 by substituting an aluminum-foil reflector for the manufacturer's white paint reflector on a 2- by 2-in.-diam NE-213 glass-encapsulated scintillator. With this, it is hoped that we can resolve n_0, n_1, n_2, and n_3 neutrons from the $^9Be(\alpha,n)^{12}C, ^{12}C^*$ reactions for alpha bombarding energies above 20 Mev and can use the relatively weak beam from the ORNL tandem Van de Graaff.

The n_0 and n_1 neutron angular distributions have been obtained with hand calculations at 7.3-, 8.2-, 9.2-, and 10.1-Mev alpha bombarding energies. In general, their structure (shape) is pronounced, with two to three maxima, and varies slowly with energy; an exception is the rather large change for the n_0 angular distribution between 7.3- and 8.2-Mev alpha energies. At 10.1 Mev, the angular distributions are in good overall agreement with the 9.8-Mev results of Kjillman and Nilsson[5] for n_0 and n_1 neutrons.

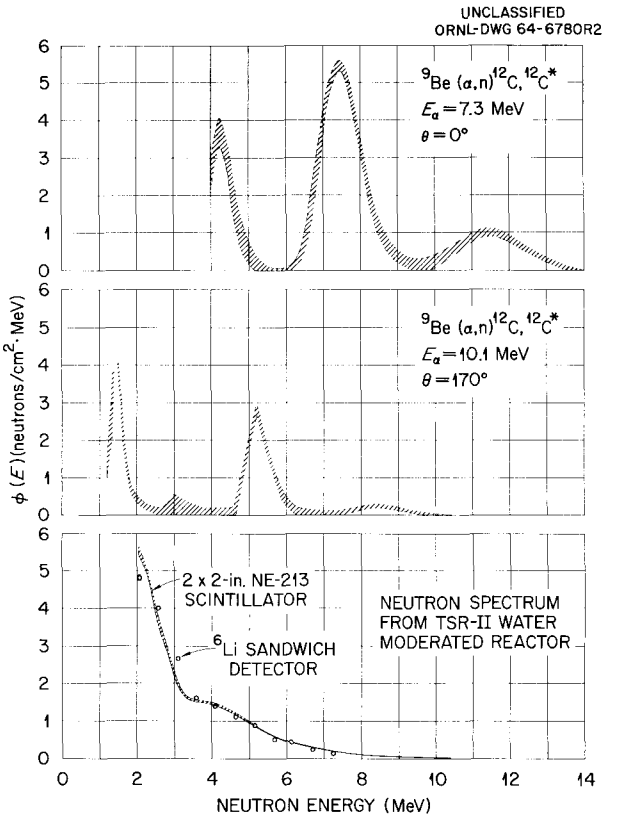

Fig. 1.17.2. Sample Energy Spectra Obtained from Unfolding Pulse-Height Distributions from the $^9Be(\alpha,n)$ Reactions. Up to four neutron groups are identified from the $^9Be(\alpha,n)^{12}C, ^{12}C^*$ Reactions.

The work reported here represents an extension of total cross-section measurements performed previously by Gibbons and Macklin.[6]

References

[1]Physics Division.

[2]Nuclear Enterprises, Ltd., Winnipeg, Manitoba, Canada.

[3]G. Deconnick *et al.*, *Nucl. Phys.* **49**, 424 (1963).

[4]V. V. Verbinski *et al.*, *Neutron Phys. Div. Ann. Progr. Rept. Sept. 1, 1962,* ORNL-3360, Fig. 6.17.2, p. 107.

[5]J. Kjillman and A. Nilsson, *Arkiv Fysik* **22**, 277 (1962); A. Nilsson and J. Kjillman, *Nucl. Phys.* **32**, 177 (1962).

[6]J. H. Gibbons and R. L. Macklin, *Phys. Rev.* **114**, 571 (1959); R. L. Macklin, *Nucl. Phys.* **1**, 335 (1963).

1.18. PHOTONEUTRON SPECTRA FROM ^{16}O, ^{12}C, AND ^{27}Al

V. V. Verbinski J. C. Courtney[1]

The giant dipole resonance in the total gamma-ray absorption cross section of a few light elements displays pronounced fine structure, some of which has been observed in a direct measurement[2] on ^{16}O. A shell model calculation[3] has reproduced two of the most prominent peaks at the correct gamma-ray energy, but the height that was predicted for the peaks is too large.[4] The giant resonance in ^{16}O is of great interest not only because of much fine structure but also because the doubly magic ^{16}O nucleus lends itself rather well to detailed calculations.

The giant dipole resonance is made up mostly of simple (γ,n) and (γ,p) reactions in light elements. The fine structure in these reactions was first reliably obtained from measurements of the inverse ground-state (p,γ_0) reaction, and the (γ,p_0) cross section was then obtained with detailed balance.[5,6] The $^{16}O(\gamma,p_0)$ cross section, obtained from the $^{15}N(p,\gamma_0)$ reaction,[7] was reproduced in much of its detail by direct measurements of the $^{16}O(\gamma,p)$ cross section. This demonstrates that the (γ,p) transitions go predominantly to the ground state of ^{15}N. A high-resolution measurement[8] of the $^{16}O(\gamma,n)$ cross section was made with 32.5-Mev bremsstrahlung. It reproduced many of the peaks in the $^{16}O(\gamma,p_0)$ ground-state transition, but they appeared to be riding on a high sea of background neutrons,[9] which gave serious disagreement in overall shape and which therefore made it impossible to determine whether the $^{16}O(\gamma,n)$ reactions mostly populate the ground state of ^{15}O. If ground-state reactions are highly favored, then the $^{16}O(\gamma,n)$ cross section can be obtained directly and with high energy resolution from a simple spectral measurement. The work reported here describes such a measurement. The technique employed reduces the background, enables the reduced background to be measured and subtracted, produces a narrow, uncluttered bremsstrahlung cone, and makes possible the measurement of angular-distribution and absolute differential cross sections. In addition to the $^{16}O(\gamma,n)$ reaction, measurements of the $^{12}C(\gamma,n)$ and $^{27}Al(\gamma,n)$ reactions were also made.

Figure 1.18.1 shows the experimental geometry. A 34-Mev burst (10 nsec) of electrons was passed through the field of a bending magnet and then through a 0.15-cm-thick bismuth converter, which produced a narrow (3.5° half angle[10]) cone of bremsstrahlung at an angle θ with respect to the drift-tube axis shown. The electrons were swept out of this cone with a magnetic field. The target material (H_2O, C, or Al) was centered on both the bremsstrahlung cone and the drift tube axis. Neutrons leaving the target at an angle θ passed down a 55-m flight path to an organic scintillator. Time-of-flight spectrometry was used.

An arsenic pellet placed behind the target monitored the time-integrated bremsstrahlung flux via the $^{75}As(\gamma,n)^{74}As$ reaction for which the cross section is known.[11] Sulfur pills placed near the bismuth converter were used to correct for a reduction in arsenic activity due to bremsstrahlung scattering in the target. The target was centered on the bremsstrahlung cone with the aid of the thin ionization chamber shown. The target was moved along the drift tube axis and just out of the bremsstrahlung cone for a measurement of the background, which arose mostly from (γ,n) reactions in the bismuth converter (an abundant and nearly isotropic source). These background neutrons were then scattered into the detector by the target, the air, and the walls of the room.

Figure 1.18.2 shows the absolute $^{16}O(\gamma,n)^{15}O$ cross section obtained from a 1-cm-thick H_2O target, with all neutrons assumed to have left ^{15}O in the ground state. There is excellent overall agreement in shape with the $^{16}O(\gamma,p_0)$ cross section obtained from detailed balance[4,5,7] (solid line), except for some differences in relative peak heights and for an apparent peak at 18.3-Mev excitation energy in the $^{16}O(\gamma,n)$ measurement. The evidence indicates that for 26- to 34-Mev bremsstrahlung (the Bi target of the present experiment

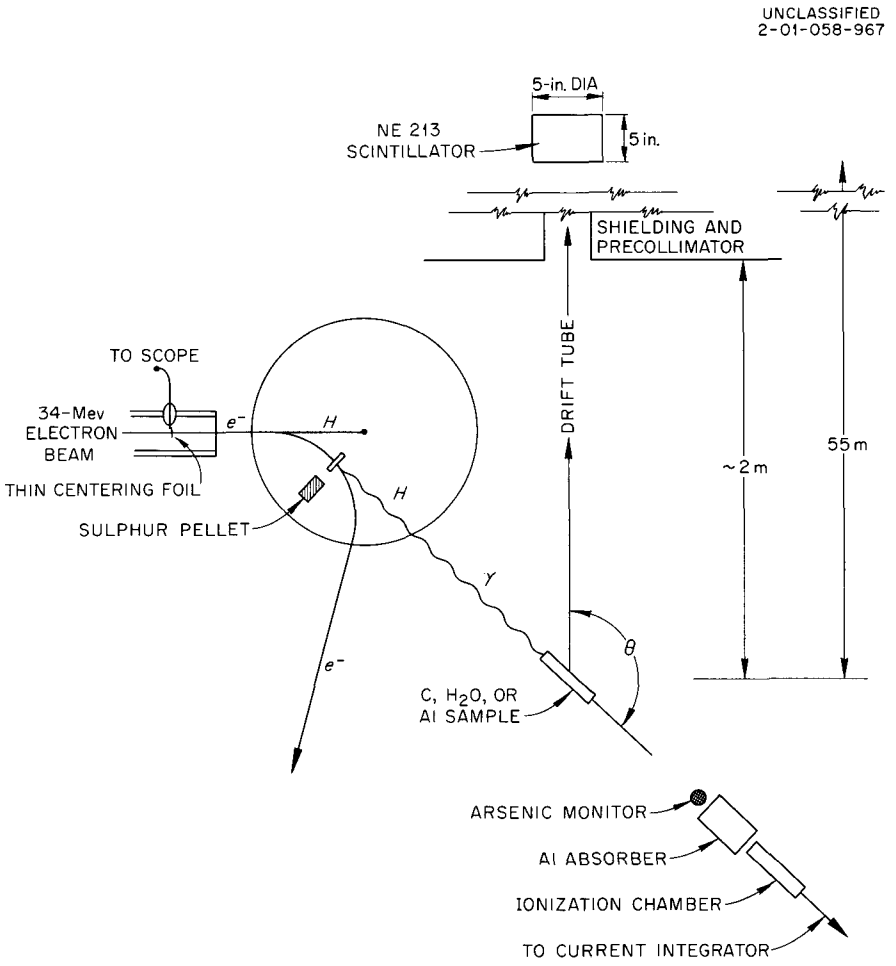

Fig. 1.18.1. Experimental Arrangement for Time-of-Flight Measurements of the Spectra of Photoneutrons from ^{16}O, ^{12}C, and ^{27}Al.

is about 8 Mev thick to 34-Mev electrons[12]) the $^{16}O(\gamma,n)^{15}O$ reaction goes predominantly to the ground state of ^{15}O. This transition is expected to be favored from both energy and angular momentum considerations. The electric dipole transitions excite (1^-) states in ^{16}O, which can decay to the ground state of ^{15}O $(\frac{1}{2}^-)$ by $l = 0$ neutron emission, whereas excitation of the 5.3-Mev doublet of ^{15}O $(\frac{5}{2}^+$ and $\frac{1}{2}^+)$ requires odd l $(l_{min} = 1)$ neutron emission.

The ^{12}C data for 55 and 93° neutron emission (Fig. 1.18.3) show very little variation with angle. However, when the two spectra are normalized at lower energies, there is about a 20% excess of 93° neutrons above 7 Mev, which suggests that direct processes are contributing in this higher energy region.

The aluminum data also produce spectral shapes that are very similar at 55 and 93°, and they agree roughly with the $^{12}C(e,pe')$ spectrum of Dodge and Barber.[6] This agreement is not very meaningful, however, because of the roughly exponential decrease with increasing energy for both cases. Therefore, our spectra for the $^{27}Al(\gamma,n)^{26}Al$ reaction at 55 and 93° have been analyzed by fitting to evaporation spectra, $\phi(E) = E \exp(-E/T)$.

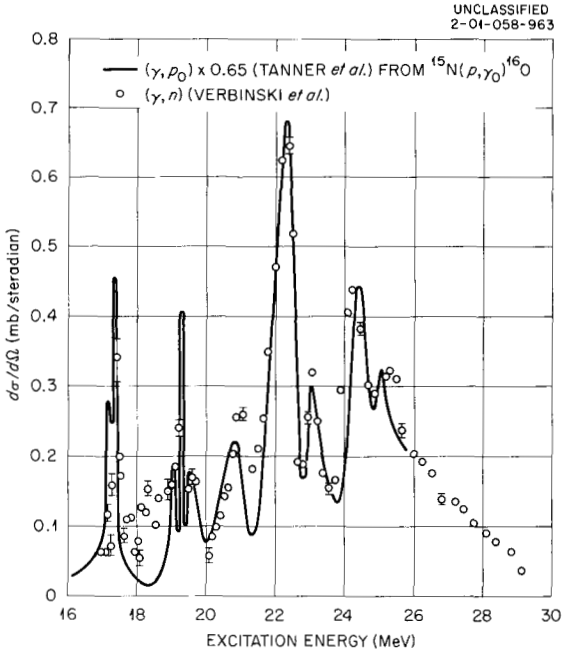

Fig. 1.18.2. Cross Sections for the $^{16}O(\gamma,n)^{15}O$ and $^{16}O(\gamma,p_0)^{15}N$ Reactions.

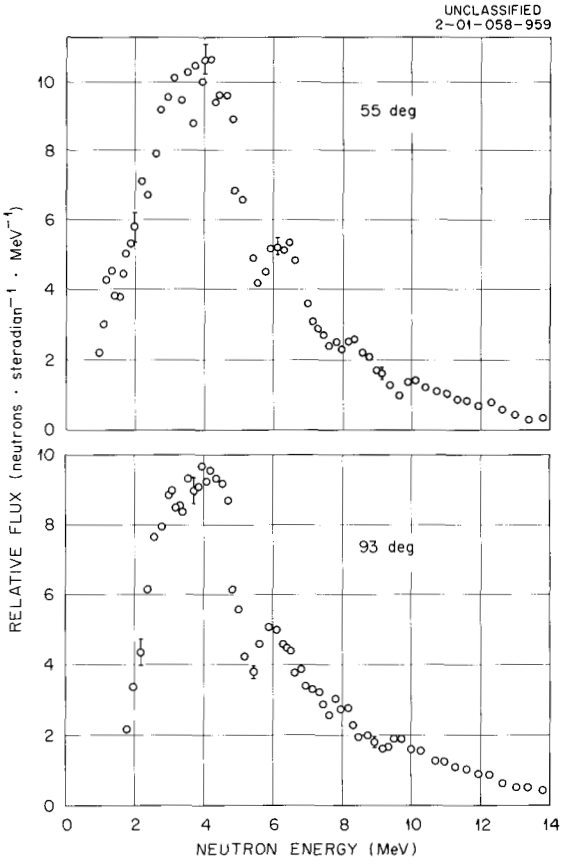

Fig. 1.18.3. Photoneutron Spectra from the $^{12}C(\gamma,n)^{11}C$ Reaction at 55 and 93°.

Since the present measurements were mostly exploratory in nature, they are by no means complete and need to be repeated at several bremsstrahlung energies and angles. However, for the case of ^{16}O, they are adequate to show the great degree of similarity between (γ,n) and (γ,p) cross sections, which is evidence that, to a good approximation, both reactions display the fine structures of the giant dipole resonance for bremsstrahlung radiation below 34 Mev.

References

[1]Catholic University, Washington, D.C.; Graduate Fellow, Oak Ridge Institute of Nuclear Studies.

[2]N. A. Burgov *et al.*, *Zh. Eksperim. i Teor. Fiz.* **43**, 70 (1962) [*Soviet Phys. JETP (English Transl.)* **16**, 50 (1963)].

[3]J. P. Elliott and B. H. Flowers, *Proc. Roy. Soc. (London)* **A242**, 57 (1957).

[4]E. Hayward, *Rev. Mod. Phys.* **35**, 324 (1963).

[5]E. G. Fuller and E. Hayward, *Nuclear Reactions* (ed. by P. M. Endt and P. B. Smith), Vol. II, Chap. 3, p. 144, North Holland Publishing Co., Amsterdam, 1962.

[6]W. R. Dodge and W. C. Barber, *Phys. Rev.* **127**, 174 (1962).

[7]N. W. Tanner *et al.*, *Proceedings of the Rutherford Jubilee International Conference, Manchester, 1961* (ed. by J. B. Birks), Academic Press, New York, 1961.

[8]F. W. K. Firk and K. H. Lokan, *Phys. Rev. Letters* **8**, 321 (1962).

[9]This was pointed out by J. Godemberg of Sao Paulo University, Brazil, who suggested that this measurement be repeated if some method of reducing the background could be included.

[10]L. I. Schiff, *Phys. Rev.* **70**, 87 (1946).

[11]L. Katz and G. B. Chidley, "Nuclear Reactions at Low Energy" [Academy of Sciences, USSR, 1958 (p. 371)]; cited on p. 191 in *Nuclear Reactions*, Vol. II (ed. by T. M. Endt and P. B. Smith), North Holland Publishing Co., Amsterdam, 1962.

[12]N. Hansen, *et al.*, *Bremsstrahlung Production in Thin and Thick Targets*, Lawrence Radiation Laboratory, University of California (unpublished).

1.19. SPECTRA OF BREMSSTRAHLUNG-PRODUCED NEUTRONS EMITTED FROM ^{206}Pb, ^{208}Pb, AND ^{209}Bi AT 90 AND 141°

V. V. Verbinski J. C. Courtney[1]

The spectra of photoneutrons produced in targets of ^{206}Pb, ^{208}Pb, and ^{209}Bi by bremsstrahlung radiation (34-Mev end point) have been measured at angles of 90 and 141° from the bremsstrahlung beam. Experimental accuracies are adequate to obtain level-density information and perhaps to give some insight into the interaction mechanism.

The experimental arrangement is shown in Fig. 1.19.1. Ten-nanosecond bursts of 34-Mev electrons produced by the General Atomic Linear Electron Accelerator (linac) passed through a bending magnet and struck the high-Z target, producing a forward cone (about 5° half width at half maximum[2]) of bremsstrahlung, which accounted for nearly all the neutron production in the target. Neutrons leaving the target at an angle θ passed

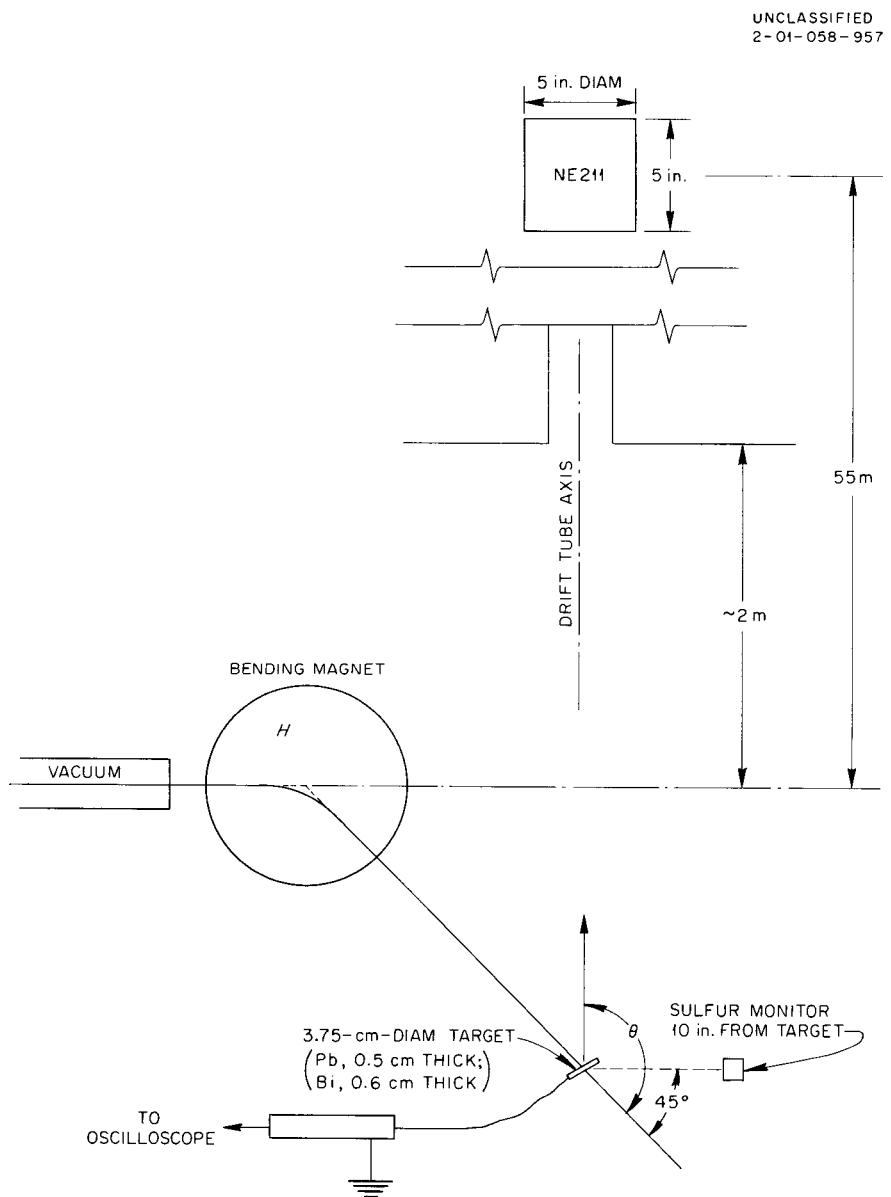

Fig. 1.19.1. Experimental Geometry for Measurements of Photoneutron Spectra.

down a 55-m drift tube to a 5- by 5-in.-diam NE-211 liquid scintillator detector, their energies being determined by time-of-flight techniques. The energy resolution of the final results was limited by statistics because of limited linac availability and not by the combined linac-spectrometer capability. Emergent angles θ of 90 and 141° were used, resulting in a factor of 2.5 variation in $\sin^2 \theta$. A sulfur-pill monitor at 45° to the electron beam facilitated proper normalization of 90 and 141° data.

The scintillator efficiency vs bias setting is known accurately from 0.8 to 11 Mev, and both limits are being extended. The efficiency was determined with a combination of measurements and calculations of the scintillator response to monoenergetic neutrons (see Sect. 6.2) and was tested by repeated time-of-flight spectral measurements of a fixed neutron spectrum with several bias settings (0.6–2.7 Mev). Each setting accurately reproduced both spectral shape and intensity (monitored with sulfur pellets) from about (E_{bias} + 0.2 Mev) to 11 Mev.

The 90 and 141° spectra for a lead target enriched to 88% in ^{208}Pb (doubly magic nucleus) are shown in Fig. 1.19.2. The steepest straight lines represent a fit to a $\phi(E) = KE \exp(-E/T)$ evaporation spectrum in the energy range 1 to 3.5 Mev. The data in Fig. 1.19.2 (as well as in Figs. 1.19.3 and 1.19.4) were plotted as $\ln [\phi(E)/E]$ vs E, whence the slope of any straight-line portion gives the nuclear temperature T directly.

At energies above 3.5 Mev, the portion of data above the solid line fitted to the 1- to 3.5-Mev data has often been interpreted as nonboiloff or direct-emission neutrons, and this component is expected to vary with angle as $a + b \sin^2 \theta$, where a and b are near unity. The fallacy of this interpretation lies in attempting to fit the poor-resolution poor-statistics data in the past with a single nuclear temperature and often with a single constant K at all angles.[3] For ^{208}Pb, the $\ln[\phi(E)/E]$ plots for θ = 90 and 141° each lie along two straight lines, which indicates an abrupt rise in nuclear temperature at 3.5 Mev. This is consistent with

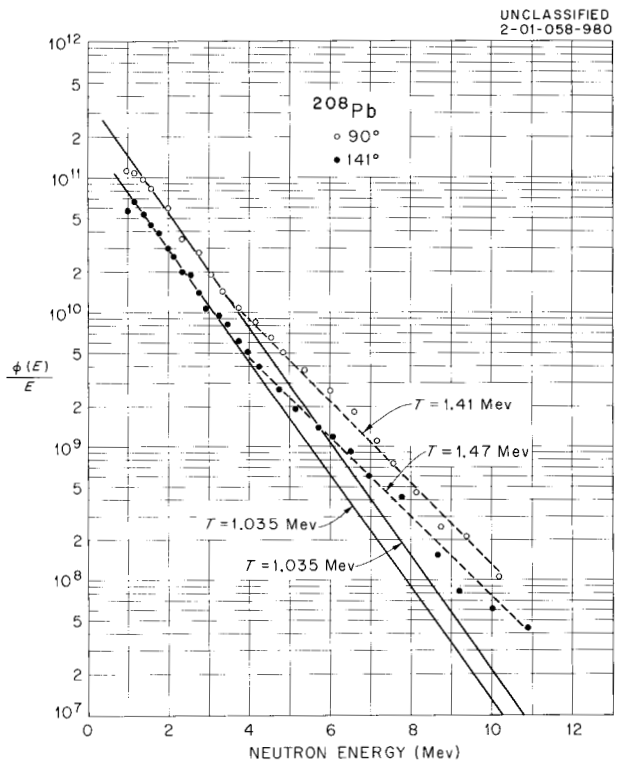

Fig. 1.19.2. Photoneutron Spectra for ^{208}Pb at 90 and 141°. The slopes of the solid lines give the nuclear temperature T in the $\ln [\phi(E)/E]$ plots.

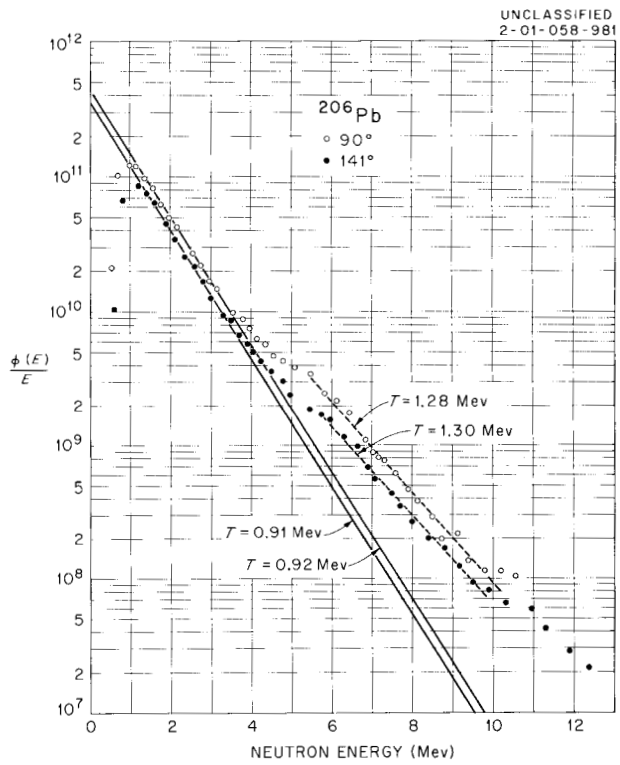

Fig. 1.19.3. Photoneutron Spectra from ^{206}Pb at 90 and 141° Plotted as $\ln [\phi(E)/E]$ vs E.

Table 1.19.1. Values of Nuclear Temperature (T) and the Energy Region (E) over Which T Is Constant

Target	Angle (deg)	T_1(Mev)	E_1(Mev)	T_2(Mev)	E_2(Mev)	T_3(Mev)	E_3(Mev)
^{208}Pb	90	1.035 ± 0.02	1–3.5	1.41 ± 0.03	>3.5		
	141	1.035 ± 0.02	1–3.5	1.47 ± 0.03	>3.5		
^{206}Pb	90	0.92 ± 0.02	1–3.5	High	3.5–5.5	1.28 ± 0.03	>5.5
	141	0.91 ± 0.02	1–3.5	High	3.5–5.5	1.30 ± 0.03	>5.5
^{209}Bi	90	1.01 ± 0.02	1–4	High	4–6	1.41 ± 0.03	>6
	141	0.93 ± 0.02	1–4	High	4–6	1.30 ± 0.03	>6

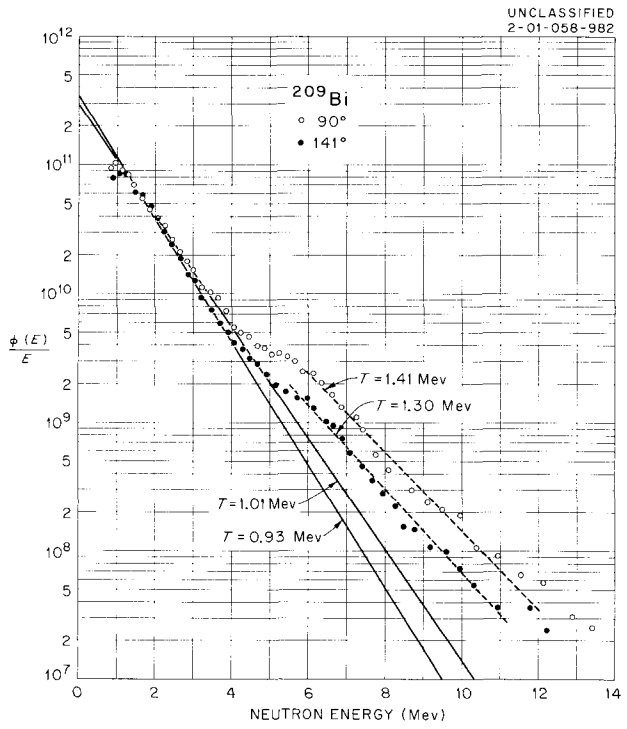

Fig. 1.19.4. Photoneutron Spectra from ^{209}Bi at 90 and 141° Plotted as ln $[\phi(E)/E]$ vs E.

the picture of a lower "available" level density below a few Mev, because in the shell model of independent particles most of the lower levels are occupied.[4] From Fig. 1.19.2 and from Table 1.19.1, where T is given as a function of neutron energy, the 90 and 141° spectra are seen to be practically identical in shape, thus ruling out all direct interactions for ^{208}Pb.

The spectra at 90 and 141° for a lead target enriched to 73% in ^{206}Pb (doubly magic minus two neutrons) (Fig. 1.19.3) are identical up to 3.5 Mev and above 5.5 Mev; from 3.5 to 5.5 Mev, the 90° spectrum displays a larger value of T than the 141° spectrum does, resulting in a relatively higher flux everywhere above 3.5 Mev. Therefore, a slight admixture of direct interactions is in evidence.

For ^{209}Bi (doubly magic plus one proton) the 141° spectrum (Fig. 1.19.4) is very similar to the ^{206}Pb 141° spectrum, but at 90°, T_1 and T_2 are much higher for ^{209}Bi (Table 1.19.1), and more structure appears. Barring serious experimental error, a possibility which is being investigated, the ^{209}Bi photoneutrons may include a significant admixture of direct interactions. As a possible explanation for the direct contribution, the odd proton could increase the coupling of the electromagnetic radiation to the closed-shell neutrons, perhaps in connection with the quasi-deuteron model that is in evidence for low-Z nuclei at higher gamma-ray energies.[5] The difference between ^{208}Pb and ^{209}Bi is not understandable from the shell model approach of Wilkinson,[6] which considers most of the photoexcitation taking place in the closed shell.

The above measurements, although interesting, should be repeated for a greater range of angle and bremsstrahlung energy, with targets substantially thinner than the 0.5-cm-thick ones used, and with efforts to obtain absolute yields, as in the work on low-Z targets (Sect. 1.18).

References

[1]Catholic University, Washington, D.C.; Graduate Fellow, Oak Ridge Institute of Nuclear Studies.

[2]L. I. Schiff, *Phys. Rev.* **70**, 87 (1946).

[3]C. Milone, *Nuovo Cimento Suppl.* **19**, 172 (1961).

[4]J. M. Blatt and V. F. Weisskopf, *Theoretical Nuclear Physics*, Wiley, New York, 1952.

[5]E. Hayward, *Rev. Mod. Phys.* **35**, 324 (1963).

[6]P. H. Wilkinson, *Physica* **22**, 1149A (1956); *Phil. Mag.* **3**, 567 (1958).

1.20. POLARIZATION OF DEUTERONS IN THE $^9Be(p,d)^8Be$ REACTION AT 3 TO 5 Mev

V. V. Verbinski M. S. Bokhari[1]

The polarization of deuterons (P_d) from the $^9Be(p,d)^8Be$ ground-state pickup reaction has been studied both as a function of angle with respect to the protons and as a function of proton energy in an experiment utilizing the double-scattering (or reaction) chamber shown schematically in Fig. 1.20.1. Protons penetrating the ^9Be target were position-monitored by two beam-pickoff electrodes. The reaction deuterons (Q = 0.56 Mev) passed through the collimator slits at an angle θ_1 (variable) and struck a carbon analyzer, where $^{12}C(d,p)^{13}C$ ground-state reactions (Q = 2.7 Mev) produced protons well separated in energy from the scattered deuterons and primary protons. Two surface-barrier diodes located in the plane of the primary reaction and 45° from the deuteron beam measured the left-right asymmetry of the $^{12}C(d,p)^{13}C$ protons.

Each measurement was repeated with the analyzer chamber rotated 180° to correct for detector misalignment. Axial alignment of the initial proton beam was achieved by removing the carbon target and moving the proton beam across the ^9Be target to maximize the count rate of the pinhole-collimated monitor. The two beam-pickoff electrodes were then centered to maintain the alignment during the measurement. Gold-foil scatterers were used to check the accuracy of calculations that were made to correct for the nonuniform irradiation of the analyzer foil, which was caused by the finite slope in $\sigma(\theta)$ from the $^9Be(p,d)^8Be$ reaction. These corrections were approximately 1 to 2%, depending on θ.

The experimental technique was tested by a measurement of the known polarization of carbon elastic scattering[2] with thin (0.4 mg/cm^2) carbon targets and incident proton energies of 5.2 Mev at the first target and 4.7 Mev at the second target. The results agreed within statistical error with the published results[2] and with those calculated from the phase shifts for proton elastic scattering on carbon.

The results for $P_d(E,\theta)$ for the $^9Be(p,d)^8Be$ reaction are shown in Table 1.20.1. The errors

UNCLASSIFIED
2-01-058-955

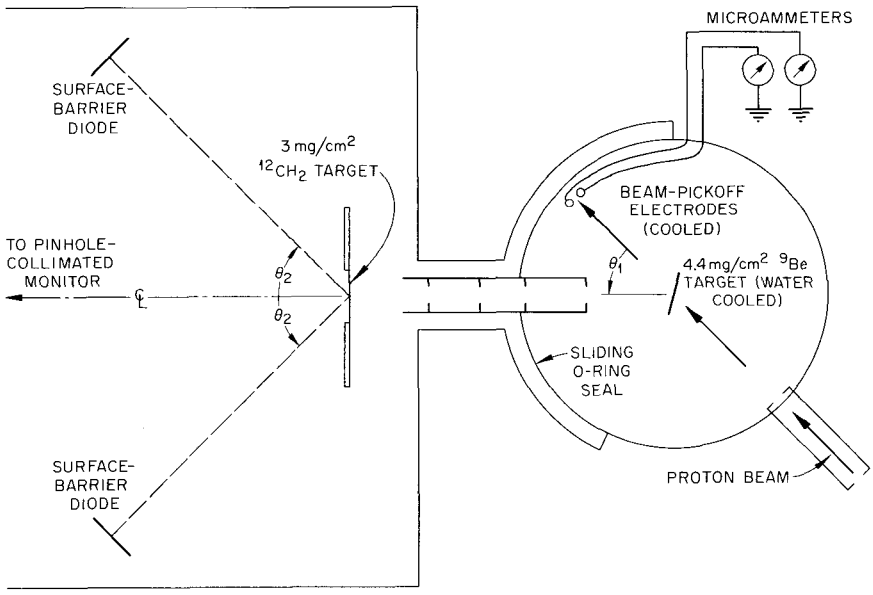

Fig. 1.20.1. Double-Scattering Chamber for Measuring Polarization of Deuterons in the $^9Be(p,d)^8Be$ reaction. The pinhole-collimated monitor is a solid-state detector. The scattering angle θ can be varied without breaking the vacuum. A quartz viewing plate can be remotely inserted in the proton beam near the beryllium target.

Table 1.20.1. Polarization for ^{9}Be(p,d) Pickup Reaction

Angle (deg)	Polarization		
	3 Mev	4 Mev	5 Mev
30	+0.11 ± 0.05[a]		
30	+0.17 ± 0.05		−0.065 ± 0.02
45	+0.18 ± 0.06	+0.06 ± 0.03	−0.045 ± 0.02
60	+0.056 ± 0.03		+0.01 ± 0.025
90	+0.06 ± 0.03[a]		

[a]J. M. Lambert *et al.*, *Phys. Rev.* **124**, 1959 (1961).

represent the statistical uncertainty of the measured left-right asymmetry, combined with the assumed uncertainty of P_p for the polarizability of the carbon analyzer. Two of the 3-Mev values, at 30 and 90°, are those taken from the work of Lambert *et al.*[3] The data of our experiment were analyzed with the assumption of ref. 3 that the left-right asymmetry is $\epsilon = 3P_dP_p$ and P_p was taken to be 0.4 ± 0.10 and to be constant with energy.[4] The sign of polarization, taken according to the convention established at Basel,[4,5] is positive when taken along $\vec{k}_{in} \times \vec{k}_{out}$, where $\vec{k}$ is the propagation vector.

It is interesting to test the results of the experiment against a few of the simpler rules[3,4,6] of polarization with respect to stripping or pickup reactions. For example, one rule states that where $j_n = l + \frac{1}{2}$ and $l = 0$, the maximum polarization for the ^{9}Be(p,d)^{8}Be reaction near the stripping (or pickoff) peak is $\frac{1}{3}$ if spin-orbit interaction is negligible[3,7] (calculations[8] indicate that it is small). No values in Table 1.20.1 are greater than $\frac{1}{3}$, but this is because the interaction model used[7] predicts that $\epsilon = 3\vec{P}_p \cdot \vec{P}_d$. If instead $\epsilon = P_pP_d$, then the polarization at 30 and 45° for 3 Mev would be well over $\frac{1}{3}$. However, this result assumes that changing $\epsilon = 3\vec{P}_p \cdot \vec{P}_d$ to $\epsilon = P_pP_d$ does not affect the prediction of $\frac{1}{3}$ as an upper limit.

A second rule of polarization – one that has been altered[8,9] from its original form[10] due to some early experimental evidence[11] – predicts the sign of polarization (near the stripping peak) in stripping and pickup reactions if the deuteron waves interact with the nucleus (that is, if they are distorted). Other experimental results[12,13] are in agreement with this prediction. For the ^{9}Be(p,d)^{8}Be pickup reaction, the sign should be positive.[3] However, the data of Table 1.20.1 show a variation in sign with proton energy (as well as reaction angle), so that at 5 Mev, where the sign becomes negative, one may conclude that either proton wave distortion is also important, and becomes greater than for deuterons, or that another rule is placed in doubt. Both above-cited rules assume negligible spin-orbit interaction, an assumption that may not be valid.

From the words of Goldfarb,[4] ". . . there is a multiplicity of rules, and what we need now are the exceptions to these rules," and from the present work it is evident that in polarization measurements large ranges of energy and angle should be covered to give significant meaning to survey-type measurements.

Thanks are due to G. R. Satchler (Physics Division) for suggesting the extension of our earlier 5-Mev measurements to other angles and energies. In this sense, the ^{9}Be(p,d)^{8}Be measurements are far from complete.

References

[1]Affiliated with Pakistan Atomic Energy Commission; formerly a visiting scientist at ORNL.

[2]R. E. Warner and W. P. Alford, *Phys. Rev.* **114**, 1338 (1959); *1960 Nuclear Data Tables*, Part 3 (ed. by J. B. Marion), GPO, Washington, D.C.

[3]J. M. Lambert *et al.*, *Phys. Rev.* **124**, 1959 (1961).

[4]L. B. J. Goldfarb, p. 479 in *Proceedings of the Rutherford Jubilee International Conference, Manchester, 1961* (ed. by J. B. Birks), Haywood, London.

[5]*Helvitica Physica Acta, Supplementum VI,* 1960 (Proceedings of the International Symposium on Phenomena of Nucleons).

[6]G. R. Satchler, *Nucl. Phys.* **6**, 543 (1958).

[7]G. L. Vysatskii and A. G. Sitenko, *Zh, Eksperim. i. Teor. Fiz.* **36**, 812 (1959).

[8]H. C. Newns and M. Y. Refai, *Proc Phys. Soc. (London)* **71**, 627 (1958).

[9]W. Tobocman, *Phys. Rev.* **115**, 98 (1959).

[10]H. C. Newns, *Proc. Phys. Soc. (London)* **A66**, 477 (1953).

[11]P. Hillman, *Phys. Rev.* **104**, 176 (1956).

[12]A. Juveland and W. Jentschke, *Phys. Rev.* **110**, 456 (1958).

[13]M. S. Bokhari *et al., Proc. Phys. Soc. (London)* **72**, 88 (1958).

1.21. MEASUREMENTS OF THE VARIATION OF THE RATIO OF THE CAPTURE AND FISSION CROSS SECTIONS OF ^{235}U

L. W. Weston R. Gwin
G. de Saussure J. E. Russell[1]
R. W. Hockenbury[1]

The analyses of the measurements of the ratio of the capture and fission cross sections (α) of ^{235}U for the neutron energy ranges from 3.25 ev to 1.8 kev and from 12 to 690 kev have been completed, and the results have been reported in detail elsewhere.[2,3]

As was reported previously,[4] the technique used for the lower energy range consisted in directing pulsed neutrons at a multiplate ^{235}U fission chamber placed in the center of a large liquid scintillator. Gamma rays from both capture events and fission events in the ^{235}U of the fission chamber were detected with high efficiency by the scintillator, while fission alone was detected by the fission chamber. The value of α was then the ratio of the scintillator counts in anticoincidence with the fission chamber counts to those in coincidence with the fission chamber counts. The incident neutrons were produced in a target bombarded by electron bursts from the Rensselaer Polytechnic Institute linear accelerator, and their energies were measured by time-of-flight methods.

The same technique was used for measurements at 30 and 64 kev except that the source neutrons were produced by protons from the ORNL Van de Graaff accelerator incident on ^{7}Li and tritium targets respectively.[5] Other measurements at the Van de Graaff in the 12- to 690-kev range also used the $^{7}Li(p,n)$ reaction, but the fission chamber was replaced with a ^{235}U sample and the liquid scintillator was loaded with gadolinium. In this case a capture event in the sample was characterized by a scintillator pulse due to a single fast cascade of gamma rays in coincidence with the beam pulse, while a fission event was characterized by a pulse due to prompt-fission gamma rays followed a few microseconds later by additional pulses due to gamma rays produced by the capture of thermalized fission neutrons in the gadolinium-loaded solution.

The values of α obtained for energies above 12 kev can be approximately described by a linear decrease from 0.374 at 12 kev to 0.177 at 310 kev followed by a less rapid linear decrease to 0.095 at 690 kev. For the energy range from 3.25 ev to 1.8 kev, large fluctuations in the data were observed, the value of α for many energies being greater than 1. The ORNL values are compared with those of other investigations in Fig. 1.21.1.

The α experiments are to be continued at the RPI linear accelerator by a method which will also utilize a pulsed beam of neutrons striking a sample positioned at the center of a large liquid scintillator, but fission and capture events will be distinguished by the difference in the pulse-height distributions of the fission gamma rays and capture gamma rays. The feasibility of the method was demonstrated by a preliminary run at General Atomic for ^{235}U in the energy range from 10 to 20 ev.[6] In preparation for these measurements, which hopefully will cover all three of the fissionable isotopes in the energy range from thermal to 20 kev, a time-of-flight (or multidimensional) analyzer is being assembled that uses a general-purpose digital computer as an integral part of its system. The analyzer will not only increase the accuracy of the measurement but will also reduce the total linac time required.

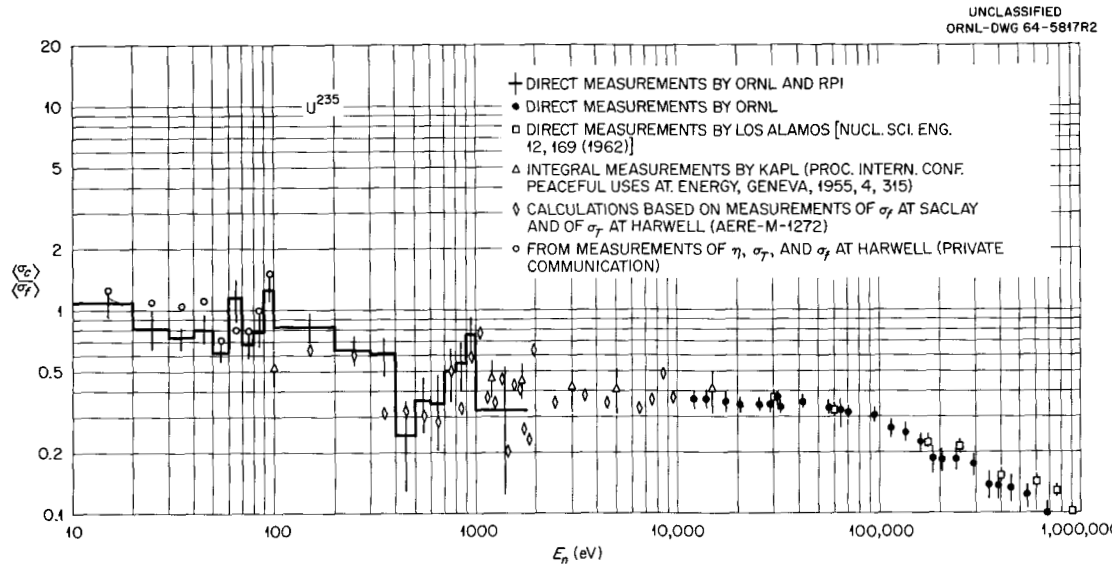

Fig. 1.21.1. Ratio of the Average Value of the ^{235}U Neutron-Capture Cross Section to the Average Value of the Fission Cross Section as a Function of Neutron Energy. The vertical lines are error bars for the energy intervals in which they appear.

References

[1]Rensselaer Polytechnic Institute.

[2]G. de Saussure *et al.*, *Measurement of α, the Ratio of the Neutron Capture Cross Section to the Fission Cross Section, for ^{235}U in the Energy Region from 3.25 eV to 1.8 keV*, ORNL-3738 (in press).

[3]L. W. Weston, G. de Saussure, and R. Gwin, *Nucl. Sci. Eng.* **20**, 80–87 (1964).

[4]G. de Saussure *et al.*, *Neutron Phys. Div. Ann. Progr. Rept. Aug. 1, 1963*, ORNL-3499, Vol. I, p. 3.

[5]L. W. Weston, G. de Saussure, and R. Gwin, ORNL-3499, Vol. I, *op. cit.*, p. 11.

[6]R. Gwin *et al.*, ORNL-3499, Vol. I, *op. cit.*, p. 15.

1.22. MEASUREMENT OF THE SLOW NEUTRON FISSION CROSS SECTION OF ^{239}Pu[1]

G. de Saussure C. Jousseaume[2]
J. Blons[2] A. Michaudon[2]
Y. Pranal[2]

The interaction of slow neutrons (E < 10 kev) and fissile nuclei is of interest for reactor calculations and for the information it provides on the excited levels of heavy nuclei and on the fission process. The isotope ^{239}Pu is especially interesting because the small value of its spin, $I = \frac{1}{2}$, causes the resonances to be farther apart and larger than in other fissile nuclei and hence facilitates their analysis. In addition the determination of the resonance spin state is made easier.[3]

The cross sections of ^{239}Pu, however, have not been investigated to much extent, and at present the resonance parameters are known only up to 50 ev.[4] Therefore it seemed desirable to take advantage of recent improvements in energy resolution and intensity of neutron spectrometers to remeasure the neutron fission cross section of ^{239}Pu by the time-of-flight technique.[5] This paper reports a measurement which was made at the Saclay linac[6] for neutron energies between 0.16 ev and 5 kev.

The linac was used to obtain a source of pulsed neutrons which impinged on a ^{239}Pu sample contained within a gaseous scintillator. The fission rate in the sample was determined from pulses from the scintillator, and the energy spectrum of the incident neutrons was determined with a BF_3 detector whose efficiency is proportional to $E^{-1/2}$. Backgrounds were obtained by placing screens with black resonances in the neutron beam. The quantity $\sigma_f\sqrt{E}$ was proportional to the

ratio of the fission count rate to the BF_3 detector count rate and was normalized at the 7.8-ev resonance whose parameters are known.[4]

The gaseous scintillator was similar to one described by Nifenecker *et al.*[7] The variations of the amplitude of fission pulses and of the alpha pile-up rate with the position of the plutonium samples in the scintillator and the pressure and composition of the scintillation gas were investigated with a spontaneous fission source. Best results were obtained with pure xenon at 200 mg/cm^2 pressure. With a 310-mg ^{239}Pu sample (plated at 1.2 mg/cm^2), the activity was $\sim 10^9$ alphas per second. With a bias allowing one alpha pileup per second, the efficiency for fissions was 65%.

Several runs were made to obtain the fission cross section over various energy ranges with appropriate resolution. Under the best conditions at high energy the resolution was 3 nsec/m. Table 1.22.1 summarizes the experimental conditions for two of the runs, and Fig. 1.22.1 shows the resulting fission cross-section curve for neutron energies from 100 to $\sim$220 ev. In the low-energy range, 22,000 counts per 0.4-μsec channel were obtained at the peak of the 11-ev resonance; in the high-energy range 6500 counts per 0.05-μsec channel were obtained at the peak of the 75-ev resonance.

Figure 1.22.2 shows the number of resonances observed up to energy E as a function of E up to 200 ev. The resonance parameters are being analyzed and will be published later.

References

[1]Submitted for a reading by the French Academy of Sciences.

[2]Centre d'Etudes Nucléaires de Saclay, France.

[3]J. S. Fraser and R. Schwartz, *Nucl. Phys.* **30**, 269 (1962).

[4]D. J. Hughes, B. A. Magurno, and M. K. Brussel, *Neutron Cross Sections, Supplement 1*, 2d ed. (Jan. 1, 1960); L. M. Bollinger, *Proc. U.N. Intern. Conf. Peaceful Uses Atomic Energy, 2nd, Geneva, 1958* **15**, 127 (1958); K. G. Ignat'ev, I. V. Kirpichnikov, and S. I. Sukhoruchkin, *Measurement of η in Partial Cross Sections of the Isotopes U^{235} and Pu^{239} for Resonance Neutrons* [translated by Lydia Venters, AEC-tr 5917 (1963)].

[5]J. Spaepen (ed.), *Proceedings of the Symposium on Neutron Time-of-Flight Methods, Saclay, France, 1961*, Euratom, Brussels, 1962.

[6]P. Ribon *et al.*, *op. cit.*, p. 97; R. Bergere, *op. cit.*, p. 329.

[7]H. Nifenecker *et al.*, *op. cit.*, p. 413.

Table 1.22.1. Experimental Conditions for Fission Cross-Section Measurements

	Low-Energy Range (0.16–100 ev)	High-Energy Range (11 ev–5 kev)[a]
Linac	500 pulses/sec of 100-nsec width	500 pulses/sec of 100-nsec width
Time analysis with variable channel width[b]	Channel width varying between 50 and 1600 nsec	Channel width set between 50 and 400 nsec
Flight path	10.80 m	19 m (perpendicular to the moderator)
Duration of run	34 hr	140 hr
Experimental resolution	1.2 μsec/m at 0.16 ev; 46 nsec/m at 100 ev	35 nsec/m at 12 ev; 11 nsec/m at 100 ev; 6 nsec/m at 5 kev

[a]A 50-hr run was made with the same settings except that the linac pulse width was 20 nsec, giving a 3-nsec/m resolution at 5 kev.

[b]J. Thenard *et al.*, *Nucl. Instr. Methods* **26**, 45–50 (1964).

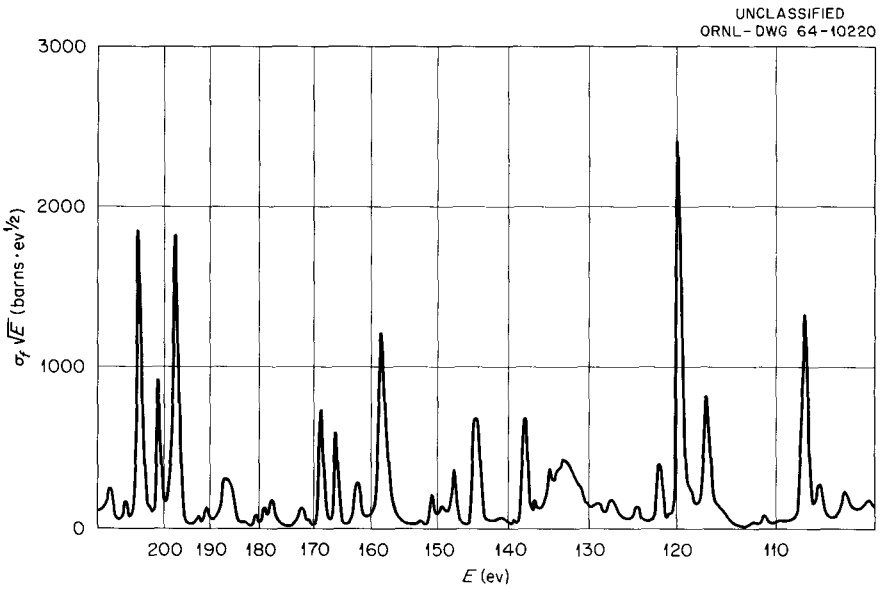

Fig. 1.22.1. ^{239}Pu Fission Cross Section for Neutron Energies from 100 to ~220 ev.

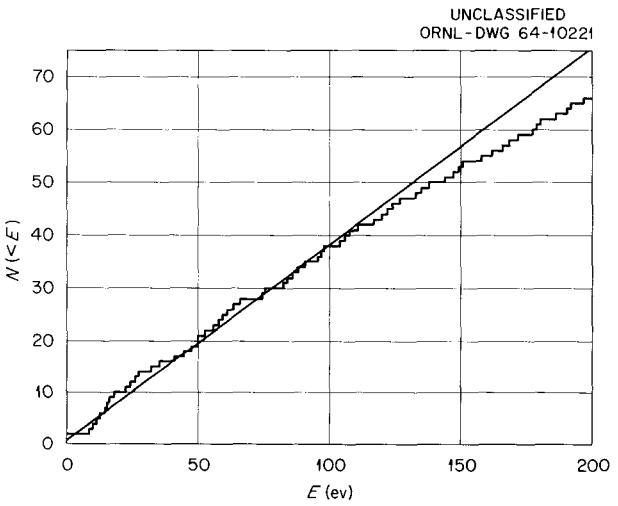

Fig. 1.22.2. Number of ^{239}Pu Resonances Observed Up to Neutron Energy E as a Function of E.

1.23. STATUS OF PULSED-NEUTRON MEASUREMENTS OF THE TEMPERATURE DEPENDENCE OF NEUTRON DIFFUSION PARAMETERS FOR LIGHT-WATER ICE

E. G. Silver

The collection of data in the experiment to determine the temperature dependence of the neutron-diffusion parameters for light-water ice has been concluded except for remeasurements of some experimental points if shown by analysis to be needed. The program of analysis outlined in the previous annual report[1] has also been completed. The decay data were analyzed with a model which assumed two exponentials and which was of the form

$$C_n = A(\Delta t) + B(\Delta t)e^{-n(\Delta t)\lambda} + C(\Delta t)e^{-2n(\Delta t)\lambda} ,$$

where C_n is the number of counts in the nth decay channel, A is the background counting rate, and B and C are the initial counting rates due to each exponential component.

The analysis was performed for each set of decay data over five subsets of the available 18 channels, namely, channels 1–18, 1–15, 2–16, 3–17, and 4–18. Table 1.23.1 shows some representative results for both large and small cylinders. For the smallest cylinders the model is apparently not a sufficiently good fit, and other methods are being sought for extracting the asymptotic value of the decay constant. However, for medium and large cylinders the results appear to be quite acceptable. The temperature seems to have little effect, for any given buckling, on the suitability of the analysis described above.

Table 1.23.1. Neutron Decay Constants for Various Light-Water Ice Cylinders

Cylinder Dimensions			Decay Constant (kc/sec)				
Height (cm)	Diameter (cm)	Temperature (°C)	Channels 1–18	Channels 1–15	Channels 2–16	Channels 3–17	Channels 4–18
25.30	20.07	−45	6.45 ± 0.02	6.43 ± 0.03	6.41 ± 0.03	6.45 ± 0.04	6.49 ± 0.05
		−85	6.08 ± 0.02	6.08 ± 0.03	6.05 ± 0.04	6.13 ± 0.04	6.10 ± 0.05
16.05	14.65	−5	8.74 ± 0.02	8.74 ± 0.03	8.73 ± 0.04	8.78 ± 0.04	8.70 ± 0.06
		−85	7.56 ± 0.03	7.53 ± 0.03	7.54 ± 0.03	7.64 ± 0.03	7.61 ± 0.04
9.07	8.38	−5	16.58 ± 0.05	16.64 ± 0.06	16.54 ± 0.07	16.50 ± 0.09	16.43 ± 0.12
		−85	13.31 ± 0.04	13.32 ± 0.05	13.24 ± 0.06	13.32 ± 0.07	13.32 ± 0.08
7.18	5.72	−5	24.97 ± 0.06	25.46 ± 0.07	24.76 ± 0.09	23.87 ± 0.13	22.73 ± 0.17
		−85	20.15 ± 0.04	20.24 ± 0.05	20.04 ± 0.06	19.89 ± 0.08	19.70 ± 0.10

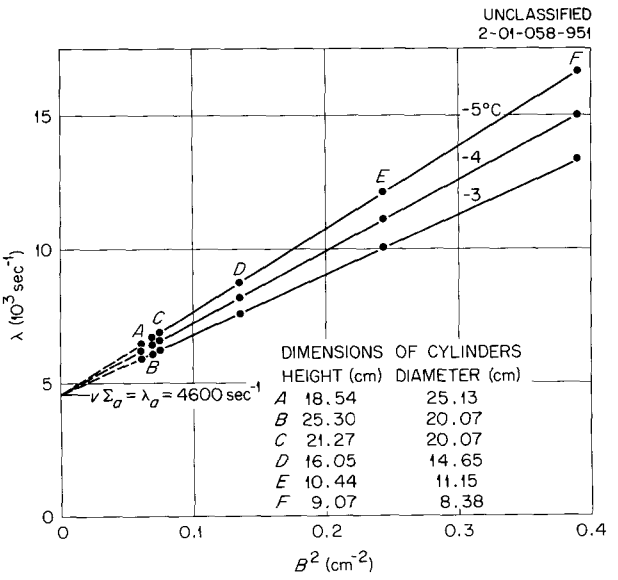

Fig. 1.23.1. Decay Constant, λ, as a Function of Buckling for Ice Cylinders at Three Different Temperatures.

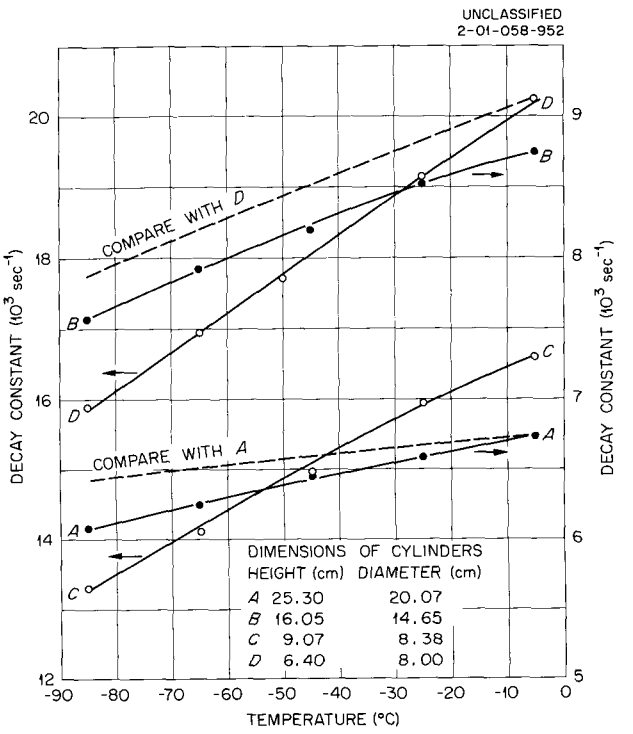

Fig. 1.23.2. Decay Constant, λ, as a Function of Temperature for Four Ice Cylinders. The slope expected, assuming the transport mean free path to be constant, is shown for two of the cylinders.

Figure 1.23.1 shows the results for the decay constant λ as a function of B^2 for three temperatures, using only the larger and medium-sized cylinders. In this domain the effect of diffusion cooling is negligible, as may be seen from the fact that a straight line fits the experimental data extremely well. The data for the smallest cylinders are not yet analyzed well enough to indicate whether they will enable a determination of the diffusion cooling coefficient C.

Figure 1.23.2 shows preliminary results of the value of the decay constant for four cylinders as a function of temperature. For two cases the curve expected for the transport mean free path λ_{tr} (assuming a constant diffusion cooling coefficient and an absorption cross section varying

as 1/v) is also shown, fitted to the observed value at –5°C. It is apparent that in each case, both for a very large cylinder and a very small one, the decay constant drops more rapidly with temperature than would be the case if λ_{tr} were constant with temperature. This implies that λ_{tr} decreases with decreasing temperature. The preliminary value for the change over the maximum range observed is $\lambda_{tr}(-5°C)/\lambda_{tr}(-85°C) = 1.22$. This value is approximately independent of the buckling of the cylinder in which it is measured, as would be expected if a true change in λ_{tr} is observed.

The effect of the refrigerator walls on the observed decay was also carefully measured by observing the decay constant at room temperature of both a cadmium-clad plastic cylinder inside the boral-lined refrigerator and a bare plastic cylinder outside the refrigerator in a low back-scattering location. The effect of the refrigerator was proved to be completely negligible, as shown in Fig. 1.23.3, which gives the decay data as well as the difference curves for both measurements.

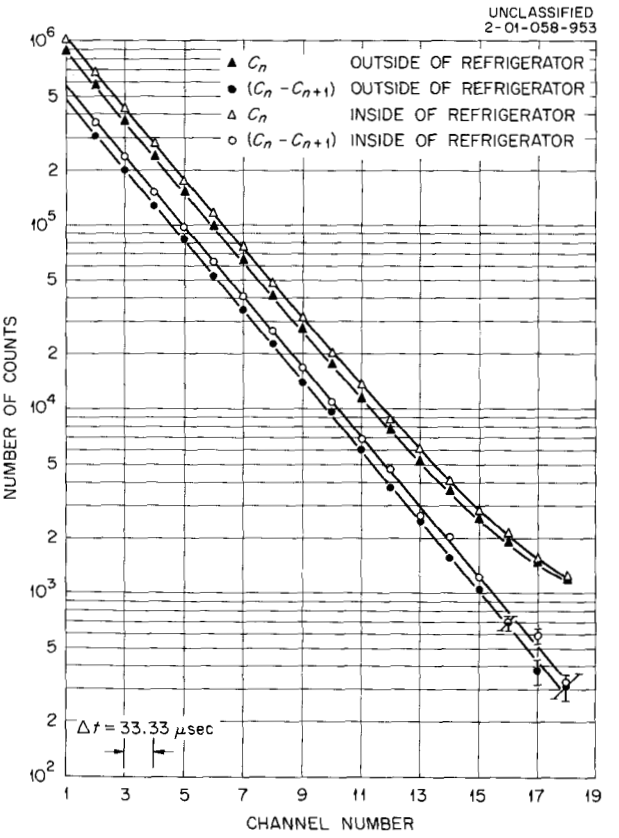

Fig. 1.23.3. Comparison of Decay in a Cadmium-Clad Teflon Cylinder in Boral-Lined Refrigerator (20°C) with Decay in Bare Teflon Cylinder Outside Refrigerator.

References

[1]E. G. Silver, *Neutron Phys. Div. Ann. Progr. Rept. Aug. 1, 1963*, ORNL-3499, Vol. I, p. 33.

2. Critical Experiments

2.1. CRITICAL THREE-DIMENSIONAL ARRAYS OF NEUTRON-INTERACTING UNITS. PART II. U(93.2) METAL[1]

J. T. Thomas

A series of critical experiments with uranium metal cylinders, enriched to 93.2% in ^{235}U and arranged in three-dimensional arrays, was a part of a continuing program in support of criticality safety in the handling of accumulations of individually subcritical units of fissile materials. Four weight groups of units, ranging from 10.5 to 26.2 kg of uranium in five sizes, were employed, and the critical surface separation between units was determined as a function of the number of units in an array. In addition, the critical uranium density (the ratio of the mass of a unit to the volume of the lattice cell it occupies in a critical array) was observed to depend upon a number of factors. Changes in the k_{eff} of the individual units, caused by alteration of their shape, produced inverse changes in the critical density, provided that the array shape was unchanged. The critical density of the array varied with its shape in a manner similar to that resulting from corresponding changes in a single critical unit. Addition of a hydrogenous reflector reduced the critical density of the array by factors much greater than those observed for similar reflection of a single critical unit. In studies of the effect of a hydrogenous moderator between units, the density was found to be minimal when the thickness of this moderator was 4.9 cm. The separate effects of moderation and reflection of arrays are not additive. In several experiments it was observed that an array comprised of half of each of two different critical arrays was subcritical.

References

[1]Abstract of ORNL-TM-868 (June 1964).

2.2. CRITICAL DIMENSIONS OF AQUEOUS UO_2F_2 SOLUTIONS CONTAINING 4.9% ^{235}U-ENRICHED URANIUM

E. B. Johnson D. F. Cronin[1]

The critical dimensions of aqueous solutions of $U(4.9)O_2F_2$ have been measured as a part of an ORNL program to provide data useful in authenticating nuclear reactor calculations and in establishing specifications for chemical processes and for transport and storage of fissile materials. Many earlier results from this program have been published previously.[2]

The high solubility of uranyl fluoride (~890 g of uranium per liter) allowed experiments with solutions having an $H/^{235}U$ atomic ratio as low as 500, approximately that for minimum critical mass and near that for minimum critical volume at this enrichment. The solution was contained in spherical or cylindrical aluminum or stainless steel vessels. The critical dimensions of a number of single units, both unreflected and surrounded by an effectively infinite water reflector, are summarized in Table 2.2.1. Some of these data have been published.[3]

In another series of experiments, as many as 25 cylinders of solution 24.1 cm in diameter were arranged in planar arrays, with the individual units in a square lattice. The number of units in a critical array as a function of the separation of their axes is shown in Fig. 2.2.1. The arrays were

located sufficiently far from massive structural members to be considered unreflected, and contained no moderator except the solvent itself. The results may be compared with those from similar experiments with a solution of highly enriched uranium.[4]

From the results of these experiments it is possible to establish some limiting dimensions useful in process designs. The following configurations of aqueous solutions at concentrations of 900 g of U(4.9) per liter and less will be subcritical: a water-reflected cylinder 30.5 cm in

Table 2.2.1. Critical Dimensions of $U(4.9)O_2F_2$[a] Aqueous Solutions in Single Units

Solution Concentration		Container	Cylindrical Critical Dimensions			
$H/^{235}U$	g of U per liter	(0.16-cm-thick wall)	Diameter (cm)	Height (cm)	Volume (liters)	^{235}U Mass (kg)
		Water-Reflected Units				
495	890	Aluminum	38.1	41.7	47.6	2.11
		Aluminum	33.0	72.4	62.1	2.75
		Aluminum	31.1	139.6	106.0	4.70
		Aluminum	30.7	173.2	128.1	5.67
524	870	Stainless steel	50.8	29.3	59.4	2.53
		Aluminum	38.1	44.8	51.1	2.17
		Stainless steel	38.1	50.4	57.4	2.44
		Stainless steel	30.5	>153	>111	>4.73
643	728	Aluminum	76.2	23.9	109.2	3.89
		Stainless steel	50.8	34.7	70.3	2.50
		Stainless steel	38.1	75.5	86.1	3.06
735	650	Aluminum	76.2	24.2	110.4	3.50
		Stainless steel	50.8	40.1	81.1	2.58
		Stainless steel	38.1	153.0	174.4	5.54
994	496	Aluminum	76.2	37.9	173.1	4.20
		Stainless steel	50.8	85.7	173.7	4.21
1099	452	Aluminum[b]	69.3		170.5	3.77
		Unreflected Units				
524	870	Stainless steel	50.8	38.7	78.3	3.33
		Stainless steel	38.1	>147	>168	>7.13
643	728	Aluminum	76.2	28.9	132	4.69
		Stainless steel	50.8	45.7	92.6	3.30
		Stainless steel	38.1	>166	>189	>6.73
735	650	Aluminum	76.2	31.5	144	4.58
		Stainless steel	50.8	54.3	110	3.50
994	496	Aluminum	76.1	44.8	204	4.96
		Stainless steel	50.8	>140	>283	>6.84
1002	492	Aluminum[c]	69.3		172.0	4.14

[a]U(4.9) designates uranium enriched to 4.9 wt % in ^{235}U.

[b]This was a spherical container 98% filled when critical.

[c]This was a spherical container 99% filled when critical.

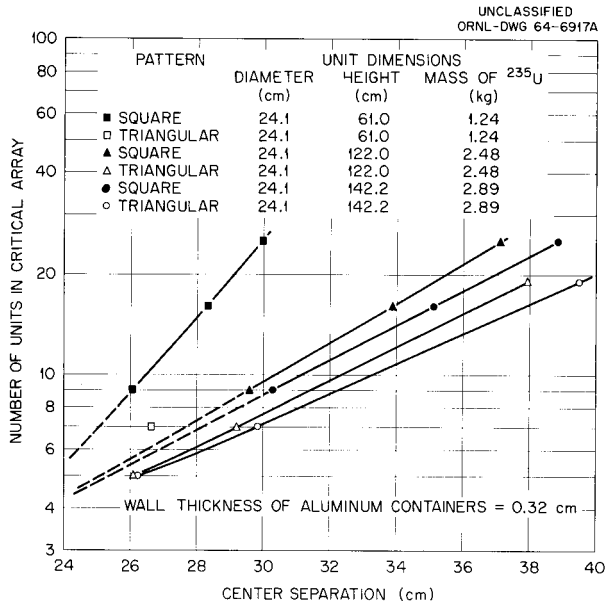

Fig. 2.2.1. Critical Planar Arrays of Cylindrical Units of $U(4.9)O_2F_2$ Aqueous Solution at an $H/^{235}U$ of 493.

diameter, provided that its height-to-diameter ratio (h/d) is less than 7; an unreflected cylinder 38 cm in diameter, provided that h/d is less than 5; three 24.1-cm-diam cylinders, 142.5 cm high and separated by 25 cm between centers in a planar array, triangular pattern, reflected by water on one face; a linear array of nine 24.1-cm-diam cylinders 61 cm high, spaced 25 cm on centers, and reflected on one side by water; and four of these cylinders in a planar array, square pattern, unreflected and separated by 25 cm.

References

[1]Present address: United Nuclear Corporation, New Haven, Conn.

[2]H. C. Paxton *et al.*, *Critical Dimensions of Systems Containing U^{235}, Pu^{239}, and U^{233}*, TID-7028 (June 1964).

[3]D. F. Cronin, *Critical Mass Studies. Part X, Uranium of Intermediate Enrichment*, ORNL-2968 (Sept. 20, 1960) (Classified).

[4]L. W. Gilley and J. T. Thomas, *Trans. Am. Nucl. Soc.* **4**, 54 (June 1961).

2.3. GEOMETRICALLY COMPLICATED CRITICAL ASSEMBLIES OF 93.2% ^{235}U-ENRICHED URANIUM METAL

J. T. Mihalczo

The capability of the 05R code (see Sect. 5.2) for handling complicated geometries exactly has been tested in a series of calculations of unmoderated and unreflected critical assemblies of 93.2 wt % ^{235}U-enriched uranium metal ($\rho = 18.69$ g/cc). The upper section of each assembly was built on a 30-in.-diam stainless steel diaphragm, and the lower section was supported by a low-mass frame that could be raised remotely.

The first three assemblies consisted of a cylindrical annulus encircling a right circular cylinder, a parallelepiped, or two parallelepipeds as shown in Table 2.3.1. In a fourth assembly, pictured in Fig. 2.3.1, the eight upper units of various geometries were slightly tilted toward the vertical axis and criticality was achieved by allowing the center piece shown in the inset to penetrate the hole in the support diaphragm.

The neutron cross sections used in the calculations are those given in BNL-325,[1] with an energy variation of $\nu^{235}(E \text{ Mev}) = 2.423 + 0.088E + 0.0088E^2$ (ref. 2). The angular distributions for elastic scattering were taken from Smith's work[3] for energies below 1.5 Mev and from BNL-400[4] for higher energies. The total inelastic cross sections were those of Smith's[5] below 1.5 Mev, those of Howerton's[6] from 1.5 to 9.0 Mev, and those obtained from optical model calculations[7] of direct neutron interactions above 9.0 Mev. The angular distribution of neutrons inelastically scattered from the low-energy levels which contribute at high energies to the measurement of $\sigma_{el}(\theta)$ was assumed to be the same as that for elastic scattering. Inelastic scattering was treated by evaporation theory except where level excitation cross sections were available. For ^{238}U the level excitation cross sections were those measured by Smith up to 1.5 Mev; for ^{235}U they were those calculated by Parker[8] and modified slightly by optical-model results.

Although the calculated multiplication constants are 1.4 to 2.1% larger than those measured, they are well within the error introduced by the ±5% uncertainty in σ_f^{235} in the Mev range (for these assemblies $\Delta\sigma_f^{235}/\Delta k = 0.8$).

Table 2.3.1. Critical Masses and Calculated Multiplication Constants[a] of 93.2 wt % ^{235}U-Enriched Uranium Metal

Assembly					
Upper Section	Lower Section	Height (in.)	Critical Mass (kg of U)	Calculated Multiplication Constant[b]	CDC-1604 Calculational Time (min)
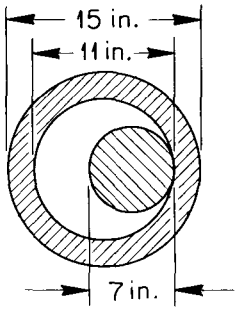	Same as upper section	3.98	147.6	1.021	65
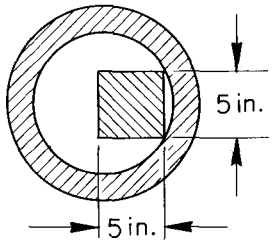	Same as upper section	5.11	166.8	1.014	64
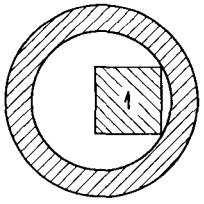	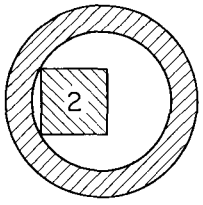	6.37, annulus 3.00, No. 1 4.40, No. 2	215.4	1.020	64
Eight-unit ring and center piece (see Fig. 2.3.1)			206.5	1.017	82

[a]A similar calculation for Godiva I required 58 min and yielded a multiplication constant of 1.015; Godiva I is described by G. E. Hansen, "Physics of Fast and Intermediate Reactors," p. 453 in *Proceedings of a Seminar*, Vol. I, International Atomic Energy Agency, Vienna, 1962.

[b]Number of histories, 20,000; standard deviation, ±0.007.

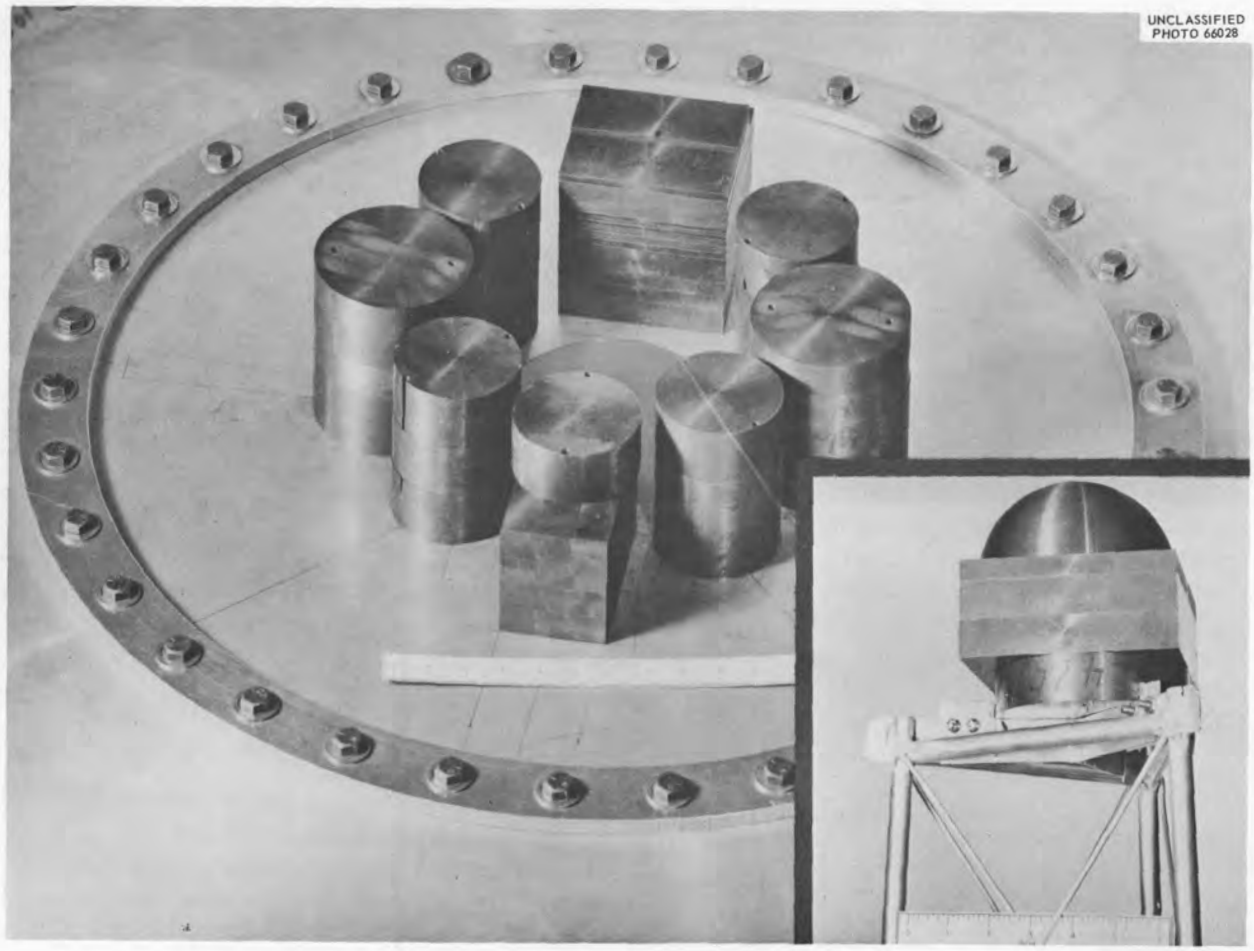

Fig. 2.3.1. Critical 93.2% ^{235}U-Enriched Uranium Metal Assembly with Eight-Unit Upper Section and an Irregularly Shaped Center Piece (Inset). The unit at the top of the photograph is an approximate parallelepiped whose base is 5 by 5 in. and whose height varies in three steps (5.14, 5.27, and 4.39 in., front to back); the opposite unit is a parallelepiped with a 3- by 5-in. base and a 3.51-in. height topped by a 3.60-in.-diam by 1.70-in.-high cylinder; the four small cylinders are 3.59 in. in diameter and 5.11 in. high; and the two large cylinders are 4.5 in. in diameter and 5.3 in. high. The center piece consists of a 4.5-in.-diam by 1.11-in.-high cylinder topped by a parallelepiped with a 5.00- by 5.00-in. base and a 2.25-in. height and by a hemisphere with a 2.39-in. radius.

References

[1]D. J. Hughes and R. B. Schwartz, *Neutron Cross Sections*, 2d ed., BNL-325 (July 1958) and D. J. Hughes, A. Magurno, and M. K. Brussel, *Supplement 1* (January 1960).

[2]D. S. Mather, P. Fieldhouse, and A. Moat, *Phys. Rev.* **113**, B1403 (1964).

[3]A. B. Smith, *Nucl. Sci. Eng.* **18**, 126 (1964).

[4]M. D. Goldberg, V. M. May, and J. R. Stehn, *Angular Distributions in Neutron-Induced Reactions*, BNL-400, 2d ed., Vol. 2 (February 1963).

[5]A. B. Smith, "The Scattering of Fast Neutrons from Natural Uranium," *Nucl. Phys.* (in press).

[6]R. J. Howerton, *Semiempirical Neutron Cross Sections*, Part III, Vol. 1, UCRL-5351 (November 1958).

[7]B. Baldoni and A. M. Sarius, "A Rotational-Optical Model Analysis of Fast Neutron Scattering by U^{238} Nucleus," *Nuovo Cimento* (in press); F. Perey, private communication.

[8]K. Parker, *Neutron Cross Sections of U^{235} and U^{238} in the Energy Range 1 KeV–15 MeV*, AWRE Report 0/82/63.

2.4. CRITICAL EXPERIMENTS AND CALCULATIONS WITH REFLECTED ANNULAR CYLINDERS OF U(93.2) METAL

J. T. Mihalczo

The previously reported[1] work with annular cylinders of uranium metal enriched to 93.2% (ρ = 18.76 g/cc) has been extended to include studies of the effect of graphite (ρ = 1.7 g/cc) and polyethylene (ρ = 0.92 g/cc) reflectors. Annuli with outside diameters as large as 15 in. and inside diameters as small as 7 in. were assembled to delayed critical with all external surfaces uniformly reflected by graphite having a maximum thickness of 10 in. or by polyethylene at least $5\frac{3}{4}$ in. thick. In some instances the central cavity was filled with the reflector material. Some typical results are shown in Figs. 2.4.1 and 2.4.2.

Multiplication constants, k_{eff}, of one annulus were calculated by multigroup transport theory using the S_N method[2] in the S_8 approximation, the TDC computer code,[3] and the 16-group cross sections of Hansen and Roach[4] for the ^{235}U and ^{238}U isotopes. Fission of ^{234}U and of ^{236}U was included, and the absorption and scattering properties of these isotopes were assumed to be the same as those of ^{238}U. The value of k_{eff} for a 7-in.-ID by 11-in.-OD critical annulus having a graphite core and a 7-in.-thick graphite reflector was calculated to be 0.9989; the value for the reflected annulus with the graphite removed from the center was 0.9975.

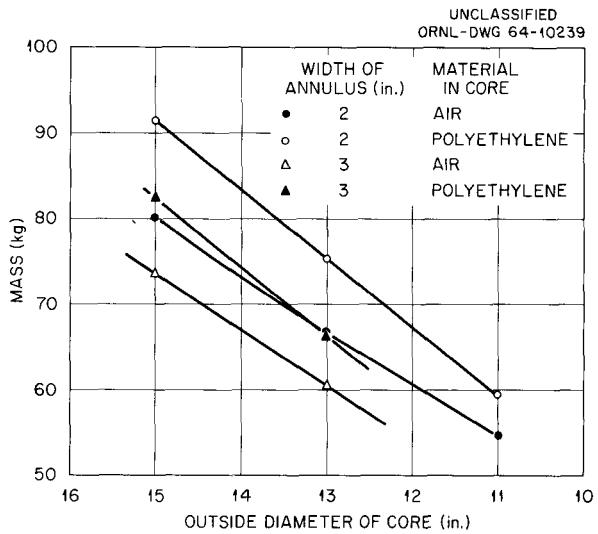

Fig. 2.4.2. Critical Mass of Cylindrical Annuli of U(93.2) Metal Reflected by Polyethylene.

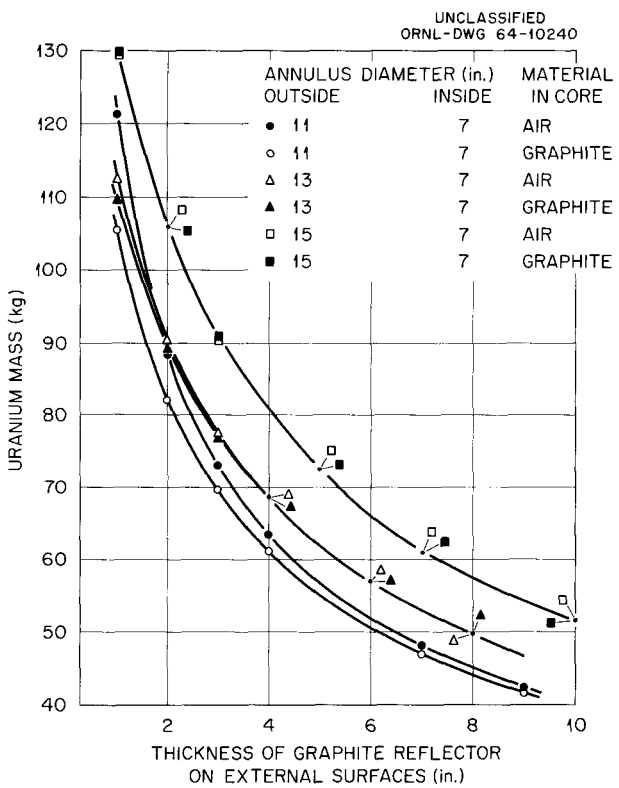

Fig. 2.4.1. Critical Mass of Cylindrical Annuli of U(93.2) Metal Reflected by Graphite.

References

[1]J. T. Mihalczo, *Neutron Phys. Div. Ann. Progr. Rept. Aug. 1, 1963*, ORNL-3499, Vol. I, p. 62.

[2]B. G. Carlson and G. I. Bell, *Proc. Intern. Conf. Peaceful Uses At. Energy, 2nd, Geneva, 1958* **16**, 535–49 (1959).

[3]B. Carlson, C. F. Lee, and J. Worlton, *The DSN and TDC Neutron Transport Codes*, LAMS-2346 (1960).

[4]G. E. Hansen and W. H. Roach, *Six and Sixteen Group Cross Sections for Fast and Intermediate Critical Assemblies*, LAMS-2543 (1961).

2.5. PROMPT-NEUTRON LIFETIME IN CRITICAL ENRICHED-URANIUM METAL CYLINDERS AND ANNULI[1]

J. T. Mihalczo

Prompt-neutron lifetimes have been determined for unreflected and unmoderated critical assemblies of enriched-uranium metal (93.15% ^{235}U) in cylindrical geometry. Five solid cylinders ranging in diameter from 7 to 15 in. and three cylindrical annuli having outside diameters as large as 15 in. were assembled to delayed critical and their prompt-neutron decay constants measured by the Rossi-α technique. The prompt-neutron lifetimes were determined from the measured decay constants and from effective delayed-neutron fractions obtained by S_n multigroup transport-theory calculations, which predicted the multiplication constants of all assemblies to within $\frac{1}{2}$%. For the solid cylinders the lifetime value is 6.25 ± 0.04 nsec, which, within the limits of experimental errors, is independent of the dimensions of the cylinders and agrees with the lifetime of 6.2 ± 0.1 nsec obtained from earlier prompt-neutron decay-constant measurements with a uranium sphere (Godiva I). For the cylindrical annuli the lifetime varied from 7.0 to 8.0 nsec. The increase in the lifetime value over that of the solid cylinders is due to the time required for neutrons to cross the center void.

References

[1]Abstract of published paper: *Nucl. Sci. Eng.* **20**, 60–65 (1964).

2.6. HIGH FLUX ISOTOPE REACTOR CRITICAL EXPERIMENT NO. 3

J. T. Thomas

The nuclear design of the High Flux Isotope Reactor (HFIR) has been supported by three series of critical experiments.[1,2] The current series, designated as HFIR Critical Experiment No. 3, utilizes a newly designed core, based upon the results of the previous experiments, in which the loading and distribution of the uranium and the distribution of boron have been altered. The loading was increased from 8.0 to 9.4 kg of ^{235}U. As was true previously, the results of these experiments are of limited interest and serve primarily as guidance in the design of the reactor. The material reported here exemplifies the program.

The relative power distribution through the core was obtained from the delayed fission-product activity induced in small samples removable from the fuel plates. Shown in Fig. 2.6.1 is an anticipated radial power distribution in the HFIR core. The values shown for the relative power were derived from the experimental data by applying, to each measurement, a factor relating the actual uranium content of the experimental core to that expected in the reactor core. Azimuthal variations in the radial power near the outer boundary of the core were as great as 10% with the control cylinders partly inserted but were negligible when sufficient boron was dissolved in the moderator water to permit complete withdrawal of the cylinders. The 10% variation is, therefore, possibly attributable to the nonuniform peripheral distribution of the absorbing materials of the control cylinders or to asymmetry of the cylinders with respect to the core.

The response of a fission counter proposed for use in the HFIR was found satisfactory by measurements using a 7.3 ± 1.5 curie ^{124}Sb source located

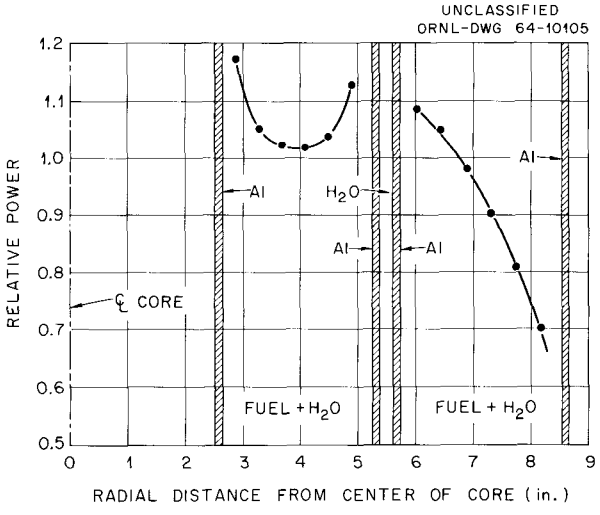

Fig. 2.6.1. Radial Power Distribution Anticipated at HFIR Midplane. Ordinates are experimental values corrected to the design uranium distribution.

within the beryllium reflector 3 in. from its inner surface and in the core midplane. The fission counter was placed on the axis of the core 21.8 in. below its midplane. Counting rates were observed with two different control-cylinder configurations, with the core flooded in both cases. In one configuration both cylinders were completely inserted, making the core ~$11 subcritical; in the other configuration, the outer cylinder was inserted and the inner one was withdrawn, resulting in the core being ~$6 subcritical.

References

[1]J. K. Fox, L. W. Gilley, and D. W. Magnuson, *Preliminary Solution Critical Experiments for the High-Flux Isotope Reactor*, ORNL-3359 (1963).

[2]D. W. Magnuson, *Neutron Phys. Div. Ann. Progr. Rept. Sept. 1, 1961*, ORNL-3193, p. 136.

2.7. EXPERIMENTAL AND CALCULATIONAL DETERMINATIONS OF THE REACTIVITY EFFECTS OF PERTURBATIONS IN A ONE-DIMENSIONAL CRITICAL EXPERIMENT

E. G. Silver E. B. Johnson

The course of a reactor transient may be affected by the reactivity change produced by possible motion of the reactor components during the transient. In particular, during power excursions in pool-type reactors, reactivity changes may result from motion of the fuel plates. In order to establish confidence in calculational methods, the reactivity effects caused by displacements of fuel plates were measured in an otherwise unperturbed critical assembly.[1] The results were compared with those calculated by using both transport- and diffusion-theory codes.

Since adequate transport-theory codes are applicable only to one-dimensional geometry, the critical assembly was a slab that had transverse dimensions large compared with its thickness and that was reflected on its faces only. The core, composed of a uranium-aluminum alloy containing 10.8 wt % uranium enriched to 93.1% in ^{235}U, was mounted in a tank which could be filled with water to provide moderator and reflector. Individual elements were 60.96 cm long, 59.94 cm high, and 0.147 cm thick and contained 156.4 g of ^{235}U. Each element was made up of eight 7.49-cm-wide plates. The unperturbed core consisted of 28 elements uniformly spaced 0.51 cm between centers by grooves in the side walls of the tank and by Plexiglas spacers. The plane of symmetry was located in a water space. In this unperturbed loading each of the outermost elements consisted of only four alloy plates, the remainder being aluminum plates of the same dimensions to preserve the metal to water volume ratio. A photograph of the core and tank is shown as Fig. 2.7.1.

Perturbations were produced in the core by the displacements of elements shown in Fig. 2.7.2. The perturbations were compensated for and evaluated by adjusting the ^{235}U loading in the two outermost elements and by varying the height of water above the core. The latter was never more than 1.5 cm, and it was found that in this range the reactivity was proportional to the thickness of the top reflector.

The unperturbed core was reassembled a number of times, and the reactivity was observed to be reproducible to $\pm 6 \times 10^{-3}\%$ in $\Delta k/k$. This uncertainty is taken to be the precision of individual measurements. The magnitude of most of the perturbations required evaluation by a series of individual measurements, even necessitating alteration of the loading in the outermost plates, so that the uncertainty of a perturbation measurement may be as great as $\pm 6 \times 10^{-2}\%$ $\Delta k/k$.

The diffusion-theory calculations were performed with a version of the MODRIC code[2] using flux-weighted 16-group cross sections.[3] Down-scattering was included by employing transfer coefficients from any group to the next ten groups below it, rather than by continuous slowing down from group to group. Since only 25 spatial regions can be considered by the MODRIC code, it was necessary to homogenize a part of the core. The fuel density in this region was modified to correct for self-shielding. Several models for the transverse leakage produced essentially the same calculated perturbation.

The transport-theory calculations utilized a one-dimensional multigroup code, DTK, a version of Carlson's[4] S_n method. In the present instance n equaled 4, and an 18-group cross-section set developed by Mills[5] was employed. Since the DTK code has no limit on the number of regions, it was possible to describe all elements explicitly as

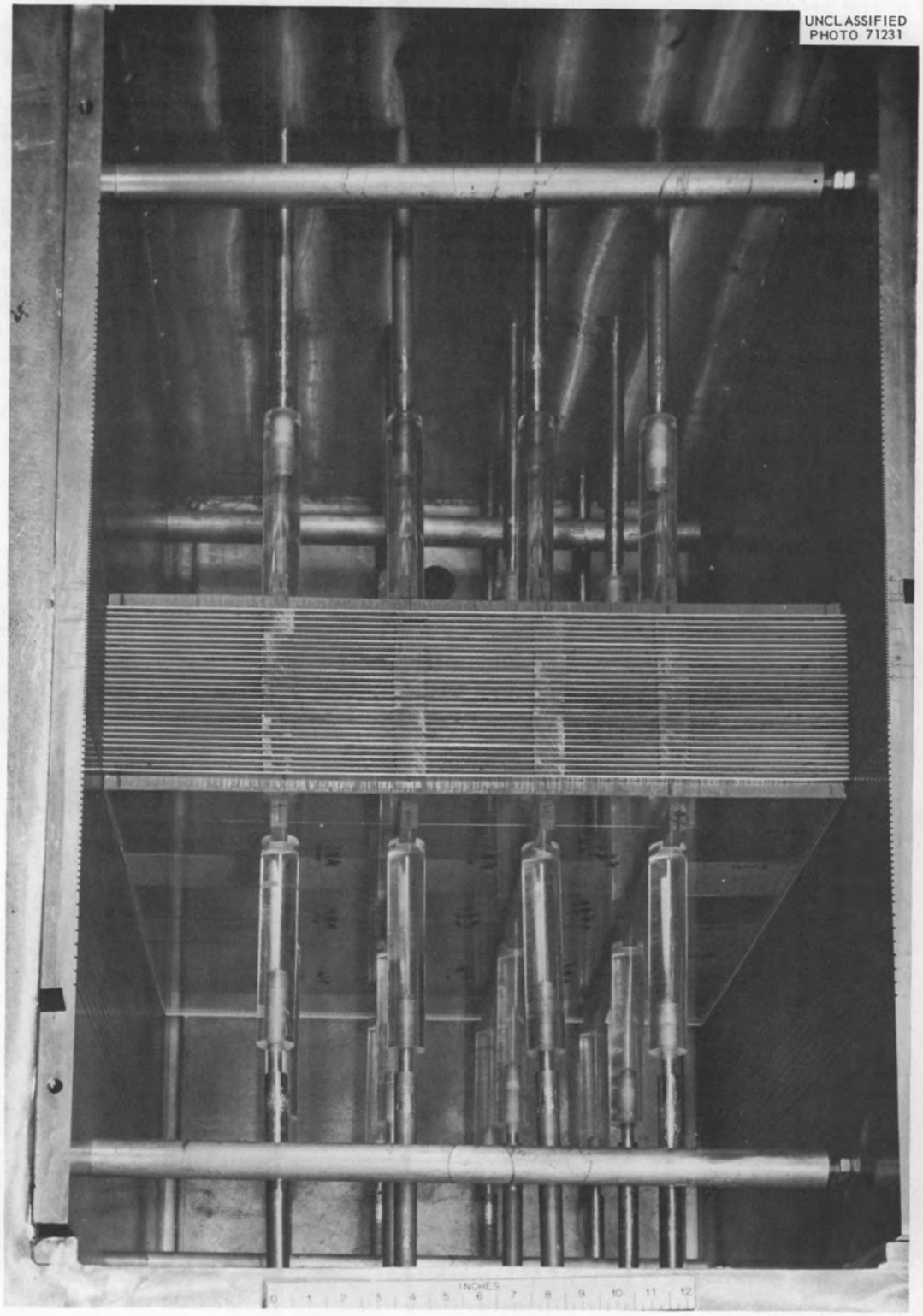

Fig. 2.7.1. Top View of Critical Experiment Tank Showing Fuel Elements in Position and the Plastic Spacing Strips and Clamping Arrangement.

well as to homogenize selected regions of the core for more direct comparison with the diffusion-theory calculations.

The effective delayed neutron fraction, β_{eff}, was calculated by both diffusion- and transport-theory methods using a modified prompt-fission-only fission spectrum. A consistent value of 0.78% resulted, and allowed conversion of the experimental values into units of $\Delta k/k$.

The experimental and calculated results, summarized in Fig. 2.7.2, show that transport theory yields substantially better results than can diffusion theory, as was expected. The mean disagreement of the former with experiment is 8.4%, whereas it is 33.8% in the latter case.

As might also be expected, the flux calculated by diffusion theory is depressed in the water regions as compared with that calculated by transport theory. This comparison is illustrated by the calculated thermal-neutron fluxes shown in Fig. 2.7.3 for the case of fuel-element displacements from positions adjacent to the core midplane to positions between the fifth and sixth elements.

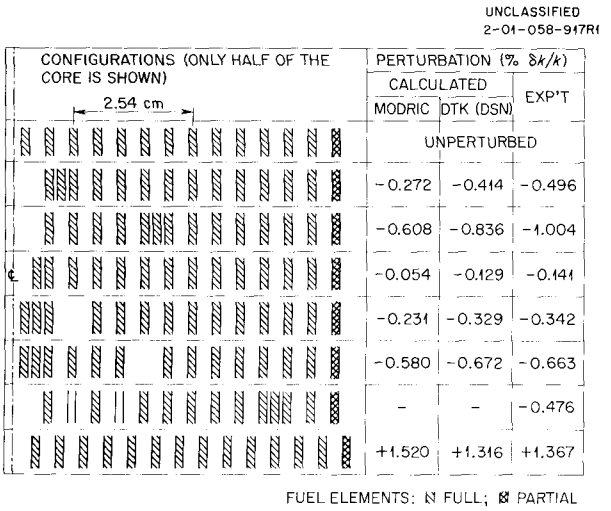

Fig. 2.7.2. Core Configurations and Corresponding Calculated and Measured Reactivity Perturbations.

References

[1]A description of the equipment was included in a preliminary report by E. G. Silver and E. B. Johnson, *Neutron Phys. Div. Ann. Progr. Rept. Aug. 1, 1963*, ORNL-3499, Vol.I, pp. 69–76.

[2]J. Replogle, *MODRIC, A One-Dimension Neutron Diffusion Code for the IBM-7090*, K-1497 (1962).

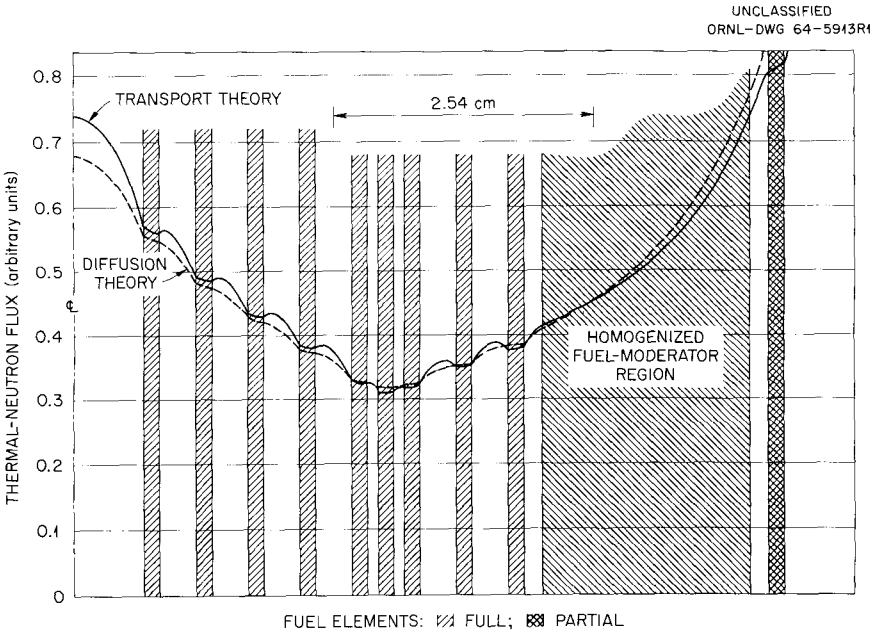

Fig. 2.7.3. Thermal-Neutron Flux Calculated by Transport- and Diffusion-Theory Codes for a Specific Perturbed Core.

[3]The derivation of this set of cross sections is given by E. G. Silver and E. B. Johnson, *Nucl. Safety Program Semiann. Progr. Rept. June 1, 1964*, ORNL-3691.

[4]B. Carlson, C. F. Lee, and J. Worlton, *The DSN and TDC Neutron Transport Codes*, LAMS-2346 (1959).

[5]C. B. Mills, *Neutron Cross Sections for Fast and Intermediate Nuclear Reactors*, LAMS-2255 (1959).

2.8. CALCULATED NEUTRON MULTIPLICATION FACTORS OF A SPHERICAL VOLUME OF FISSILE MATERIAL IN AQUEOUS SOLUTION ENCLOSED IN COMBINATIONS OF ABSORBERS AND REFLECTORS

D. W. Magnuson

Calculations using the DSN transport code in the S_4 approximation and the 16-group cross sections of Hansen and Roach[1] have evaluated the neutron multiplication factor of a sphere of aqueous $U(92.44)O_2(NO_3)_2$ solution contained in aluminum and surrounded by various reflectors. These reflectors consisted of spherical shells of water of various thickness and, in cases with an effectively infinite water thickness, of a thin layer of neutron absorber adjacent to the aluminum. The absorber was an 0.08-cm-thick sheet of cadmium or a 0.03-cm-thick layer of Lindsay mix, the latter being a mixture of rare-earth oxides, principally those of gadolinium and samarium, and having a density of 5.9 g/cm^3. For the calculations the concentration of the solution was taken as 64.90 g of uranium per liter, the radius of the solution sphere as 18.35 cm, and the thickness of the aluminum container as 0.15 cm since this assembly had been found by experiment to be critical when unreflected. Scatter and absorption in neutron-energy groups 1 to 13 were not included in the calculations.

The results of these calculations, including neutron lifetimes, for the various absorber-reflector configurations are given in Table 2.8.1. It is seen that cadmium is slightly more effective than the Lindsay mix in decreasing the multiplication factor. This result is expected from the comparison of neutron attenuation factors, the product of the thickness and the macroscopic absorption

Table 2.8.1. DSN Transport Calculations of an 18.35-cm-radius Sphere of $U(92.44)O_2(NO_3)_2$ Solution

(Solution concentration 64.90 g of uranium per liter)

Material Surrounding Solution Sphere	Multiplication Factor, k_{eff}	Neutron Lifetime[a] (μsec)
None	0.9919	20.58
0.15 cm Al	0.9941	20.67
0.15 cm Al plus 1 cm water	1.0302	22.34
0.15 cm Al plus 2 cm water	1.0595	24.99
0.15 cm Al plus 3 cm water	1.0822	28.76
0.15 cm Al plus 30 cm water	1.1296	90.75
0.15 cm Al plus 0.08 cm Cd plus 30 cm water	1.0408	69.91
0.15 cm Al plus 0.03 cm Lindsay mix[b] plus 30 cm water	1.0424	70.22
0.15 cm Al (experimental)	1.0000	

[a]The neutron lifetime is calculated from $l = \dfrac{\sum_n \phi_n (1/v)_n}{\sum_n (\text{leakage} + \text{absorption})}$.

[b]A mixture of 45% Sm_2O_3, 45% Gd_2O_3, 1% Fe_2O_3, and 9% Er_2O_3, Eu_2O_3, and Yb_2O_3. The density of this material when sprayed on a metallic surface with a plasma torch was 5.9 g/cm^3.

Table 2.8.2. Neutron Attenuation Through Cadmium and Lindsay Mix

Neutron Energy Group		Attenuation Factor, $\Sigma_a t$	
Number	Energy Limits (ev)	Cadmium	Lindsay Mix
16	Thermal	11.12	13.77
15	0.1–0.4	11.12	2.05
14	0.4–1.0	0.22	0.23

cross section, shown in Table 2.8.2. Both cadmium and the rare-earth materials absorb more than 99.9% of the thermal neutrons. Cadmium, however, absorbs more group-15 neutrons (0.1 to 0.4 ev) than does the Lindsay mix, increasing its total effectiveness.

As may be observed in Table 2.8.1, the calculations show that a composite reflector of the Lindsay mix (0.03 cm thick) backed by a 30-cm-thick water reflector is equivalent to a 1.39-cm-thick water reflector, and that the 0.08-cm-thick cadmium–30-cm-thick water combination is equivalent to a 1.34-cm-thick water reflector. Experiments with various reflectors surrounding a 17.72-cm-radius (23.22 liter), 0.11-cm-thick stainless steel sphere filled with plutonium nitrate solution showed that a composite of 0.08-cm-thick cadmium backed by thick water was equivalent to a 1.8-cm-thick paraffin reflector.[2] The plutonium concentration was about 70 g per liter.

The results of this investigation indicate that selection of neutron absorbers for nuclear safety application should be governed by the cost of the absorber and the permanency of its application rather than by the slight differences in calculated reactivities.

References

[1]G. E. Hansen and W. H. Roach, *Six and Sixteen Group Cross Sections for Fast and Intermediate Critical Assemblies*, LAMS-2543 (1961).

[2]R. C. Lloyd, E. D. Clayton, and C. R. Richey, *Physics Research Quarterly Report for July, August, and September, 1962*, HW-75228 (Oct. 15, 1962).

2.9. CRITICAL DIMENSIONS OF SYSTEMS CONTAINING ^{235}U, ^{239}Pu, AND ^{233}U[1]

H. C. Paxton[2] D. Callihan
J. T. Thomas E. B. Johnson

A compilation of critical data obtained from experiments performed since 1945, both in this country and in Europe, is presented. The report supplements the Nuclear Safety Guide[3] and shows the bases of the recommendations that appear in the Guide. Conversions to standard geometries are shown. Results are given for single units and multiple-unit arrays.

References

[1]Abstract of TID-7028 (1964) as presented in *Nucl. Sci. Abstr.* **18**, 4153 (1964).

[2]Los Alamos Scientific Laboratory.

[3]TID-7016, Rev. 1.

3. Reactor Shielding

3.1. MEASUREMENTS AND CALCULATIONS OF NEUTRON SPECTRAL INTENSITIES THROUGHOUT A REACTOR WATER SHIELD

M. S. Bokhari[1] V. V. Verbinski

Measurements have been made of the spectral intensity of fast neutrons throughout the water shield of the Bulk Shielding Reactor I and the results compared with two numerical transport calculations. An ^{6}Li shielded-diode neutron spectrometer,[2] which was operable in gamma-ray fields of up to 3×10^6 r/hr, was used to measure the spectrum of directed neutron flux, $\phi(\mu,r,E)$, for $r = 0$ to 50 cm and $\mu = 1$, 0.755, and 0.617, where $\mu = \cos\theta$ and θ and r are shown in Fig. 3.1.1.

Figure 3.1.1 shows the relative positions of the reactor and spectrometer, along with the ^{6}Li and ^{7}Li foils used for foreground and background

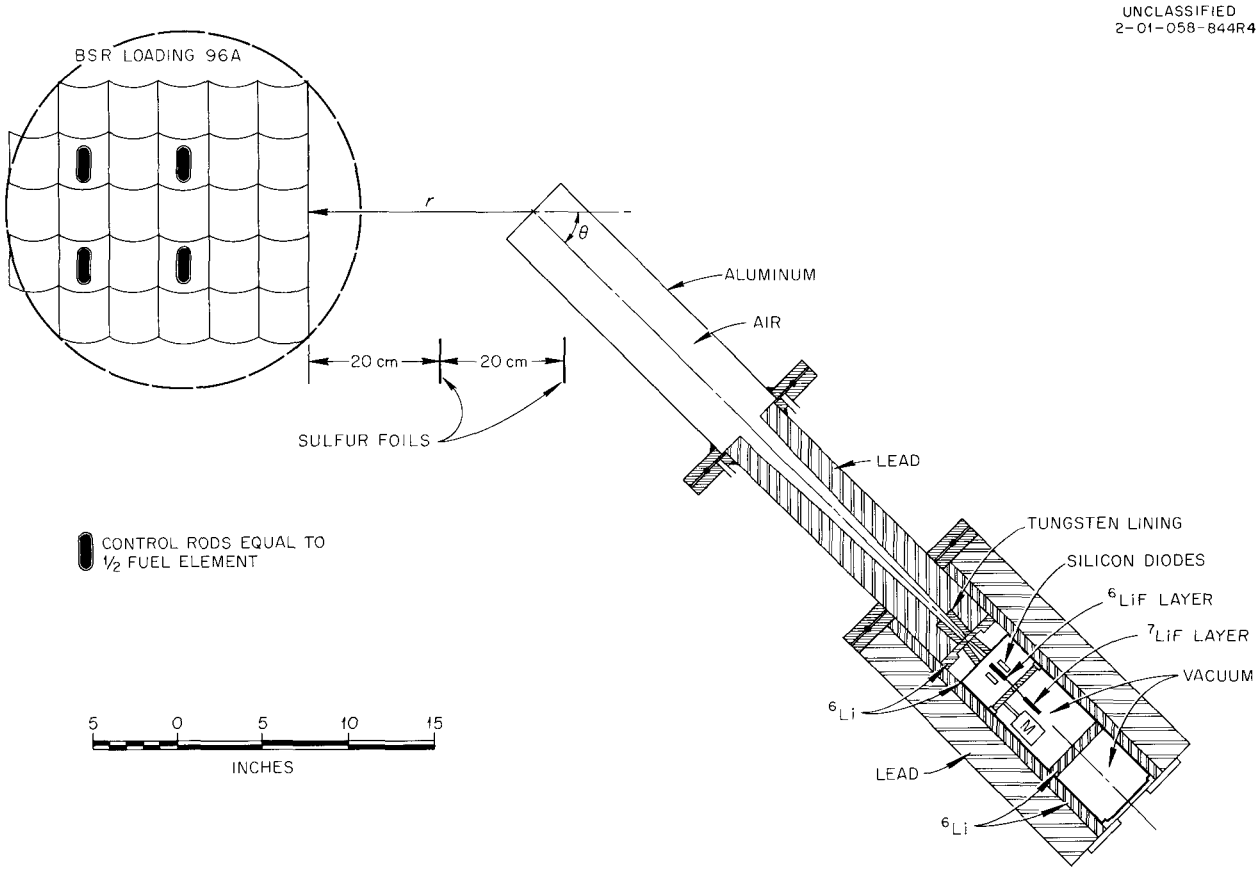

Fig. 3.1.1. Experimental Arrangement of BSR-I and Shielded-Diode Spectrometer in the BSF Pool. The sulfur foils are 38 cm lateral to and 35 cm above the midplane of the center line.

measurements [utilizing the $^6Li(n,\alpha)^3H$ reaction, $Q = +4.76$ Mev] and the two diodes whose outputs were added and sent to a pulse-height analyzer when in coincidence.[2] The sulfur foils shown in the figure monitored the absolute reactor power. They were calibrated during a measurement of absolute power density throughout the reactor (see Sect. 3.2).

The calculations were performed with the NIOBE code[3] and the DTF-2 code,[4] both of which required spherical symmetry and utilized a spherical source region whose radial dependence was that measured along the midplane center line of the reactor. Therefore, the $\theta = 0°$ ($\mu = 1$) spectra can be compared directly with measurement. In Fig. 3.1.2, the NIOBE results for $\phi(\mu = 1,r,E)$ and the measurements are shown to agree everywhere within a factor of 2, except in the region below 1.5 Mev, where the spectrometer is least reliable. Because of the coarse group structure of the DTF-2 code, only group 2 (1.4 to 3 Mev) can be compared favorably with the measurements. The DTF results differ with the measurements by a factor of 3 at $r = 0$, but, like the NIOBE results, almost agree with the measurements at $r = 50$ cm and $E = 2$ Mev.

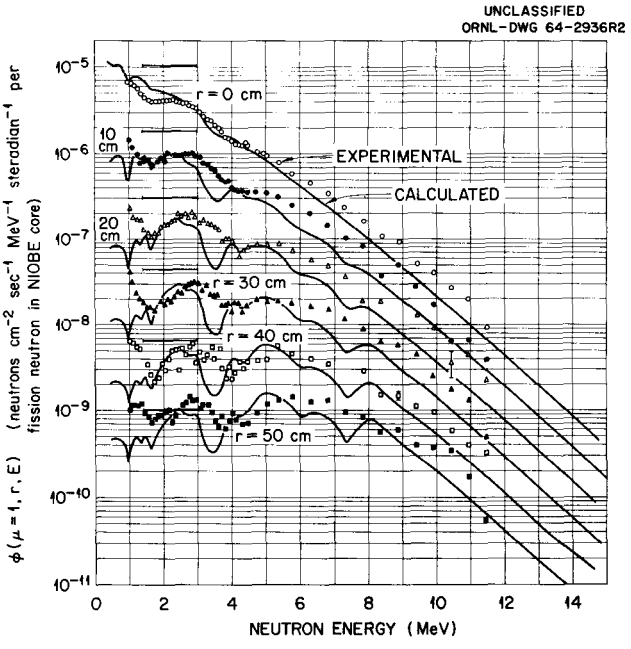

Fig. 3.1.2. A Comparison Between Measured and Calculated Values of $\phi(\mu = 1, r, E)$. The solid curves are NIOBE calculations; the horizontal bars are DTF-2 calculations.

References

[1]Affiliated with Pakistan Atomic Energy Commission; formerly a visiting scientist at ORNL.

[2]V. V. Verbinski *et al.*, *Neutron Phys. Div. Ann. Progr. Rept. Aug. 1, 1963*, ORNL-3499, Vol. I, p. 181.

[3]S. Preiser *et al.*, *A Program for the Numerical Integration of the Boltzmann Equation*, A.R.L. Technical Report 60-314, U.S. Department of Commerce, Washington, D.C. (1960).

[4]DTF-2 is a version of the DSN Code that has improved convergence capabilities; it was obtained for this problem by E. Whitesides, Oak Ridge Gaseous Diffusion Plant, from B. W. Colston, Atomics International.

3.2. POWER CALIBRATION OF THE BULK SHIELDING REACTOR I

M. S. Bokhari[1] V. V. Verbinski T. V. Blosser
G. T. Chapman A. Bakeshloo[2]

Recent measurements of the spatial and spectral details of the fast-neutron flux at points in a water shield surrounding the Bulk Shielding Reactor I are discussed in Section 3.1. These data were obtained for evaluation of neutron transport calculational methods, but before a complete and meaningful comparison of experimental and calculated results could be made, it was necessary to perform a power calibration of the BSR-I loading shown in Fig. 3.1.1 of Sect. 3.1 since the absolute source density and the total power of the reactor are the required inputs to the transport calculation.

In performing the calibration, the thermal-neutron flux was mapped throughout the reactor core by means of thin copper wires inserted vertically between the fuel plates of the fuel elements. The entire flux mapping was accomplished with about 12 copper wires per fuel element. The resulting relative flux values were converted to absolute flux values by cross calibrating them against very thin uranium foils that had nearly the same ^{235}U enrichment as the fuel elements and had been exposed first in the reactor and then in the ORNL Standard Pile.[3] The activation ratios plus the flux value at the Standard Pile gave the fission rates in the fuel element. The flux in the Standard Pile was assumed to be completely thermal, and

the average thermal fission cross section was taken as 582/1.126 = 516 barns per ^{235}U atom (582 is the value of the fission cross section at 0.025 ev, and the dividing factor of 1.126 converts this cross section to the average over the thermal spectrum). A horizontal flux plot along the center line of the midplane of the BSR-I is shown in Fig. 3.2.1.

The sulfur foils shown in Fig. 3.1.1 of Sect. 3.1 were used to monitor the relative power during both the spectral measurements and the power calibration experiment. The ratio of their activations during the two experiments was then used to determine the power of the reactor at the time the spectral measurements were made.

No corrections were made for differences in copper and uranium activation arising from variation of the neutron spectrum (thermal and epithermal) with position in the reactor. The ratio of these two activations vs distance along the second central fuel element from the reactor face is plotted in Fig. 3.2.2. The plot shows that the ratio is very nearly the same throughout the central region and at the ends of a fuel element and that the variation is within statistical and systematic errors in the measurement.

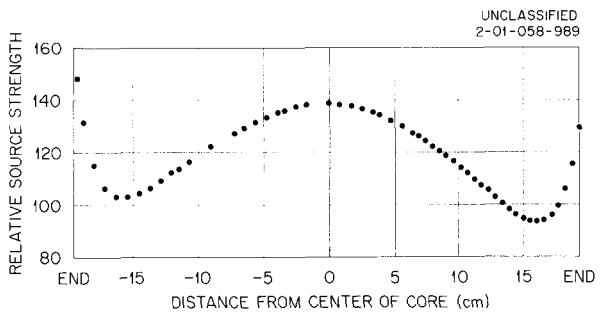

Fig. 3.2.1. Relative Power Distribution in the Midplane of the Bulk Shielding Reactor I.

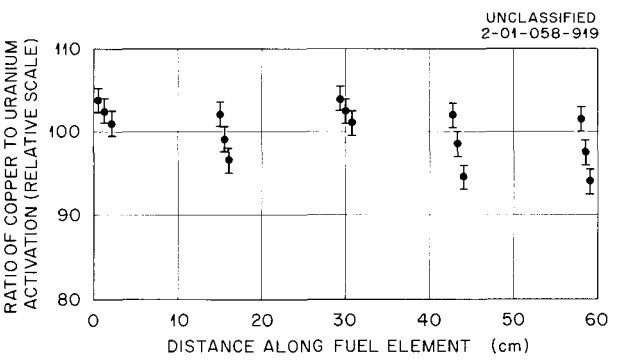

Fig. 3.2.2. Cu/^{235}U Activation Ratio as a Function of Distance Along BSR-I Fuel Element.

References

[1]Affiliated with Pakistan Atomic Energy Commission; formerly a visiting scientist at ORNL.

[2]Government of Iran; sponsored by the Department of State, Agency for International Development.

[3]E. D. Klema *et al.*, *Recalibration of the X-10 Standard Graphite Pile*, ORNL-1398 (October 1952).

3.3. PULSE-HEIGHT SPECTRA OF GAMMA RAYS EMITTED BY THE STAINLESS-STEEL-CLAD BULK SHIELDING REACTOR II (BSR-II)[1]

G. T. Chapman K. M. Henry J. D. Jarrard

Measurements have been made of the pulse-height spectra of gamma rays emitted from the core of the Bulk Shielding Reactor II (BSR-II). Preliminary analysis of the data indicates that the gamma rays having energies above 5 Mev originate primarily from thermal-neutron capture in the stainless steel reactor structure. Below 5 Mev the spectrum is apparently composed of the expected continua of prompt-fission and fission-product gamma rays plus a large contribution from thermal-neutron captures in the hydrogen of the water that moderates and reflects the core. Except for reduced intensity, little change was noticed in the structure of the distribution as the amount of water between the reactor surface and the spectrometer was increased from 1 to 60 cm. Angular-distribution measurements were also made about two points at 10 and 25 cm from the surface of the reactor. A simple calculation of the expected spectra at the surface of a homogeneous reactor compared favorably with a measured spectrum.

References

[1]Abstract of ORNL-3609 (November 1964).

3.4. DETERMINATION OF THERMAL-NEUTRON FLUX DISTRIBUTIONS IN THE BULK SHIELDING REACTOR II BY COPPER WIRE ACTIVATION TECHNIQUES[1]

G. T. Chapman

The thermal-neutron flux distribution within the stainless steel ORNL Bulk Shielding Reactor II has been determined by exposing copper wires at selected locations in the core during reactor operation. The gamma-ray activity resulting from thermal-neutron activation of the copper was counted as a function of position along the wire, and the results were converted to estimates of the thermal-neutron flux by methods which are described in this report. The use of copper for determining the thermal-neutron distribution was checked by independently exposing gold and copper wires at a common location in the reactor. The thermal-neutron fluxes obtained from analysis of both sets of data were in agreement within ~3%. The results of the analysis of the copper activation were compared with calculations of the distribution made by the PDQ reactor code. Agreement was good in statistically important regions.

References

[1]Abstract of ORNL-TM-846 (in press).

3.5. AN EXPERIMENTAL VERIFICATION OF A SOURCE GEOMETRY TRANSFORMATION FOR SHIELDING CALCULATIONS

L. Jung

The comparison method of shield design, which uses data from a known source-shield configuration to predict the performance of a source-shield configuration for which no data are available, is based upon the assumption that the known and unknown configurations can be converted to the same geometry. Using only the theorem of additivity of effects, Blizard[1] has presented a number of source-geometry transformations to accomplish such conversions. In particular he has shown that the dose from a disk source of radius $\sqrt{m}\,a$, as measured at a distance z on its axis, is equal to the sum of m terms at distances z, $(z^2 + a^2)^{1/2}$, $(z^2 + 2a^2)^{1/2}$, etc., from the dose data for a smaller disk of radius a.[2] The work reported here is intended to demonstrate the validity of this transformation applied to an experimental facility.

The experiment, which was performed at the ORNL Lid Tank Shielding Facility (LTSF),[3] consisted of measurements of thermal-neutron fluxes in the water of the LTSF as a function of axial distance z from a number of disk sources having radii smaller than the 14-in. radius (A) of the LTSF source plate (the SP-II). Blizard's transformation, written in the form

$$D(z,A) = \sum_{n=1}^{m} D\left(\sqrt{z^2 + \frac{(n-1)A^2}{m}},\, a\right), \quad (1)$$

where n and m are integers and $a = A/\sqrt{m}$, was then applied to the results to predict the fluxes at the same distances from SP-II. The predictions were compared with the fluxes measured at those distances from SP-II.

Values of m in Eq. (1) were chosen to be 16, 9, 4, and 2, which, since the diameter of the large disk source was 28 in., resulted in values for the small-source diameters of 7, 9.33, 14, and 19.80 in. These small source plates were simulated by masking the large disk with 25-mil-thick cadmium diaphragms having circular openings of the appropriate diameters; they were inserted between the thermal-neutron beam from the ORNL Graphite Reactor and the large source plate. The large plate was so constructed, however, that the closest location possible for the cadmium diaphragms was $^3/_8$ in. from the uranium plate. This $^3/_8$-in. gap of aluminum and air allowed neutrons from the thermal beam to scatter behind the cadmium and to produce fissions in the annular regions beyond the nominal limits of the diaphragm opening. The magnitude of this effect is shown in Fig. 3.5.1, where the configuration numbers correspond to the rounded-off diameters of the sources. The measured z-axis flux was corrected for the effect of

fissions in annular regions by the use of the following equation:

$$D(z,a) = \frac{D_M(z,a)}{1 + ATTEN\left[E_1\left(\frac{\sqrt{z^2+a^2}}{\lambda_n}\right) - E_1\left(\frac{\sqrt{z^2+A^2}}{\lambda_n}\right) \Big/ E_1\left(\frac{z}{\lambda_n}\right) - E_1\left(\frac{\sqrt{z^2+a^2}}{\lambda_n}\right)\right]}, \tag{2}$$

where $D_M(z,a)$ is the measured flux at z, $ATTEN$ is the ratio of the flux behind the cadmium diaphragm to the flux with the diaphragm removed, and λ_n is the neutron relaxation length. The functions within the brackets are the well-known exponential integral functions. Since the ratio $ATTEN$ varied rapidly with radius, this term in the denominator of the fraction, $1 + ATTEN\ [\ldots]$, was computed for each centimeter of radius and summed over the annular distance $A - a$ to obtain the corrected value of $D(z,a)$.

A second correction to the measured fluxes was required because the flux distribution was not uniform over the entire diameter of SP-II, as is shown in Fig. 3.5.1. The conditions of the transformation being tested require a uniform distribution of source strength. Since the distribution across each of the smaller sources was nearly uniform, it was necessary only to correct the data from the large plate. The corrected flux at a distance z from the large plate is given by

$$D(z,A) = \frac{D_M(z,A)\left[E_1\left(\frac{z}{\lambda_n}\right) - E_1\left(\frac{\sqrt{z^2+A^2}}{\lambda_n}\right)\right]}{E_1\left(\frac{z}{\lambda_n}\right) - E_1\left(\frac{\sqrt{z^2+a^2}}{\lambda_n}\right) + \frac{\bar{\phi}_a}{\phi_0}\left[E_1\left(\frac{\sqrt{z^2+a^2}}{\lambda_n}\right) - E_1\left(\frac{\sqrt{z^2+A^2}}{\lambda_n}\right)\right]}, \tag{3}$$

where ϕ_0 is the thermal-neutron flux in the region of uniformity, assumed to extend from the center radially for 22.5 cm, and $\bar{\phi}_a$ is the average thermal-neutron flux over the region of nonuniformity, computed to be 13.7% lower than the uniform flux.

The experimental data are plotted as data points and solid curves in Figs. 3.5.2 and 3.5.3, where the various symbols differentiate between the instruments used.[4] The broken curves are the corrected experimental data. For configurations 7, 9, 14, and 20, the correction was for annular fissions and was as large as 11.4% only for configuration 7 at z = 160 cm. For configuration 28, the correction for nonuniformity of flux reached a maximum of 7.5% at z = 160 cm.

The test of the source geometry transformation was accomplished by using values obtained from the corrected (broken) curves of Figs. 3.5.2 and 3.5.3, configurations 7, 9, 14, and 20, as input to predict values for configuration 28 (Fig. 3.5.3). The calculation was programmed for the CDC-1604A computer, and the predicted values are compared with the corrected experimental data from configuration 28 in Table 3.5.1. Agreement in the region close to the source is not expected because of abrupt changes in the neutron-scattering medium caused by the source plate and a ½-in.-thick sheet of boral added to reduce albedo neutron effects with the smaller sources. Likewise, agreement is not expected at large z distances because photoneutrons due to gamma rays from thermal-neutron captures in the cadmium diaphragms make a contribution to the observed flux that is difficult to evaluate. For configuration 7 the average disagreement between prediction and measurement for z = 10 to 90 cm is 0.07%, with an isolated maximum of 5%. For configuration 9 the average disagreement is 0.07%, with an isolated maximum of 5.4% over the same range of z. For configuration 14 the average deviation is but 0.04% over the range z = 5 to 120 cm, with a maximum of 5.8%. The poorest agreement is shown by configuration 20, with an average deviation of 2.7% and a maximum of 10.6% over the range 5 to 160 cm.

As a cross check upon this work, the flux to be expected with configuration 14 was computed from the measurements of configuration 7 with m = 4. The comparison of predicted results with

measured values is shown in Table 3.5.2. Agreement is seen to be excellent, both in shape and magnitude, at reasonable values of z.

From the results presented above, it may be concluded that the source geometry transformation relating data from a small disk source to those from a large disk source has been thoroughly validated. By association, confidence is reinforced in the similar transformation, derived in the same way, relating a disk source to an infinite plane source. It should be emphasized, however, that it is important in using these transformations to correctly compensate for nonuniform power distributions over the experimental source plate.

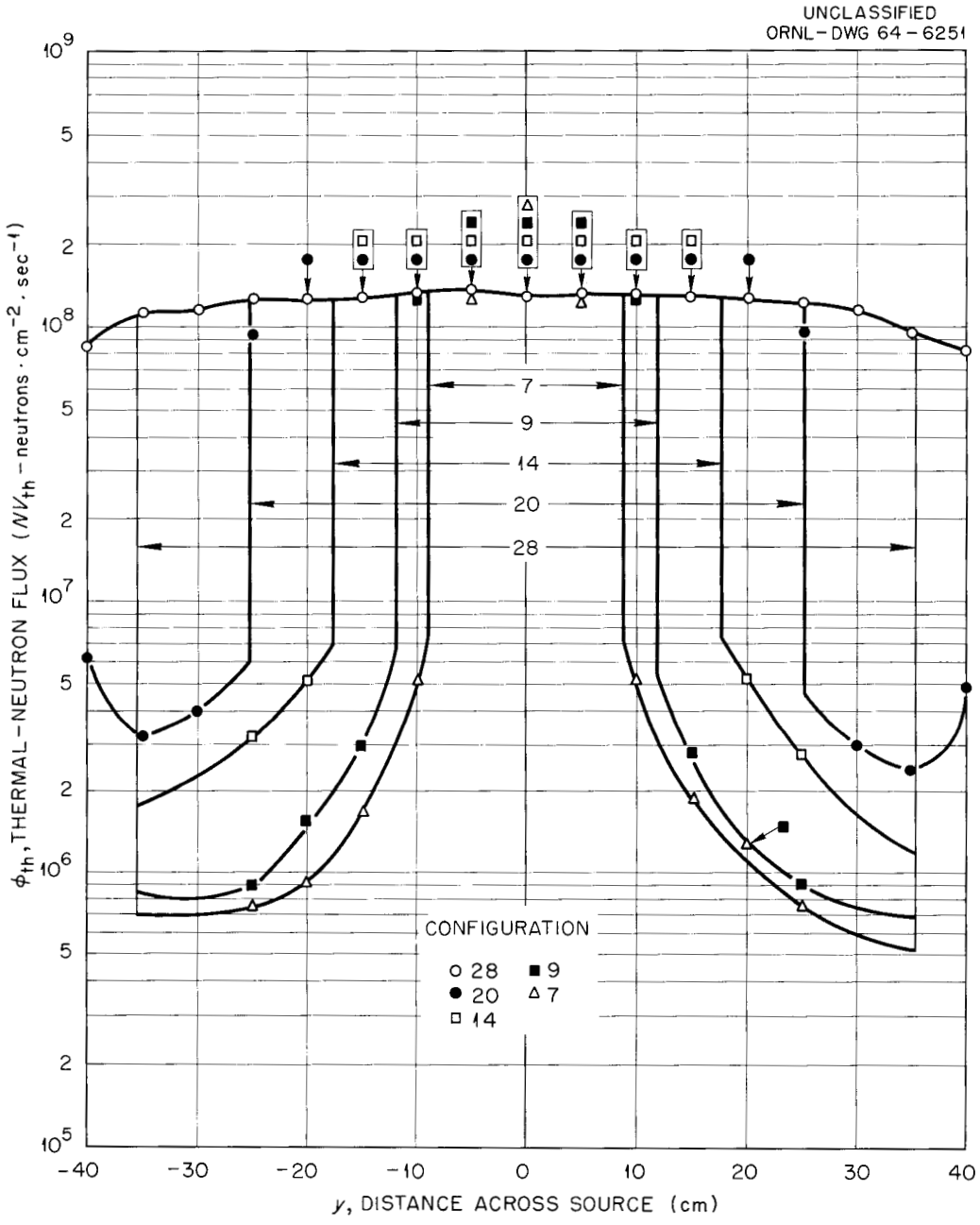

Fig. 3.5.1. Measured Thermal-Neutron Flux Between the Cadmium Diaphragms and the LTSF Source Plate: Configurations 7, 9, 14, 20, and 28.

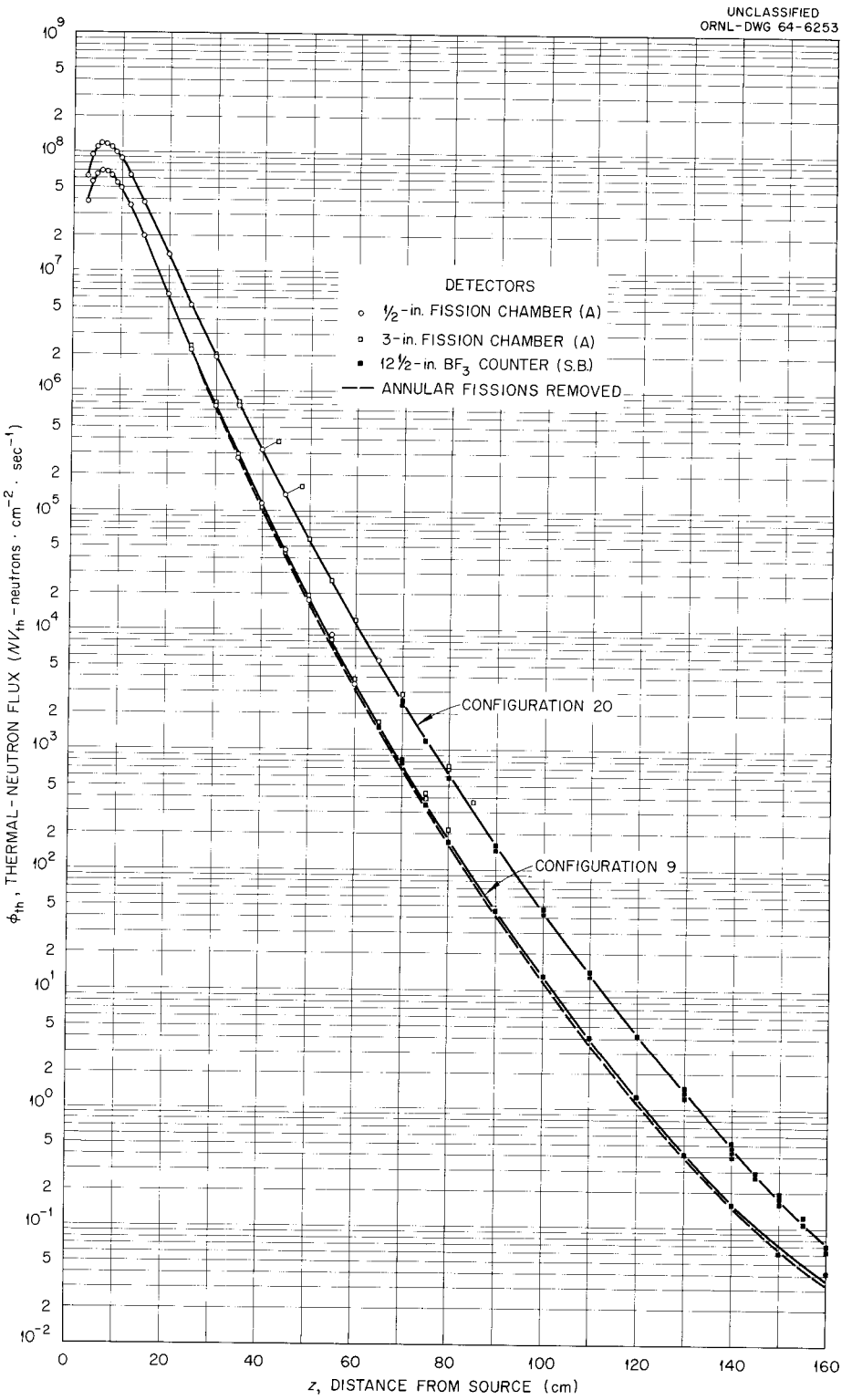

Fig. 3.5.2. Comparison of Measured and Corrected Thermal-Neutron Fluxes as Functions of Distance from Source: Configurations 9 and 20.

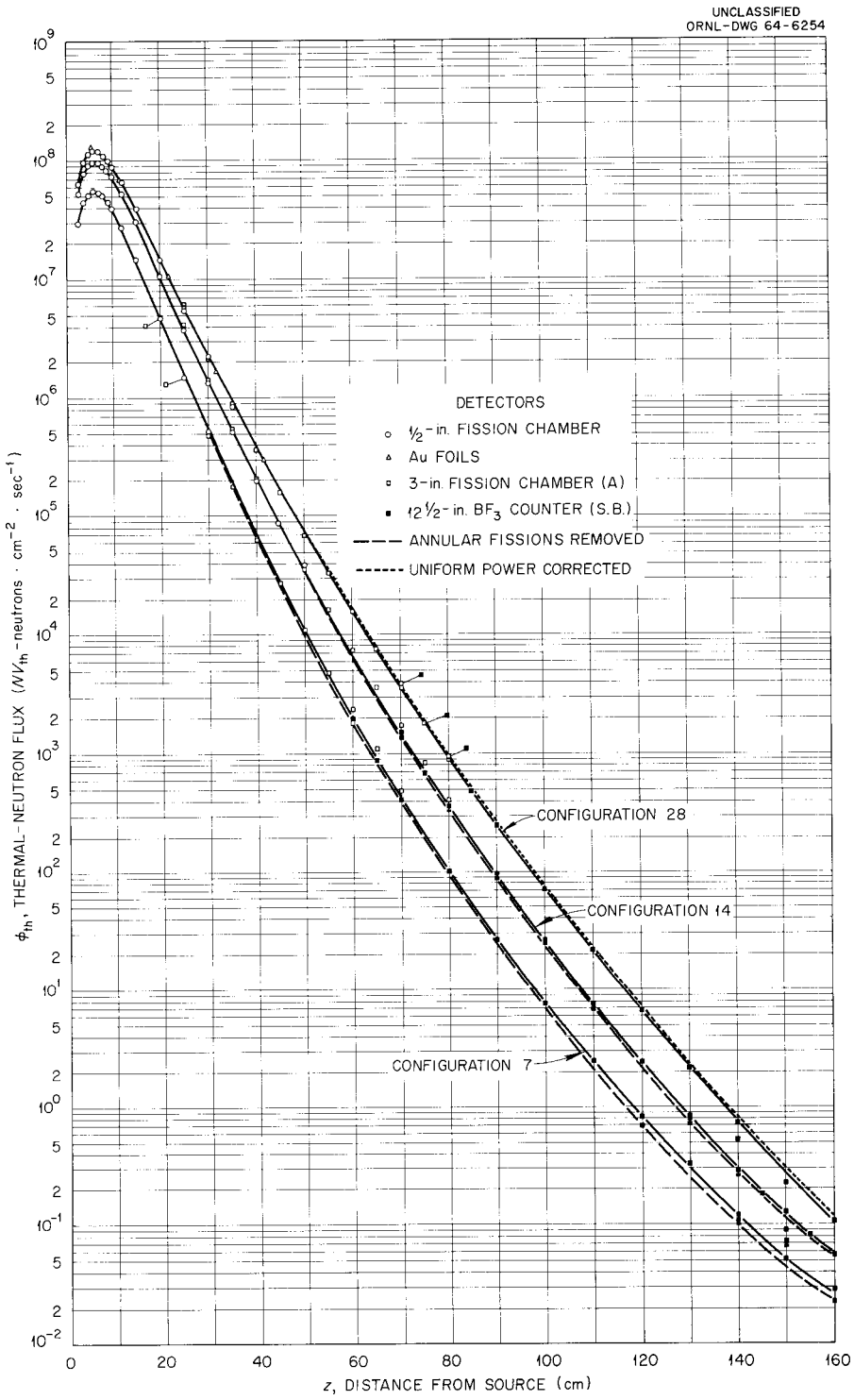

Fig. 3.5.3. Comparison of Measured and Corrected Thermal-Neutron Fluxes as Functions of Distance from Source: Configurations 7, 14, and 28.

Table 3.5.1. Computed Thermal-Neutron Fluxes from Configurations 7, 9, 14, and 20 Compared with Corrected Thermal-Neutron Fluxes of Configuration 28

z, Distance from Source (cm)	Thermal-Neutron Flux (NV_{th})				
	Configuration 7	Configuration 9	Configuration 14	Configuration 20	Configuration 28 (Corrected)
0	1.04×10^8	6.39×10^7	2.55×10^7	9.04×10^6	
5	1.37×10^8	1.18×10^8	1.10×10^8	1.14×10^8	1.12×10^8
10	8.88×10^7	8.14×10^7	8.52×10^7	8.93×10^7	8.82×10^7
15	3.78×10^7	3.59×10^7	3.73×10^7	3.93×10^7	3.85×10^7
20	1.45×10^7	1.39×10^7	1.43×10^7	1.50×10^7	1.47×10^7
25	5.49×10^6	5.38×10^6	5.58×10^6	5.75×10^6	5.52×10^6
30	2.15×10^6	2.14×10^6	2.23×10^6	2.26×10^6	2.14×10^6
35	8.80×10^5	8.99×10^5	9.18×10^5	9.19×10^5	8.73×10^5
40	3.76×10^5	3.93×10^5	3.80×10^5	3.99×10^5	3.73×10^5
45	1.66×10^5	1.71×10^5	1.63×10^5	1.77×10^5	1.61×10^5
50	7.39×10^4	7.42×10^4	7.17×10^4	7.58×10^4	7.10×10^4
55	3.28×10^4	3.36×10^4	3.22×10^4	3.57×10^4	3.23×10^4
60	1.47×10^4	1.57×10^4	1.50×10^4	1.62×10^4	1.53×10^4
65	7.17×10^3	7.55×10^3	7.24×10^3	7.61×10^3	7.55×10^3
70	3.60×10^3	3.72×10^3	3.62×10^3	3.60×10^3	3.73×10^3
75	1.82×10^3	1.85×10^3	1.84×10^3	1.77×10^3	1.87×10^3
80	9.39×10^2	9.59×10^2	9.48×10^2	9.30×10^2	9.71×10^2
85	4.97×10^2	5.12×10^2	4.97×10^2	4.89×10^2	5.06×10^2
90	2.66×10^2	2.77×10^2	2.59×10^2	2.57×10^2	2.65×10^2
95	1.44×10^2	1.50×10^2	1.36×10^2	1.38×10^2	1.38×10^2
100	7.92×10^1	8.18×10^1	7.34×10^1	7.49×10^1	7.54×10^1
105	4.43×10^1	4.57×10^1	4.05×10^1	4.11×10^1	3.99×10^1
110	2.50×10^1	2.58×10^1	2.27×10^1	2.29×10^1	2.26×10^1
115	1.43×10^1	1.47×10^1	1.27×10^1	1.27×10^1	1.20×10^1
120	8.33×10^0	8.41×10^0	7.25×10^0	7.07×10^0	6.80×10^1
125	5.03×10^0	4.75×10^0	4.21×10^0	4.01×10^0	3.90×10^0
130	3.11×10^0	2.75×10^0	2.54×10^0	2.30×10^0	2.29×10^0
135	1.96×10^0	1.69×10^0	1.54×10^0	1.36×10^0	1.31×10^0
140	1.27×10^0	1.07×10^0	9.68×10^{-1}	8.15×10^{-1}	7.74×10^{-1}
145	8.62×10^{-1}	6.70×10^{-1}	6.17×10^{-1}	4.95×10^{-1}	4.63×10^{-1}
150	6.08×10^{-1}	4.47×10^{-1}	3.97×10^{-1}	3.07×10^{-1}	2.91×10^{-1}
155	4.41×10^{-1}	3.62×10^{-1}	2.67×10^{-1}	1.90×10^{-1}	1.88×10^{-1}
160	3.31×10^{-1}	3.34×10^{-1}	1.87×10^{-1}	1.24×10^{-1}	1.24×10^{-1}

Table 3.5.2. Computed Thermal-Neutron Fluxes From Configuration 7 Compared with Corrected Thermal-Neutron Fluxes of Configuration 14

z, Distance from Source (cm)	Thermal-Neutron Flux (NV_{th})	
	Configuration 7	Configuration 14 (Corrected)
0	8.23×10^{7}	
5	1.18×10^{8}	9.15×10^{7}
10	7.59×10^{7}	7.24×10^{7}
15	3.04×10^{7}	2.99×10^{7}
20	1.08×10^{7}	1.04×10^{7}
25	3.72×10^{6}	3.72×10^{6}
30	1.32×10^{6}	1.35×10^{6}
35	4.96×10^{5}	5.21×10^{5}
40	1.95×10^{5}	1.98×10^{5}
45	8.11×10^{4}	7.91×10^{4}
50	3.45×10^{4}	3.31×10^{4}
55	1.51×10^{4}	1.39×10^{4}
60	6.17×10^{3}	6.20×10^{3}
65	2.86×10^{3}	2.82×10^{3}
70	1.39×10^{3}	1.36×10^{3}
75	6.89×10^{2}	6.72×10^{2}
80	3.43×10^{2}	3.36×10^{2}
85	1.77×10^{2}	1.72×10^{2}
90	9.32×10^{1}	8.79×10^{1}
95	4.97×10^{1}	4.48×10^{1}
100	2.67×10^{1}	2.39×10^{1}
105	1.47×10^{1}	1.29×10^{1}
110	8.20×10^{0}	7.14×10^{0}
115	4.64×10^{0}	3.97×10^{0}
120	2.65×10^{0}	2.23×10^{0}
125	1.58×10^{0}	1.27×10^{0}
130	9.63×10^{-1}	7.55×10^{-1}
135	5.98×10^{-1}	4.55×10^{-1}
140	3.81×10^{-1}	2.80×10^{-1}
145	2.55×10^{-1}	1.78×10^{-1}
150	1.77×10^{-1}	1.12×10^{-1}
155	1.27×10^{-1}	7.46×10^{-2}
160	9.44×10^{-2}	5.15×10^{-2}

References

[1]E. P. Blizard, p. 131 in "Shielding," Volume III, Part B of *Reactor Handbook*, 2d ed. (ed. by E. P. Blizard and L. S. Abbott), Interscience, New York, 1962.

[2]The original derivation of the transformation is credited to H. Hurwitz of Knolls Atomic Power Laboratory.

[3]D. R. Otis, *The Lid Tank Shielding Facility at Oak Ridge National Laboratory. Part II*, ORNL-2350 (1959).

[4]This instrumentation has been described by D. W. Cady, *The Lid Tank Shielding Facility at Oak Ridge National Laboratory. Part III. Instrumentation*, ORNL-2587 (Rev.) (1960).

3.6. A COMPARISON OF FIRST- AND LAST-FLIGHT EXPECTATION VALUES USED IN AN O5R MONTE CARLO CALCULATION OF THE NEUTRON DISTRIBUTION IN WATER[1]

D. K. Trubey M. B. Emmett[2]

In the solution of particle transport problems by Monte Carlo, a common method of scoring in the analysis of particle random walks is the use of expectation values or statistical estimation.[3] The technique introduces the concept of detectors placed at arbitrary positions. The probability that a particular collision contributes to the quantity being calculated is summed over each history and averaged for each detector. The usual procedure is to calculate the probability that a particle will arrive at the detector from each collision without further scatterings. This may be called the "last-flight" expectation value since the probability is calculated for the particle's last flight before being observed at the detector.

It is possible in many cases, however, to compute the flux expectation value for any particular flight. The technique is to "stretch" the flight so that the collision being examined in the analysis is located at the detector site. This amounts to calculating a sequence of random walks by Monte Carlo except for one flight length, which is determined. The probability for this flight length is calculated analytically.

In most physical problems involving particle slowing down the cross section rises with decreasing energy. Hence most of the transport (associated with long flight paths) is accomplished at high energy. This is particularly true with neutrons in hydrogenous media. Therefore it is expected that first-flight stretching might be more successful than last-flight stretching.

In the calculation reported here, the O5R Monte Carlo code (see Sect. 5.3) was used to generate neutron histories in an infinite water medium. All collisions were treated by both the first- and the last-flight technique.

The first-flight estimator, or score, is determined as follows. The location of the end point of each flight is translated parallel to the neutron's original direction until it coincides with the detector sphere. This determines the location of the first collision. The flux is then given by

$$4\pi R^2 \ \phi(R) = \frac{1}{N} \sum_i \frac{W_i \Sigma_0 \, e^{-\Sigma_0 z}}{\Sigma \, |\cos \alpha|} ,$$

where

R = distance from source,

$\phi(R)$ = flux,

W = statistical weight,

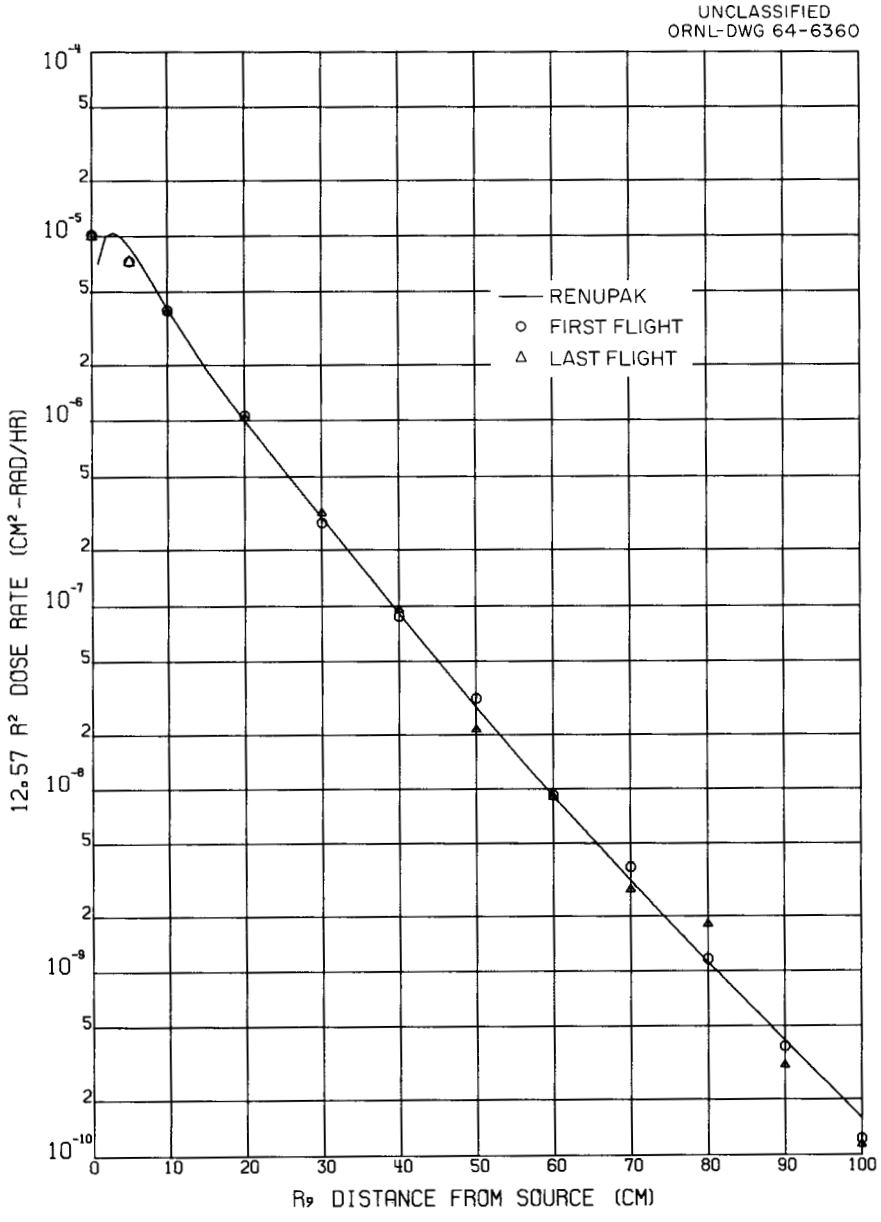

Fig. 3.6.1. Neutron Dose Rate in Water from a Fission Source (Picked Uniformly).

z = "stretched" flight distance,

Σ_0 = total cross section at energy of particle on stretched flight,

Σ = total cross section at energy of particle on flight i,

α = angle of collision location on sphere measured from neutron's initial direction, and

N = number of case histories.

The last-flight estimator is calculated similarly except that the angle α is the angle between the stretched-flight direction and the detector sphere normal.

Both methods gave results for water and a Watt fission source that agree very well with RENUPAK[4] moments method results (see Sect. 3.7) out to about 40 to 50 cm from the source, which in turn agree well with experimental results.[5] The first-flight results generally have a smaller variance; this is particularly noticeable in the energy spectra results.

Results were also obtained with the source energy picked uniformly and weighted with the fission spectrum. These results (10,000 case histories) were generally satisfactory to about twice as far (see Fig. 3.6.1).

References

[1]Summary of report to be published as RSIC-3.
[2]Mathematics Division.
[3]G. Goertzel and M. H. Kalos, p. 315 in *Progress in Nuclear Energy, Series I, Physics and Mathematics*, Vol. 2, Pergamon, New York, 1958.
[4]J. Certaine, E. deDufour, and G. Rabinowitz, *Nucl. Sci. Eng.* **12**, 446 (1962).
[5]D. R. Otis, *Neutron and Gamma-Ray Attenuation for a Fission Source in Water – Comparison of Theory with LTSF Measurements*, ORNL-CF-57-3-48 (1957).

3.7. CALCULATION OF FISSION-SOURCE THERMAL-NEUTRON DISTRIBUTION IN WATER BY THE TRANSFUSION METHOD[1]

D. K. Trubey

A calculational method which combines transport theory and diffusion theory, called the "transfusion" method, has been used to obtain the thermal-neutron flux from a point isotropic fission source in water. The transport theory code RENUPAK, which utilizes the moments method, was used to calculate the energy-spatial neutron distribution above 1 kev, and the multigroup diffusion code MODRIC was used to continue the calculation down to thermal energies. The resulting thermal-neutron fluxes agree very well with experimental results for distances out to 70 cm from the source, but the calculated fluxes are as much as 40% higher for greater distances.

References

[1]Abstract of ORNL-3487 (August 1964).

3.8. SOME CALCULATIONS OF THE FAST-NEUTRON DISTRIBUTION IN ORDINARY CONCRETE FROM POINT AND PLANE ISOTROPIC FISSION SOURCES[1]

D. K. Trubey M. B. Emmett[2]

The fast-neutron dose rates and energy distributions for point and plane isotropic fission sources in an infinite medium of ordinary concrete have been calculated by the moments method code RENUPAK. The effect of varying the concrete composition (especially hydrogen content) and lower energy cutoff was examined for several cases and was found to be significant. Detailed tables of energy spectra are given at lethargy steps of 0.1 from 0.001 to 18 Mev. Monte Carlo calculations were performed as a check and gave results that were in good agreement with the RENUPAK results.

References

[1]Abstract of ORNL-RSIC-4 (in press).
[2]Mathematics Division.

3.9. A CALCULATION OF THE NEUTRON DOSE IN ORDINARY CONCRETE DUE TO AIR-SCATTERED NEUTRONS FROM A POINT FISSION SOURCE[1]

D. K. Trubey

The results of a calculation of the fast-neutron dose at various depths within an infinite concrete

slab located at a distance of 100 g/cm^2 from a point fission source in air are given. These results may be used to predict the dose in bomb shelters. The moments method code, RENUPAK, was used successively to produce the energy spectrum in air from the point source and the energy spectrum in the concrete from the air-scattered source. Angular distribution conversion factors and data to convert to other amounts of air attenuation are given.

References

[1]Abstract of TM-973 (in press).

3.10. MEASUREMENTS OF THE ANGULAR DEPENDENCE OF FAST-NEUTRON DOSE REFLECTED FROM CONCRETE[1]

F. J. Muckenthaler K. M. Henry L. B. Holland
J. L. Hull J. J. Manning D. R. Ward

In connection with predicting radiation intensities in concrete structures of interest to the Defense Atomic Support Agency, research has been completed to determine in detail the fast-neutron differential dose albedo of concrete. An experimental program was performed at the Tower Shielding Facility concurrently with a Monte Carlo calculation (see Sect. 3.11) to obtain the dose rate

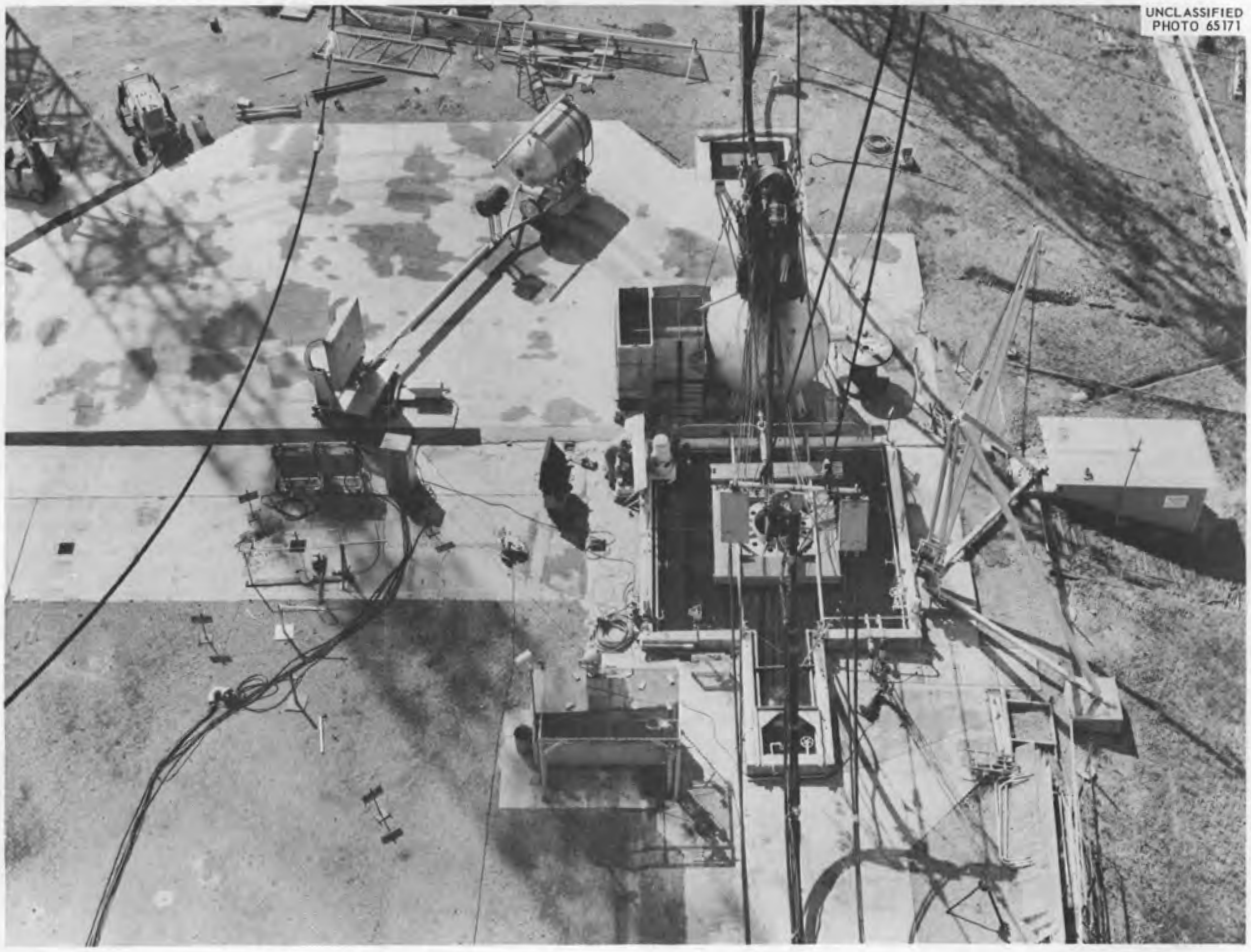

Fig. 3.10.1. Experimental Arrangement for Measurements of Fast Neutrons Reflected from Concrete.

scattered from a concrete slab as a function of the angle of incidence and emergence. This provided two independent determinations of many of the quantities of interest, and their agreement validates the results.

A highly collimated beam of neutrons was obtained for this experiment by placing a 92-in.-thick water shield adjacent to the 15-in.-diam beam port of the Tower Shielding Reactor II beam shield as shown in Fig. 3.10.1. This additional shielding contained a stepped collimator with the neutron beam emerging through a duct $2\frac{3}{4}$ in. in diameter and 36 in. long. Neutron dose rates were measured at points 8 and 24 ft from the end of the collimator in planes perpendicular to its axis. These results were integrated to obtain the total dose rate incident upon the surface of a concrete slab placed at these locations. The neutron spectrum from this reactor was determined earlier.[2]

The concrete slab, 6 ft square and 9 in. thick, was attached to a turntable that rotated the slab about both its vertical and horizontal axes. The pivot point was located in the middle of the surface of the slab upon which the neutrons were incident. The slab was placed at the 24-ft location, where it was rotated through angles of 45° or less with respect to the reactor collimator center line. For angles of rotation between 45 and 75° it was necessary to move the slab to the 8-ft location so that it would completely intercept the neutron beam.

A fast-neutron dosimeter and a modified long counter were used to measure the scattered neutron dose rate at a fixed distance of 31 ft from the center of the slab surface. The detectors were moved through an arc in the horizontal plane that passed through the reactor beam center line while the slab was rotated about both its horizontal and vertical axes. This permitted the determination of scattered dose rates for nearly all combinations of four angles of beam incidence (θ_0) and nine polar (θ) and six azimuthal (ϕ) angles of emergence.

Typical results are compared with Monte Carlo calculations made for each configuration in Table 3.10.1. The agreement between the individual calculated values and the measured results is such that the computed root mean square deviation $\left\{\sum_{\text{all } 151} [1-(\text{calc/meas})]^2\right\}^{1/2}/151$ is 3.0% and the largest deviation is 9%.

Table 3.10.1. Dose Rates for Fast Neutrons Scattered from Concrete

(Neutron beam incident at 60°; detector 31 ft from slab)

θ (deg)	ϕ (deg)	Fast-Neutron Dose Rates (ergs g^{-1} hr^{-1} w^{-1})	
		Calculated	Measured
19	15	4.69×10^{-7}	4.92×10^{-7}
19	45	4.66×10^{-7}	4.90×10^{-7}
19	75	4.67×10^{-7}	4.83×10^{-7}
19	105	4.74×10^{-7}	4.88×10^{-7}
19	135	4.82×10^{-7}	4.92×10^{-7}
19	165	4.86×10^{-7}	5.02×10^{-7}
33.5	15	4.54×10^{-7}	4.77×10^{-7}
33.5	45	4.45×10^{-7}	4.61×10^{-7}
33.5	75	4.37×10^{-7}	4.58×10^{-7}
33.5	105	4.43×10^{-7}	4.56×10^{-7}
33.5	135	4.57×10^{-7}	4.77×10^{-7}
44	15	4.31×10^{-7}	4.58×10^{-7}
44	45	4.19×10^{-7}	4.26×10^{-7}
44	75	4.04×10^{-7}	4.10×10^{-7}
44	105	4.08×10^{-7}	4.15×10^{-7}
44	135	4.22×10^{-7}	4.31×10^{-7}
52	15	4.13×10^{-7}	4.51×10^{-7}
52	45	3.85×10^{-7}	4.08×10^{-7}
52	75	3.66×10^{-7}	3.78×10^{-7}
52	105	3.66×10^{-7}	3.67×10^{-7}
52	135	3.80×10^{-7}	3.90×10^{-7}
60	15	3.98×10^{-7}	4.26×10^{-7}
60	45	3.44×10^{-7}	3.67×10^{-7}
60	75	3.21×10^{-7}	3.24×10^{-7}
60	105	3.16×10^{-7}	3.19×10^{-7}
60	135	3.30×10^{-7}	3.35×10^{-7}
67	15	3.78×10^{-7}	3.92×10^{-7}
67	45	2.99×10^{-7}	3.19×10^{-7}
67	75	2.66×10^{-7}	2.69×10^{-7}
67	105	2.59×10^{-7}	2.60×10^{-7}
67	135	2.72×10^{-7}	2.76×10^{-7}
74	15	3.33×10^{-7}	3.33×10^{-7}
74	45	2.43×10^{-7}	2.62×10^{-7}
74	75	2.03×10^{-7}	2.06×10^{-7}
74	105	1.95×10^{-7}	1.88×10^{-7}
74	135	2.05×10^{-7}	2.03×10^{-7}
80.4	15	2.47×10^{-7}	2.58×10^{-7}
80.4	45	1.68×10^{-7}	1.68×10^{-7}
80.4	75	1.28×10^{-7}	1.28×10^{-7}
80.4	105	1.22×10^{-7}	1.22×10^{-7}
80.4	135	1.29×10^{-7}	1.24×10^{-7}
86.8	15	1.01×10^{-7}	1.06×10^{-7}
86.8	45	6.41×10^{-8}	6.48×10^{-8}
86.8	75	4.42×10^{-8}	4.47×10^{-8}
86.8	105	4.17×10^{-8}	4.06×10^{-8}
86.8	135	4.37×10^{-8}	4.13×10^{-8}

References

[1]Work funded by Defense Atomic Support Agency under DASA Order Nos. E-0-800-63 and -64.

[2]F. J. Muckenthaler *et al.*, *Neutron Phys. Div. Ann. Progr. Rept. Aug. 1, 1963*, ORNL-3499, Vol. I, Fig. 3.12.2, p. 159.

3.11. A CALCULATION OF THE FAST-NEUTRON DIFFERENTIAL DOSE ALBEDO FOR CONCRETE[1]

R. E. Maerker

Interest in obtaining fast-neutron differential albedo information for various materials has been generated recently in connection with solving multibend air-duct transmission problems. It is conjectured that the duct problem can be divided into two simpler problems: (1) determination of all those parameters which adequately describe the reflection process for the wall material, assumed to be infinitely thick and to have a planar surface, and (2) use of this information in a Monte Carlo calculation or some other geometry-dependent calculation to obtain the duct transmission.

Monte Carlo results for the first of these two problems have been obtained for the case of fast neutrons incident on concrete in considerably more detail than those published previously.[2] In particular, the results reported here are for incident neutrons in groups having an energy spread of the order of 1 Mev, which averages over fluctuations in the cross sections. Six incident energy groups were used, encompassing the range 200 kev to 8 Mev, each group being a "gun barrel" source incident on the planar concrete surface at each of five angles to the normal: 0, 45, 60, 75, and 85°. In each of the 30 problems run, determined by the combination of the incident energy spread ΔE_0 and the angle to the normal θ_0, the following quantities were calculated: (1) the distribution of the reflected neutrons in the radial distance R along the surface with respect to their point of incidence as a function of θ, the emergent polar angle, and ϕ, the emergent azimuthal angle, (2) the same as (1) for singly scattered neutrons only, (3) the differential energy spectra of the reflected neutrons as a function of θ and ϕ, and (4) the distribution in depth within the concrete of the collision density, which gives rise to the reflected neutrons, as a function of R and θ.

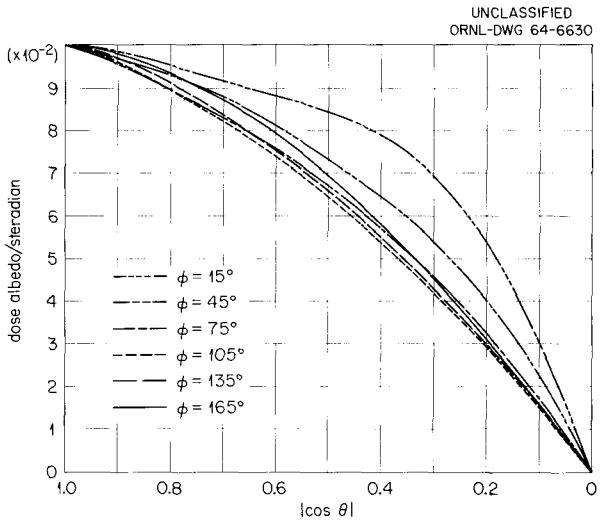

Fig. 3.11.1. Dose Albedo per Steradian for 1.5- to 3-Mev Neutrons Incident on Concrete at 60° from the Normal as a Function of θ and ϕ.

The differential angular dose albedo (reflected angular flux integrated over the surface in dose units per incident neutron in dose units) has a statistical uncertainty of around 5%, and the double differential dose albedo (per steradian per Mev) an uncertainty averaging around 10%. This accuracy was achieved by employing the technique of statistical estimation at each scattering point to calculate the probability of escape into each of 54 discrete directions, determined by a space-fixed grid of nine values of θ and six values of ϕ.

Figure 3.11.1 shows the behavior of the Monte Carlo results for the differential angular dose albedo as a function of θ and ϕ for the case $\theta_0 = 60°$ and $\Delta E_0 = 1.5$ to 3 Mev.

References

[1]Work funded by Defense Atomic Support Agency under DASA Order Nos. EO-800-63 and -64.

[2]F. J. Allen, A. Futterer, and W. Wright, *Neutron Reflection and Flux Versus Depth for Concrete*, BRL-1189 (January 1963).

3.12. AN ANGLE-DEPENDENT ALBEDO FOR FAST-NEUTRON REFLECTION CALCULATIONS[1]

R. L. French[2] M. B. Wells[2]

An albedo model for calculating the dose due to fast neutrons reflected from materials of low to moderate hydrogen content has been developed through analysis of extensive Monte Carlo data. The model, which was developed from reflection data for iron, concrete, and three types of soil, is for reflection to a unit nondirectional receiver and is of the form

$$\alpha(E_0) \cos^{2/3} \theta_0 \cos \theta ,$$

where $\alpha(E_0)$ is a coefficient tabulated as a function of incident energy E_0 for the various materials and θ_0 and θ are, respectively, the angles of incidence and reflection (both measured from the normal). The differential albedo, in units of reflected dose per steradian per unit dose incident at angle θ_0, may be converted to a total albedo by multiplying by π. The total dose albedo for normally incident fission neutrons was found to be closely approximated by $0.435\ (\Sigma_T - \Sigma_H)/\Sigma_T$, where Σ_T is the macroscopic total cross section of all elements of the material and Σ_H is the macroscopic cross section of the hydrogen of the material, both weighted by the fission spectrum.

References

[1]Abstract of published paper: *Nucl. Sci. Eng.* **19**, 441–48 (1964); work performed for Oak Ridge National Laboratory under Subcontract No. 2267; work funded by Defense Atomic Support Agency under DASA Order EO-800-63.

[2]Radiation Research Associates, Inc., Fort Worth, Tex.

3.13. A FIRST-LAST COLLISION MODEL OF THE AIR-GROUND INTERFACE EFFECTS ON FISSION NEUTRON DISTRIBUTIONS[1]

R. L. French[2]

A method has been developed for predicting the effect of an air-ground interface on the fast-neutron flux or dose at large distances from a point isotropic source of neutrons in air. The method yields numerical values for functions $f(H_S)$ and $f(H_D)$, which may be used to express the fast-neutron intensity as a function of source height H_S, receiver height H_D, and source-receiver separation distance R, in terms of the corresponding infinite air medium intensity $I(R)$. Thus

$$I(H_S, H_D R) = f(H_S) f(H_D) I(R) .$$

The method is called the "first-last collision model" because it is based on the influence of the ground upon the distribution of "first" collisions of neutrons about the source and of "last" collisions about the receiver. Generalized numerical results have been computed and means have been developed for applying these results to specific cases of interest. Comparisons of these results with those derived from Monte Carlo calculations and from experiments performed at the ORNL Tower Shielding Facility and the Nevada Test Site indicate that the first-last collision model predicts the fraction of the infinite air medium intensity within 5% in almost all cases.

References

[1]Abstract of RRA-M32 (November 1963); work performed for Oak Ridge National Laboratory under Subcontract No. 2267; work funded by Defense Atomic Support Agency under DASA Order EO-800-63.

[2]Radiation Research Associates, Inc., Fort Worth, Tex.

3.14. ANGULAR DISTRIBUTION OF THE AIR-SCATTERED FAST-NEUTRON DOSE RATE AT THE AIR-GROUND INTERFACE[1]

M. B. Wells[2]

The spatial and angular distributions of the fast-neutron dose rate in air as calculated by Monte Carlo methods are used to predict the results of fast-neutron dose-rate measurements taken in unshielded vertical concrete-lined cylindrical holes at the ORNL Tower Shielding Facility. The agreement of the predictions with the measured

data demonstrates that (1) the air-scattered fast-neutron dose rate entering the holes is not appreciably affected by the presence of the air-ground interface, (2) the angular distribution of the air-scattered fast-neutron dose rate entering the holes for a given reactor angle does not vary significantly with distance for source-detector separation distances between 100 and 450 ft, and (3) simplified calculational techniques based on the use of infinite-medium air-transport data for fast neutrons can be used to adequately predict the fast-neutron radiation environment incident upon and in the holes.

References

[1]Abstract of RRA-M33 (November 1963); work performed for Oak Ridge National Laboratory under Subcontract No. 2267; work funded by Defense Atomic Support Agency under DASA Order EO-800-63.

[2]Radiation Research Associates, Inc., Fort Worth, Tex.

3.15. REFLECTION OF THERMAL NEUTRONS AND NEUTRON-CAPTURE GAMMA RAYS FROM CONCRETE[1]

M. B. Wells[2]

Monte Carlo methods were used to compute thermal-neutron and thermal-neutron-capture gamma-ray differential albedos for portland concrete and for the concrete used in several underground structures at the ORNL Tower Shielding Facility. The results obtained for the thermal-neutron differential albedo for portland concrete were fitted by the expression $0.21 \cos^{2/3} \theta_0 \cos \theta$, where θ_0 and θ are the angles of incidence and reflection respectively. The total thermal-neutron flux reflected per unit incident flux was found to be given by $0.414 \pi \cos \theta_0$ for the TSF concrete and by $0.42 \pi \cos^{2/3} \theta_0$ for portland concrete.

The results for the neutron-capture gamma-ray dose reflected from concrete per unit incident thermal-neutron flux were fitted by the expression $1.046 \times 10^{-5} \cos^{5/4} \theta_0 \cos^{2/3} \theta$ for the TSF concrete and by the expression $6.986 \times 10^{-6} \cos \theta_0 \cos \theta$ for the portland concrete. The units of the above albedos are ergs g^{-1} hr^{-1} steradian^{-1} per unit incident thermal-neutron flux.

The results for the total thermal-neutron reflection from both the TSF and the portland concretes were found to be in reasonably good agreement with those obtained from albedo expressions derived by Fermi[3] and by Halpern *et al.*[4] Calculations of the neutron-capture gamma-ray dose rates inside 4-ft-diam concrete-lined cylindrical holes dug in the ground at the TSF show, when compared with measured data, that the major component of the gamma-ray dose rate in the holes is that resulting from thermal-neutron capture in the concrete walls.

(Editor's Note: The following paragraph reports work performed subsequent to the publication of RRA-M44.) The results of a Monte Carlo calculation of the neutron-capture gamma-ray dose albedo in which the measured thermal-neutron flux profile in a 12-in.-thick slab of TSF-type concrete was used as input data were fitted by the expression $6.14 \times 10^{-6} \cos \theta$ (ergs g^{-1} hr^{-1} steradian^{-1} per unit thermal-neutron flux measured at the slab surface). This expression, when used in calculations to predict the thermal-neutron-capture gamma-ray dose rates inside concrete-lined cylindrical holes, was found to produce calculated results which are in good agreement with measured gamma-ray dose rates for the holes.

References

[1]Abstract of RRA-M44 (June 1964); work performed for Oak Ridge National Laboratory under Subcontract No. 2267; work funded by Defense Atomic Support Agency under DASA Order EO-800-63.

[2]Radiation Research Associates, Inc., Fort Worth, Tex.

[3]E. Fermi, *On the Motion of Neutrons in Hydrogenous Substances*, NP-2385 (1951).

[4]O. Halpern *et al.*, *Phys. Rev.* **53**, 173 (1938).

3.16. A STUDY OF THE RADIATION SHIELDING CHARACTERISTICS OF BASIC CONCRETE STRUCTURES AT THE TOWER SHIELDING FACILITY[1]

V. R. Cain

In the first of a series of experiments performed for the Department of Defense to investigate the protection afforded by various typical structures

against prompt weapons radiation, radiation-intensity measurements were made at the Tower Shielding Facility in two concrete-shielded bunkers and in an interconnecting tunnel. Prompt weapons radiation was simulated by the Tower Shielding Reactor II (TSR-II), which was operated 100 ft above the ground. The distance between the reactor and the bunkers was approximately 700 ft. The bunkers were each 12-ft cubes and were constructed so that the shield thickness on the front face of one and on the top face of the other could be varied in 4-in. steps from 0 to 20 in. The thickness of concrete and dirt surrounding all other faces was sufficient to make them black to incident radiation.

The immediate goals of the experiment were to study (1) the attenuation of radiations by various thicknesses of ordinary concrete slabs, (2) the buildup of radiation intensities within the cavities by scattering of radiation in the walls, and (3) the transmission of radiation down a tunnel with two right-angle bends. Also reported are the gamma-ray and fast-neutron dose rates and thermal-neutron fluxes measured at various positions within the bunkers and in the tunnel and the pulse-height spectra from a 3-in. sodium iodide crystal determined at one position in the top bunker and one position in the tunnel.

References

[1]Abstract of ORNL-3464 (January 1964); work funded by Office of Civil Defense under Subcontract OCD-OS-62-145.

3.17. MEASUREMENTS OF RADIATION INTENSITIES IN VERTICAL CONCRETE-LINED HOLES AND AN ADJOINING TUNNEL AT THE TOWER SHIELDING FACILITY[1]

V. R. Cain C. E. Clifford L. B. Holland

Fast-neutron and gamma-ray dose rates within 4-ft-diam, 20-ft-deep, concrete-lined holes have been measured at the ORNL Tower Shielding Facility. The radiation source was the Tower Shielding Reactor II (TSR-II) enclosed in a shield which modified the neutron to gamma-ray ratio of the reactor leakage spectrum to more closely resemble that of a weapon spectrum. The holes were located at horizontal distances of 100, 228, and 450 ft from the reactor. From the hole at 100 ft extended a reinforced concrete-lined tunnel, 6 ft high, $2\frac{1}{2}$ ft wide, and 20 ft long, with its ceiling 10 ft below ground level. The experimental measurements consisted of vertical traverses in the three holes and horizontal traverses in the tunnel. The parameters varied included distance from the reactor, the angle of elevation of the reactor with respect to the horizontal at the hole, and the material and thickness of the shield over the hole. Reactor elevation angles ranged from 15 to 90°. The shields over the holes were concrete, iron, and laminated iron and concrete slabs.

References

[1]Abstract of ORNL-3513 (March 1964); work funded by the U.S. Air Force and the Office of Civil Defense under Subcontracts AF-(04-694)-62-2 and OCD-OS-62-145.

3.18. CALCULATIONS OF THERMAL-NEUTRON FLUX DISTRIBUTIONS IN CONCRETE-WALLED DUCTS USING AN ALBEDO MODEL WITH MONTE CARLO TECHNIQUES[1,2]

V. R. Cain

When radiation shields are penetrated by ducts, the gamma rays resulting from the radiative capture of low-energy neutrons in the duct walls can be principal contributors to the total dose along the duct. In order to calculate the effect of these capture gamma rays, the distribution of low-energy neutrons in the ducts must be known. This report presents calculations of low-energy neutron distributions in concrete-walled ducts by a method in which an albedo model and a Monte Carlo technique were used. One series of calculations was performed for straight ducts so that comparisons could be made with the Simon-Clifford analytic approximation. Another series was for three-legged rectangular ducts similar to those used in a Tower Shielding Facility experiment. When an albedo similar to that to be expected for a pure thermal-neutron source was used, the results agreed very closely with the TSF data. A digital computer code was written to perform the calculations.

References

[1]Abstract of ORNL-3507 (January 1964).
[2]Work funded by Defense Atomic Support Agency under DASA Order EO-800-63.

3.19. PENETRATION OF NEUTRONS AND GAMMA RADIATION THROUGH THE OPENINGS OF UNDERGROUND STRUCTURES[1]

R. L. French[2] M. B. Wells[2] N. M. Schaeffer[2]

Calculations were performed of the radiation intensities in open concrete-lined cylindrical holes and in open concrete bunkers due to a fission source located in air at distances of 100 to 700 ft. The calculations are part of an analysis of experiments performed with the ORNL Tower Shielding Reactor II (TSR-II), which included numerous radiation measurements in the underground structures with and without shields over the openings (see Sects. 3.16 and 3.17). The approach followed in the calculations was to determine, from geometric considerations, the portion of the incident radiation intensities that could enter the structures. Methods were developed to account for effects of the air-ground interface, and albedo models were devised to simplify calculation of the wall-scattered dose and production of secondary radiation in the walls. In general, the calculated and measured data agree within approximately 25%.

References

[1]Abstract of RRA-T41 (in press); work performed for Oak Ridge National Laboratory under Subcontract No. 2267; work funded by Defense Atomic Support Agency under DASA Order EO-800-63.
[2]Radiation Research Associates, Inc., Fort Worth, Tex.

3.20. MEASUREMENT OF FAST-NEUTRON TRANSMISSION THROUGH AN "INFINITE" SLAB OF LiH

F. J. Muckenthaler J. L. Hull
K. M. Henry J. J. Manning
L. B. Holland D. R. Ward

As part of the SNAP Shielding Program, extensive measurements utilizing simple source and infinite-slab geometries have been made of the fast-neutron dose transmitted through thick lithium hydride shields, and most of the results have been compared with Monte Carlo predictions (see Sect. 3.21). Transmission measurements were made for both a normally incident beam and for slant-incident beams up to 60° and for slab thicknesses that varied from 1 to 30 in. Detectors were located both near the back surface of the slab and far from it. For some of the slant-incident cases, emergent dose angular distributions were also measured with a tightly collimated detector.

The Tower Shielding Reactor II was placed inside a lead-water shield which contained a stepped opening at the horizontal midplane of the shield from which a collimated beam of neutrons emerged. The diameter of the opening was 15 in. for the outer 2-ft section and 10 in. for the inner 2-ft section. For part of the experiments the outer section was plugged with a 6-in.-ID collimator 30 in. long. The neutron intensity incident on the LiH shield surface was measured in a plane perpendicular to the collimator center line in the vertical and horizontal direction for both collimator configurations. The neutron spectrum of the beam was measured with a shielded diode fast-neutron spectrometer.[1]

The slabs of LiH used in this experiment were 5 ft square and 1, 2, 6, and 12 in. thick, each contained in $\frac{1}{8}$-in.-thick aluminum. The measurements of the transmitted neutron dose were made with a Hurst neutron dosimeter and a Hornyak button on the beam center line 4 in. from the back of the slab and at several distances from the front of the slab. Measurements were also made with a modified long counter.

Experimental results for the normally incident beam are compared in Table 3.20.1 with some Monte Carlo calculations for the same shield-detector configuration. The neutron beam was approximated as a source uniformly distributed over a disk, constant in solid angle up to the half angle of the reactor collimator and zero elsewhere, with the disk located at an appropriate distance from the slab.

References

[1]F. J. Muckenthaler *et al.*, *Neutron Phys. Div. Ann. Progr. Rept. Aug. 1, 1963,* ORNL-3499, Vol. I, Fig. 3.12.2, p. 159.

Table 3.20.1. Experimental and Calculated Dose Rates of Fast Neutrons Transmitted Through LiH

LiH Thickness (in.)	Fast-Neutron Dose Rate (ergs g^{-1} hr^{-1} w^{-1})			
	6-in.-diam Beam		15-in.-diam Beam	
	Measured	Calculated	Measured	Calculated
	Detector 4 in. Behind LiH			
0	9.36×10^{-1}	9.36×10^{-1}	1.20×10^{0}	1.20×10^{0}
1	4.49×10^{-1}	4.46×10^{-1}	7.34×10^{-1}	7.94×10^{-1}
3	1.64×10^{-1}	1.58×10^{-1}	3.19×10^{-1}	3.59×10^{-1}
6	3.85×10^{-2}	3.87×10^{-2}	8.75×10^{-2}	1.27×10^{-1}
9	8.12×10^{-3}	8.70×10^{-3}	2.30×10^{-2}	3.45×10^{-2}
12	1.86×10^{-3}	2.30×10^{-3}	5.59×10^{-3}	1.03×10^{-2}
18	1.30×10^{-4}	1.88×10^{-4}	5.31×10^{-4}	9.06×10^{-4}
24	1.12×10^{-5}	2.40×10^{-5}	4.58×10^{-5}	9.32×10^{-5}
30	1.30×10^{-6}	2.16×10^{-6}	7.13×10^{-6}	9.20×10^{-6}
	Detector 16.5 ft from Source for 6-in. Beam; 18.5 ft for 15-in. Beam			
0	3.67×10^{-2}	3.67×10^{-2}	7.98×10^{-2}	7.98×10^{-2}
1	1.90×10^{-2}	1.93×10^{-2}	4.47×10^{-2}	4.28×10^{-2}
3	5.51×10^{-3}	5.67×10^{-3}	1.37×10^{-2}	1.31×10^{-2}
6	9.18×10^{-4}	9.77×10^{-4}	2.69×10^{-3}	2.56×10^{-3}
9	1.89×10^{-4}	1.99×10^{-4}	6.27×10^{-4}	5.70×10^{-4}
12	3.73×10^{-5}	4.66×10^{-5}	1.40×10^{-4}	1.53×10^{-4}
18	2.67×10^{-6}	3.43×10^{-6}	1.27×10^{-5}	1.43×10^{-5}
24	2.58×10^{-7}	3.28×10^{-7}	1.61×10^{-6}	1.52×10^{-6}
30	3.56×10^{-8}	5.15×10^{-8}	2.51×10^{-7}	2.10×10^{-7}

3.21. MONTE CARLO CALCULATIONS OF NEUTRON TRANSMISSION THROUGH LITHIUM HYDRIDE

F. H. Clark F. B. K. Kam

The O5R Monte Carlo code (see Sect. 5.2) has been used with apparent success in computing neutron penetrations through infinite lithium hydride slabs. Thicknesses up to about 60 g/cm^2 have been considered. Sources used were isotropic distributions on a disk and collimated beams whose energy spectra resemble a fission spectrum.[1] The code has also been used to study conical-shell and disk-type shields (Fig. 3.21.1) for a point source.

The results of the isotropic-source study for the slab shields have been reported elsewhere,[2] and it need only be stated here that measurements subsequently reported[3] have been in agreement with the calculations. The results of the collimated-beam source are compared in Fig. 3.21.2 with measurements made at the Tower Shielding Facility (see also Sect. 3.20).

The calculations for the conical-shell shield were performed to explore the advantages, if any, of using this shape rather than a disk shape for space satellite power plants. The fact that the shield material was lithium hydride was incidental to the geometry. The results showed that the disk configurations yielded lighter weight shields for the same dose at the payload on any reasonable basis of comparison (see Sect. 3.22).

Importance sampling was employed in all these calculations. Among the techniques used to good advantage were (1) biased selection of source energy, (2) biased selection of direction from source, (3) biased selection of the region of first collision, (4) biased path length, and (5) Russian Roulette with phase-space dependent standards.

UNCLASSIFIED
ORNL-DWG 64-6850

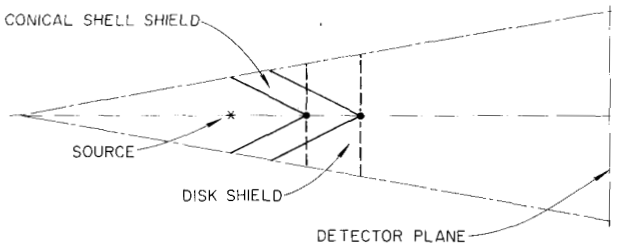

Fig. 3.21.1. Layout for Conical-Shell and Disk Shields.

Other techniques tried, but from which we have no clear demonstration of benefit, are splitting and biasing of the angle of scatter. This latter remark should not be construed to mean that these techniques are not valuable when appropriately used in a proper context.

There were some computations which did not compare favorably with measurement; however, in each such case there were flaws in the model used for computation, or the magnitude of the problem undertaken was sufficiently great to suggest the need for larger statistical samples or for more severe biasing techniques.

It appears that the existing computing system, that is, the O5R code as adapted to the lithium hydride penetration problem and the accompanying package of cross sections, is effective through 60 g/cm^2 for determining nondifferential output. This range of effectiveness can be increased with some further investment of effort.

References

[1]V. R. Cain, *A Study of the Radiation Shielding Characteristics of Basic Concrete Structures at the Tower Shielding Facility*, Fig. 4 (COOL-II spectrum), ORNL-3464 (1964).

[2]F. H. S. Clark, F. B. K. Kam, and N. A. Betz, *Trans. Am. Nucl. Soc.* **6**, 426 (1963).

[3]S. G. Wogulis and K. L. Rooney, *Experimental Studies of Neutron Attenuation in Natural Lithium Hydride Shields*, NAA-SR-9364 (1964).

UNCLASSIFIED
ORNL-DWG 64-6854

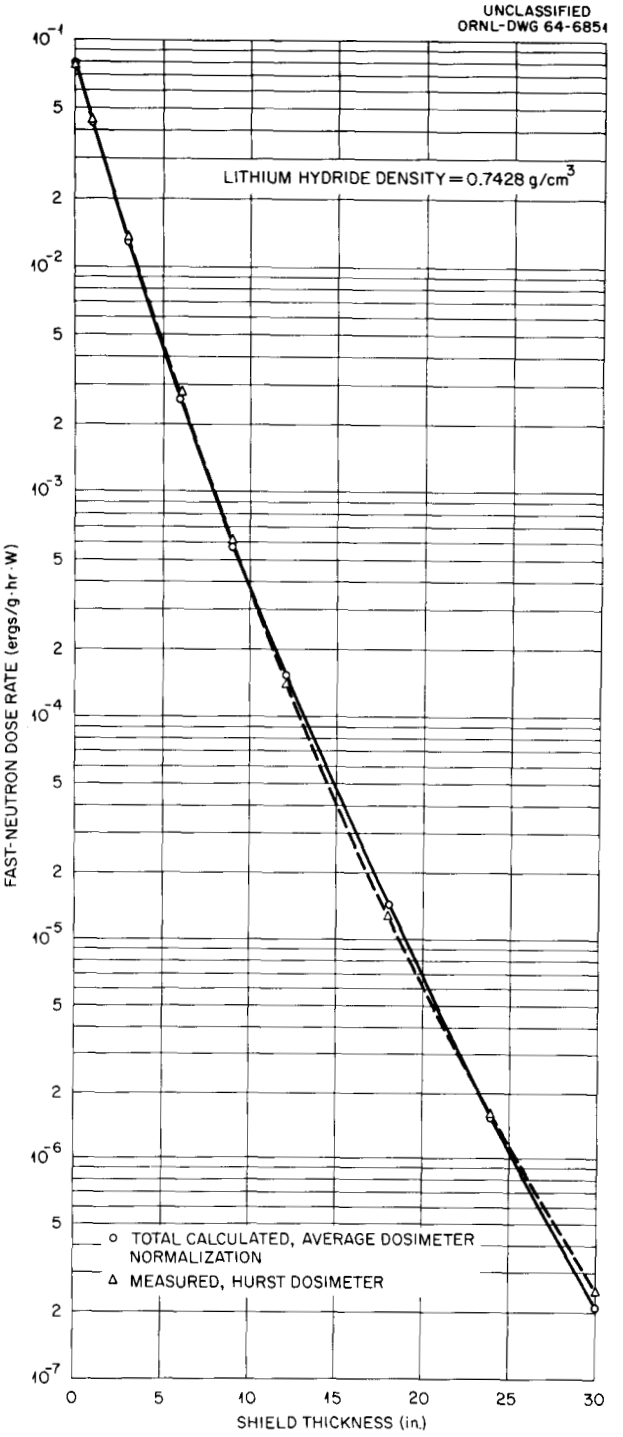

Fig. 3.21.2. Fast-Neutron Dose Rate 18.5 ft from Source for 15-in.-diam Collimated Beam.

3.22. A LITHIUM HYDRIDE CONICAL-SHELL NEUTRON SHADOW SHIELD[1]

F. H. Clark N. A. Betz[2]

A study has been made of the effectiveness of a (natural) lithium hydride shield that is formed into a conical shell and "wrapped around" a point neutron source with a near-fission spectrum. The source, detector, and cone axis are collinear with the detector 40 ft from the source. Additionally, the study covered disk shields of the same material located in approximately the same location. [Note: These geometries are shown in Fig. 3.21.1. Ed.] Evidently, there is some arbitrariness in positioning when one replaces a conical shell by a disk. If a comparison is made of a disk and a conical shell whose thicknesses measured parallel to the axis are the same, and, if the surfaces of the disk coincide with the apices of the conical shell, then the disk will provide much greater attenuation but will weigh much more. The conical shell appears to be slightly less effective than a disk which has the same normal thickness occluding the same solid angle at the source. Further, the weight of such a conical shell would exceed that of the corresponding disk.

References

[1]Abstract of TM-981 (in press).
[2]Mathematics Division.

3.23. SCATTERING OF FAST NEUTRONS FROM CYLINDERS OF LITHIUM HYDRIDE, GRAPHITE, CONCRETE, ALUMINUM, AND STEEL[1]

J. C. Courtney[2] V. V. Verbinski

Time-of-flight methods have been used to measure the spectra of neutrons scattered at several angles from small cylindrical samples of steel, aluminum, concrete, graphite, and lithium hydride. These measurements will not yield elastic- and inelastic-differential-scattering cross sections directly because the incident neutrons were not monoenergetic, and therefore no distinction can be made between an inelastic- and an elastic-scattering event. However, the data will serve as an inexpensive and useful check on the cross-section compilations used in neutron scattering calculations currently being performed in SNAP (Space Nuclear Auxiliary Power) and DASA (Defense Atomic Support Agency) shielding programs.[3] The measured source spectrum can be used as input to a scattering calculation, and the resulting calculated spectral intensities of the scattered neutrons can be compared with the measured spectral intensities. If the disagreement between the measurements and the calculations is small, as is expected, it can be compensated for in the calculations by adjusting either the elastic or the inelastic cross sections – whichever are the least well known.

The materials chosen for these measurements are those of specific interest to the SNAP and DASA shielding programs. The LiH cylinders were $1\frac{1}{2}$ and 3 in. in diameter; the concrete cylinders were $1\frac{3}{4}$ in. in diameter; and all other samples were 2 in. in diameter. The composition of the concrete is shown in Table 3.23.1.

The measurements were made at the General Atomic Electron Linear Accelerator (LINAC), where a pulsed source of bremsstrahlung-produced neutrons was obtained by irradiating a lead target with 14-nsec bursts of 34-Mev electrons. The energy spectrum of the neutrons approximated the spectrum of neutrons emitted by a pool-type reactor.[4] Some of these neutrons struck the scattering cylinder placed 13 in. from the lead target (see Fig. 3.23.1) and passed through a system of collimators and down a drift tube (55 m long) to an NE-213 liquid-scintillator fast-neutron detector.[5] Time-of-flight techniques were used to obtain the energies of the scattered neutrons.

Table 3.23.1. Composition of Concrete Cylinders

Element	Amount (wt %)
Oxygen	44.1
Silicon	23.8
Calcium	8.5
Aluminum	6.8
Sodium	2.5
Potassium	2.0
Iron	1.9
Others	10.4

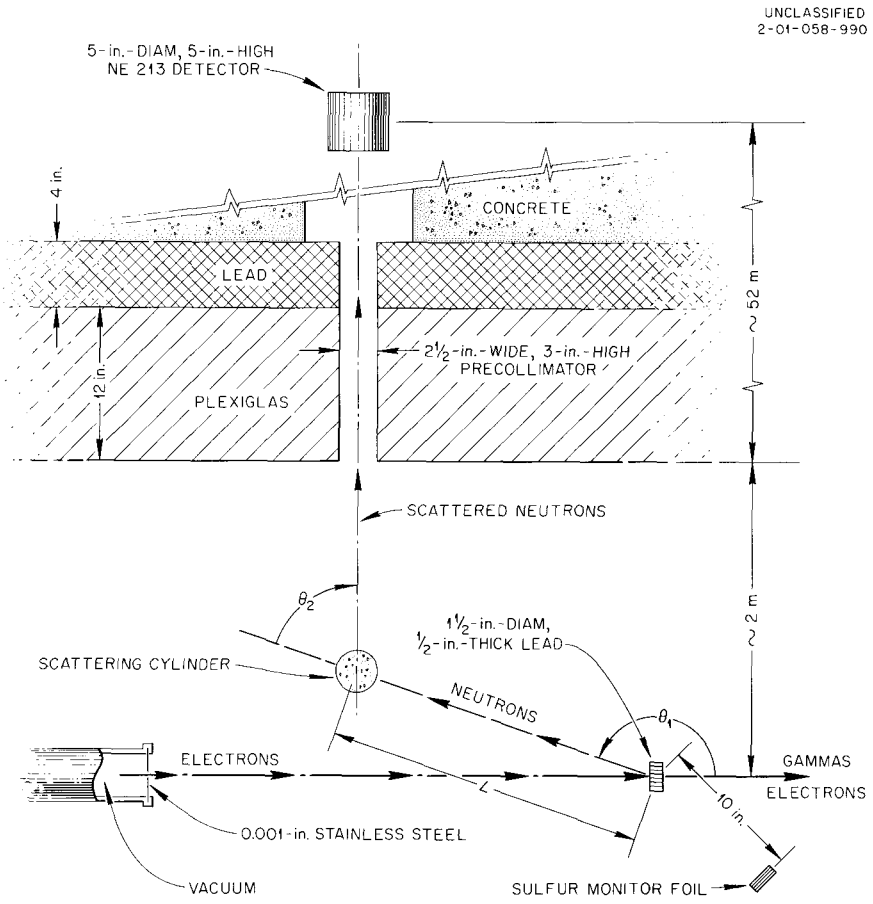

Fig. 3.23.1. Geometry for Time-of-Flight Measurements of Neutrons Scattered from Small Cylinders of Various Materials.

Pulse-shape discrimination circuitry was used during the experiment to eliminate pulses due to any gamma-ray background.[6] At the 14-nsec pulse width, the 55-m flight path afforded an energy resolution of 1% for 1-Mev neutrons and 3% for 10-Mev neutrons. A major effort has been undertaken to determine the efficiency of the detector as a function of bias setting when it is used for time-of-flight measurements such as these, and also to obtain the response function of the detector when it is used as an ordinary pulse-height spectrometer (see Sects. 6.1 and 6.2).

The measurements were made for eight values of the scattering angle θ_2 between 45 and 135° and four values of θ_1, the angle between the electron beam and the direction of the neutrons which hit the scattering cylinder. (As can be seen from Fig. 3.23.1, the geometry of the experiment is such that for a given value of θ_1 there are two values of θ_2.) The spectrum of source neutrons was obtained for each source angle through the use of a bending magnet on the LINAC beam. The time-integrated source intensity was monitored during each run by exposing a sulfur foil at a position 45° from the electron beam. This yielded a measure of the total integrated fast-neutron flux emitted from the lead during each run and also provided a means for properly normalizing the scattered flux to the source flux.

Typical results obtained during these measurements are given in Fig. 3.23.2, which shows the source spectrum for θ_1 = 135° and the spectral intensities of neutrons scattered from a 1¾-in.-diam by 2½-in.-long concrete cylinder at angles of 45

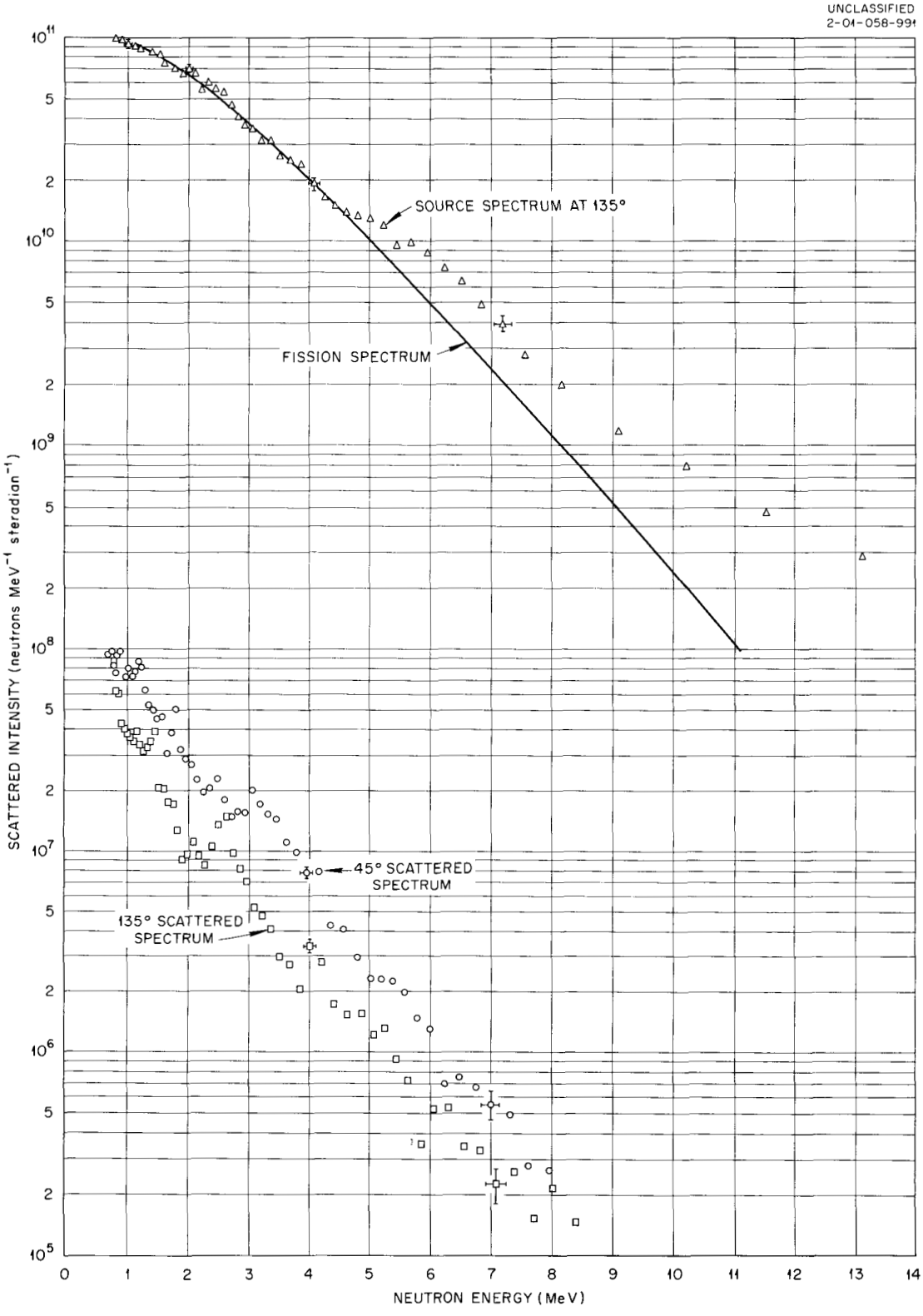

Fig. 3.23.2. Spectra of Neutrons Scattered for $1\frac{3}{4}$-in.-diam by $2\frac{1}{2}$-in.-long Concrete Cylinders.

and 135°. Also shown is a fission spectrum for comparison with the source spectrum. Note the shift in the resonances in the scattered spectra due to the change in scattering angle.

References

[1]Work partially funded by the U.S. Army Nuclear Defense Laboratory, Edgewood Arsenal, Md., under Order NDL-23-63.

[2]Catholic University, Washington, D.C.; Graduate Fellow, Oak Ridge Institute of Nuclear Studies.

[3]See, for example, F. B. K. Kam, F. H. Clark, and J. G. LaTorre, *Neutron Phys. Div. Ann. Progr. Rept. Aug. 1, 1963,* ORNL-3499, Vol. 1, p. 159, and sect. 3.15.

[4]See Fig. 3.3.5, ORNL-3499, Vol. I, *op. cit.*, p. 107.

[5]Nuclear Enterprises, Ltd., Winnepeg, Manitoba, Canada.

[6]V. V. Verbinski *et al.*, *Neutron Phys. Div. Ann. Progr. Rept. Sept. 1, 1962,* ORNL-3360, p. 105.

4. Radiation Shielding Information Center

4.1. PROGRAM OF THE RADIATION SHIELDING INFORMATION CENTER (RSIC)

S. K. Penny D. K. Trubey
B. F. Maskewitz

The program of the Radiation Shielding Information Center (RSIC) has been expanded to include shielding from weapons radiation,[1] and the technical functions of the Center have been intensified. Work has begun on state-of-the-art reports, and intercomparisons of the results produced by various digital computer codes are well under way.

RSIC is continually involved in its library functions. It has collected a large amount of shielding literature and has been responsible for a large number of translations of foreign shielding literature. New ways of presenting bibliographic references to the shielding community are continually being analyzed. The RSIC Computer Codes Section is also developing new methods for informing the shielding community about computer codes.

The technical function of providing advice and services to the community upon request is being utilized at the rate of approximately two requests per day.

The outlook for the next calendar year is that RSIC will become more of a technical institute and less of a library, hopefully in a more nearly optimum ratio.

References

[1]Work partially funded by Defense Atomic Support Agency under DASA Order No. EO-800-64.

4.2. RSIC INFORMATION RETRIEVAL SYSTEM

S. K. Penny M. B. Emmett[1]
D. K. Trubey L. Jung

The information retrieval system described previously[2] has been used in several important ways by the RSIC staff. The second cumulative bibliography of shielding literature produced by the system was issued,[3] and a third one (to be published as RSIC-5) is now in preparation. The second bibliography is much like the first one, although corrections and revisions were made and at least 200 more literature specimens were added. Also, a new role indicator was included to show whether the shielding data presented in the literature specimen are compared with similar data in some other publication. The third bibliography will be accompanied by abstracts of the literature. Its format is being made more convenient for the user.

The computer programs for revising and correcting the files of the retrieval system have been completed to the extent that many literature specimens actually have been replaced by others. Several retrieval and edit codes have been written, among which are codes that predicate the search on any of the various logical combinations of one to five subject categories. The system has been modified to include selective dissemination of information to individuals as the system is updated. The information, which is stored on magnetic tape, is in the form of bibliographic data and abstracts. It is also classified by authors and by fields of interest.

A modified version of the retrieval system will soon be used for shielding codes and the corresponding literature.

References

[1]Mathematics Division.

[2]S. K. Penny, D. K. Trubey, and M. B. Emmett, *Neutron Phys. Div. Ann. Progr. Rept. Aug. 1, 1963*, ORNL-3499, Vol. I, p. 166.

[3]S. K. Penny *et al.*, *Cumulative Bibliography of Literature Examined by the Radiation Shielding Information Center*, ORNL-RSIC-2 (1964).

4.3. COLLECTION OF SHIELDING COMPUTER CODES

B. F. Maskewitz S. K. Penny
D. K. Trubey

The Center's function of collecting computer codes written for shielding calculations has advanced to the extent that 32 programs are operable by RSIC on the IBM 7090/94 and two programs are operable on the CDC 1604A. These include codes utilizing the methods of Monte Carlo, point-to-point kernel integration, numerical integration, and Spinney (removal-diffusion). The calculations performed include penetration, reflection, heating, scattering in ducts, scattering from structural components such as those encountered in SNAP (Space Nuclear Auxiliary Power) geometries, and transport of charged particles.

All these programs, including data preparation and other auxiliary codes, have been used successfully with sample problems supplied by the contributor. To acquire experience and information on data preparation, operability, and intercomparison, RSIC has, in addition, designed simple problems which have been run on several codes. This will continue for all applicable codes.

The placing of code packages with manufacturers has proceeded slowly, as the staff wanted first to gain as much experience with each code as possible in order to be a more competent reference. However, many requests for codes not yet placed with a manufacturer have been filled directly from the RSIC collection.

The Computer Codes Section has had several visitors. Several persons have been interested in learning how to use a particular code, some to the extent that they have volunteered to assist in writing new data for a code and in making the code operable. A few contributors have personally delivered their codes, simultaneously giving valuable counsel to the RSIC staff.

The Computer Codes Section has performed some very special services for installations that are attempting to use certain shielding codes. These services include effecting the transition from one computer monitor system to another very different monitor system, aiding in an economic feasibility study to determine whether a code should be changed so that it could be operated on a computer which was different from the computer for which it was originally written, and "trouble shooting" input data for codes which require very complicated and exacting input. The codes collection is housed and serviced at the Central Data Processing Facility.[1]

A review of literature on nuclear codes, in general, and shielding codes, in particular, is continuing. Several hundred documents have been collected and indexed for ready reference. Many requests have been filled for references to literature concerning descriptions of codes useful in solving specific problems.

The codes document collection has become extensive enough to be entered into the RSIC information retrieval system. A categorization scheme has been devised, and analysis of documents is in process. It is expected that a bibliography of computer codes literature will be published in a few months. Abstracts of the codes in the collection are written, and one set has been distributed. A second distribution is expected soon.

Cooperation with the Argonne Code Center and with the European Nuclear Energy Agency (ENEA) Computer Programme Library is well established. Communication lines have also been set up with nuclear data compilation centers to secure data for use in shielding codes.

References

[1]Hemma E. Francis and Henrietta Hendrickson, members of the CDPF staff, assist in all phases of this RSIC operation, as well as handle production codes for the Neutron Physics Division research staff.

5. Mathematics and Computer Programs

5.1. HAUSER-FESHBACH COMPUTER PROGRAMS

W. R. Smith

Several CDC-1604 computer programs have been written which calculate the angular distributions of nuclear reaction products using the Hauser-Feshbach theory[1] modified to include the effects of spin-orbit coupling.[2] One program computes the compound-elastic scattering of neutrons or protons – together with the shape-elastic scattering – compares the sum of the two with experimental elastic-scattering angular distributions, and automatically varies the optical-model parameters in such a way as to optimize the agreement between theory and experiment. This program is restricted to use with zero-spin targets.

Another program forms the basis for the remaining programs. If the required penetrabilities are supplied, together with all the spins and parities involved, it will compute an angular distribution for virtually any nuclear reaction for which, in every channel, two particles enter and two emerge. With this program as a subroutine, another program automatically calculates the required optical-model penetrabilities and proceeds to generate the angular distribution for any reaction involving channels having incoming and outgoing particles with spin 0, $\frac{1}{2}$, or 1. It is limited to a maximum of 16 partial waves in any one channel, but it is not restricted with respect to the spins of the target or residual nuclei.

Two additional programs compute the angular distributions of inelastically scattered neutrons or protons, provided that the necessary penetrabilities are supplied. In one case the penetrabilities must correspond to the exact energies involved.[3] The other program interpolates the penetrabilities from values supplied in tabular form. Both programs compute in one pass the angular distributions corresponding to all the excited levels of the target having energies below the bombarding energy. In addition, in the latter program provision is made for automatically incrementing the bombarding energy and repeating the calculations without any further input.

References

[1]W. Hauser and H. Feshbach, *Phys. Rev.* **87**, 366 (1952).

[2]G. R. Satchler, *Proc. Phys. Soc. (London)* **A68**, 1041 (1955).

[3]W. R. Smith, *Hauser-Feshbach Computer Program for Spin-$\frac{1}{2}$ Particles*, ORNL-TM-875 (1964).

5.2. O5R: A GENERAL-PURPOSE MONTE CARLO NEUTRON TRANSPORT CODE[1]

R. R. Coveyou, F. B. K. Kam, D. C. Irving, J. G. Sullivan[2]

The O5R code is a highly versatile Monte Carlo neutron transport code covering the energy range from 77.13 Mev to 0.070×10^{-3} ev. It is distinguished by its detailed representation of cross-section data. In this representation the energy range is divided into 40 supergroups, each a factor of 2 apart, and each supergroup is divided into 2^n subgroups, where n may range from zero to nine at the option of the user. Cross sections are held constant across each subgroup. Practical use of so much information is made possible by storing in the machine memory the cross sections for only a single supergroup and by processing batches of from 200 to 2000 neutrons through the energy range of the supergroup. Cross sections for the next lower energy supergroup are then read in from tape, and the process is repeated.

O5R does not allow a neutron to be absorbed by a nucleus. Instead, statistical variances in analyses are improved by taking into account the probability of absorption by a reduction in the statistical weight of a neutron at each collision. Splitting and Russian Roulette can be employed at the option of the user. Both fast fissioning and thermal fissioning are permitted in appropriate systems. Diffusion of thermal-energy neutrons may be ignored, treated by a simple one-velocity model, or handled by special routines written by the user.

Anisotropic scattering is allowed by utilizing a technique for selecting from anisotropic angular distributions that gives the same accuracy as a straightforward selection from a Legendre expansion but requires considerably less computer time.

A general geometry routine permitting as many as 16 media bounded by planes or quadric surfaces, as well as special routines for simpler geometries, is included in the O5R package.

In using O5R, only two routines, a source routine and a routine to treat inelastic scattering, must be written (in FORTRAN-63) by the user. Efficient random number generating routines are contained within the code package, as are routines for performing a variety of manipulations with cross sections. The latter include routines for preparing master tapes, deleting specific data from master tapes, editing master tapes, performing cross-section arithmetic, preparing the cross-section data tapes needed by O5R, and preparing an input tape for the Calcomp plotter for drawing cross-section curves.

The output of O5R is one or more "collision" tapes that contain, for every collision suffered by a neutron, any or all of 32 distinct parameters describing the event. Analysis of these collision tapes to extract the information desired is done by separate analysis routines, which must be written by the user.

A detailed user's manual and input instructions for all parts of the O5R package are given, as well as program descriptions, flow charts, and full-scale sample problems against which the proper operation of all parts of the code may be checked.

References

[1]Abstract of ORNL-3622 (to be published).
[2]Mathematics Division.

5.3. AN O5R ANALYSIS ROUTINE TO ESTIMATE NEUTRON FLUXES IN ANISOTROPIC SCATTERING MEDIA[1]

W. E. Kinney

There are several techniques that are commonly used to reduce the variance of Monte Carlo estimates of neutron fluxes below that obtained from a straightforward analog Monte Carlo computation.[2,3] One is the method of statistical estimation wherein an analog Monte Carlo calculation diffuses neutrons through a medium, but at each collision the probability that the neutron reaches the point of interest is computed. For each collision the product of the probability that the neutron has survived to undergo the collision and the probability that the neutron scatters to the detector point is added into the estimate of the flux. Each collision contributes to the estimate in this manner so that the variance is reduced simply because there are more samples taken.

A FORTRAN analysis routine for the O5R code (Sect. 5.2) has been written to estimate fluxes by this method as a function of energy at as many as ten selected detector points in a system containing three anisotropic scatterers in two media, each of which contain a total of ten scatterers.

The O5R system data tape is used to supply the mean free flight times for the media if it contains no more than 64 points per supergroup. In addition, a tape containing Legendre expansion coefficients averaged by the code 7 averager[4] is required to describe the anisotropic-scattering angular distributions.

The analysis routine is written to put all the mean free flight times and expansion coefficients into the memory at once. This saves time but sacrifices flexibility. A P_8 approximation to the angular distributions is the maximum allowed as the code was originally written. This, as well as the maximum number of media, the maximum number of anisotropic scatterers, the maximum number of detector points, etc. may, of course, be changed by changing dimension statements, provided that the machine core storage restrictions are observed. As written, fluxes and standard deviations are estimated in a maximum of 50 energy groups.

References

[1]For more detailed information, see W. E. Kinney, *Program STATEST, An Application of the Method of Statistical Estimation to the Calculation of Neutron Flux in Anisotropically Scattering Media by Monte Carlo,* ORNL-3715 (1964).

[2]H. Kahn, *Applications of Monte Carlo,* AECU-3259 (1954).

[3]G. Goertzel and M. H. Kalos, *Progress in Nuclear Energy,* Ser. I, Vol. 2, Pergamon, New York, 1958.

[4]R. R. Coveyou *et al., O5R: A General Purpose Monte Carlo Neutron Transport Code,* ORNL-3622 (to be published).

5.4. A MONTE CARLO TECHNIQUE FOR SELECTING NEUTRON SCATTERING ANGLES FROM ANISOTROPIC DISTRIBUTIONS[1]

R. R. Coveyou

A technique has been devised for use in the O5R code (Sect. 5.2) for selecting a scattering angle ($\cos^{-1}\mu$) from an anisotropic-scattering angular distribution which gives the same accuracy as that obtained by a straightforward selection from a Legendre expansion but which requires considerably less computer time. Briefly, the method consists in selecting μ from a finite number of scattering angle cosines obtained from the distribution function

$$G(\mu) = \sum_{k=0}^{n} \phi_k \, \delta(\mu - \theta_k) , \qquad (1)$$

which can be shown to give the same order of accuracy as the appropriate Lengendre series when both are truncated at n. After calculation of the coefficients ϕ_k, when all the ϕ_k's are positive, a value of μ is selected from the θ_k's by choosing a random number R and letting $\mu = \theta_j$, if

$$\sum_{k=0}^{j-1} \phi_k < R \leq \sum_{k=0}^{j} \phi_k . \qquad (2)$$

When any of the ϕ_k's are negative, then the technique is modified somewhat. With negative ϕ_k's a situation may exist in which negative statistical weights may be assigned to individual neutrons, which in turn may give a negative value for an estimate. This simply means that an insufficient number of samples has been taken or that a higher order approximation is required.

References

[1]Abstract of a "Letter to the Editor" to be published in *Nucl. Sci. Eng.* **21** (January or February, 1965).

5.5. SOME TESTS OF THE TECHNIQUE USED BY THE O5R NEUTRON TRANSPORT CODE FOR SELECTING FROM ANISOTROPIC ANGULAR SCATTERING DISTRIBUTIONS[1]

W. E. Kinney

The application of R. R. Coveyou's time-saving technique for choosing a scattering angle from an anisotropic angular distribution and for properly including it in the O5R code (Sects. 5.2 and 5.4), has been tested by several calculations of problems for which analytic or semianalytic solutions have been obtained by other investigators. The first of these was the calculation of the flux from a plane isotropic source in a medium having a scattering cross section equal to one-half the total cross section. Both the fluxes as a function of distance and the angular distributions as calculated by the O5R code were in essentially good agreement with the semianalytic results, the points of disagreement being readily explainable in terms of characteristic deficiencies of the Monte Carlo method.

The second test of the anisotropic-scattering selection technique was the calculation of the multiplication constant for one-velocity neutrons in infinite slabs, in infinite cylinders, and in spheres of media having isotropic scattering in the laboratory system. Again the results were in agreement with published results of exact calculations.

The results of both tests indicate that the Coveyou selection technique is appropriate and has been properly incorporated in the O5R code.

References

[1]Abstract of a "Letter to the Editor" to be published in *Nucl. Sci. Eng.* **21** (January or February, 1965).

5.6. AN IMPROVED METHOD FOR HANDLING ANGULAR DISTRIBUTIONS IN THE O5R CODE

R. MacPherson R. R. Coveyou

The method presently used in the O5R code (Sect. 5.4) to select scattering angles from an angular distribution specified by a finite set of Legendre coefficients has the defect, awkward in certain problems, of giving negative probabilities for some angles of scattering. Although this defect can be partially compensated for by judicious weight juggling, it would be desirable to have a method that is free from this difficulty. Such a method has been discovered (more precisely, rediscovered) and the theory has been thoroughly developed. The method is soon to be installed in O5R.

The method now being used concentrates all probability on a finite set of points, the zeros of a certain Legendre polynomial, for all angular distributions. The new method concentrates all probability on the set of zeros of one of the sets of polynomials orthogonal with respect to the angular distribution itself; hence the set of values changes from one distribution to another. The result is that for any possible set of moments the associated probabilities are positive. Computer storage requirements will be about the same as before.

5.7. A CDC-1604A CODE TO PROCESS O5R COLLISION TAPES

F. B. K. Kam K. Franz[1]

Analysis of the collision histories generated by the O5R code (Sect. 5.2) usually requires recourse to procedures somewhat more sophisticated than simple analog techniques, in order to obtain some reasonable degree of statistical confidence in the results. Application of such procedures as, for instance, statistical estimation, has been facilitated by the construction of a code for the CDC-1604A computer which performs the major part of the "bookkeeping" tasks required. As with O5R, the code is written as a master control code which guides the many subroutines that perform the actual computations. With two exceptions these subroutines are written in the FORTRAN-63 language. The subroutine which buffers in the information given on the collision tapes and the one which computes the subgroup number for a given neutron energy are both written in CODAP, the 1604A machine language.

Many of the features of this code have been patterned after the O5R code. In particular, the representation of cross sections is the same, so that the O5R cross-section package, XSECT, can be used. In addition, a subroutine, EUCLID, permits the user to employ any of the O5R geometry subroutines. The input to the code is so written that the user familiar with O5R input will find little difference in them.

Since large blocks of storage with dimension statements do not have to be reserved in the present code, machine storage locations are more efficiently used. The code computes the amount of storage required for each block of data and loads the blocks one behind the other without wasting locations. The first address of each block is made available, so that there is rapid access to any block. In addition, through the use of duplicate tapes containing the same set of Legendre coefficients the running time is reduced.

A number of useful subroutines are built into the code, the names and functions of which are listed below.

1. INIT AND DIST: These subroutines compute a frequency distribution table from a set of values for any given parameter.

2. GTXSECT: Given the neutron energy and the medium within which the neutron is located, this subroutine obtains the appropriate cross section from storage.

3. GTFETA: Given the incident neutron energy, E, the cosine of the scattering angle in the center-of-mass system, η, and the scatterer, this subprogram returns with $f(\eta)$, the probability of scattering through η.

4. O5RSET and O5RREAD: These subroutines buffer in the information from the collision tapes and make it available for use.

5. FIXINPUT: This subroutine reads in the input required by the code.

6. ELAS: This subroutine computes the energy of the neutron after an elastic collision.

7. INELAS: This subroutine computes the energy of the neutron after an inelastic collision.

Because of the many different ways in which data may be analyzed, the user is required to insert

a few subroutines which depend directly on his problem. A routine, STBATCH, must be written to read in data for the particular job. The subroutines which perform the actual analysis of each of the eight allowable collision events must be coded. Although usually only one or two of the eight will be of interest, dummy subroutines must be inserted for the others. Subroutine NBATCH, which processes the data after each batch, and subroutine NRUN, which prints out a frequency distribution table after all batches have been run, are included in the code but an input option allows them to be replaced by routines written by the user.

References

[1]Central Data Processing Facility, Oak Ridge Gaseous Diffusion Plant.

5.8. DERIVATION OF FIRST- AND LAST-FLIGHT ESTIMATORS FOR MONTE CARLO COMPUTATIONS OF SCATTERED PARTICLE FLUXES IN ATTENUATING MEDIA WITH SPHERICAL OR PLANE SYMMETRY[1]

S. K. Penny

Estimators for the first, last, and in-between flights have been derived for use in Monte Carlo computations of scattered particle fluxes in attenuating media with spherical or plane symmetry. The derivation is based upon the integral form of the Boltzmann equation.

References

[1]Abstract of ORNL-TM-974 (1964).

5.9. OGREISH-P1 – A MONTE CARLO CODE UTILIZING IMPORTANCE SAMPLING FOR THE COMPUTATION OF GAMMA-RAY TRANSMISSION THROUGH LAMINATED SLABS[1]

T. W. Armstrong S. K. Penny

A Monte Carlo code, OGREISH-P1, has been written to perform computations of the transmitted dose rate due to gamma rays impinging on laminated infinite slabs. The gamma rays are monoenergetic, and their angular distributions may be isotropic, "cosine," or monodirectional. The code is essentially a modernization of the TRIGR-P code in that the importance sampling techniques are similar and the code is written in FORTRAN in a modern Monte Carlo system called "OGRE."

References

[1]Abstract of ORNL-TM-953 (November 1964).

5.10. AN ALGORITHM FOR THE WORKING INVERSE OF A MATRIX

W. R. Burrus C. Schneeberger
B. Rust[1]

A common numerical problem is that of finding the inverse A^{-1} of a matrix A. The inverse has the theoretical property that $A^{-1}A = I$, the identity matrix. The primary use of the inverse is in solving linear systems of equations, since if $Ax = b$, $x = A^{-1}b$. Sometimes, however, we confuse theory with practice and forget that the property $A^{-1}A = I$ holds theoretically but not necessarily when the computations are performed on a digital computer with finite accuracy. For example, consider a 10 by 10 section of the famous Hilbert matrix:

$$H = \begin{bmatrix} 1 & 1/2 & \dots & 1/10 \\ 1/2 & 1/3 & \dots & 1/11 \\ \dots & \dots & \dots & \dots \\ 1/9 & 1/10 & \dots & 1/18 \\ 1/10 & 1/11 & \dots & 1/19 \end{bmatrix}.$$

The exact inverse is given by the formula

$$H_{ij}^{-1} = (-1)^{i+j} \frac{(n+i-1)!\,(n+j-1)!}{(i+j-1)!\,[(i-1)!\,(j-1)!]^2\,(n-i)!\,(n-j)!}, \qquad (1)$$

where $n = 10$. The result to six significant figures is

$$H^{-1}_{6\ \mathrm{figs}} = \begin{bmatrix} 1.00000 \times 10^2 & -4.95000 \times 10^3 & 7.92000 \times 10^4 & \cdots & -9.23780 \times 10^5 \\ -4.95000 \times 10^3 & 3.26700 \times 10^5 & -5.88060 \times 10^5 & \cdots & 8.31402 \times 10^7 \\ \cdots & \cdots & \cdots & & \cdots \\ 4.37580 \times 10^6 & -3.89884 \times 10^8 & 8.50655 \times 10^9 & \cdots & -2.02114 \times 10^{11} \\ -9.23780 \times 10^5 & 8.31402 \times 10^7 & 1.82908 \times 10^9 & \cdots & 4.49142 \times 10^{10} \end{bmatrix}.$$

If the inverse is obtained by using a standard matrix inversion routine, such as the familiar Gauss-Jordan elimination method with partial pivoting, the following result is obtained by single-precision arithmetic on the IBM-7090 computer:

$$H^{-1}_{\mathrm{Gauss}} = \begin{bmatrix} 5.71245 \times 10^1 & -1.58848 \times 10^3 & 1.38303 \times 10^4 & \cdots & 1.00300 \times 10^4 \\ -1.83928 \times 10^3 & 6.69172 \times 10^4 & -6.08180 \times 10^5 & \cdots & 1.76242 \times 10^6 \\ \cdots & \cdots & \cdots & & \cdots \\ -5.88363 \times 10^5 & 1.99866 \times 10^7 & -1.00191 \times 10^8 & \cdots & 4.77521 \times 10^9 \\ 1.89423 \times 10^5 & -6.28228 \times 10^6 & 2.81649 \times 10^7 & \cdots & -1.60654 \times 10^9 \end{bmatrix}.$$

This result is obviously very far from the correct inverse, having an average magnitude error for each element of 4.190×10^{11}! Yet it is presumptuous to assume that $H^{-1}_{\mathrm{Gauss}} H$ will be greatly different from the identity matrix. In fact,

$$H^{-1}_{\mathrm{Gauss}} H = \begin{bmatrix} 1.00000 \times 10^0 & 7.32442 \times 10^{-4} & -6.10352 \times 10^{-4} & \cdots & 2.44141 \times 10^{-4} \\ 7.81250 \times 10^{-3} & 1.23438 \times 10^0 & 7.81250 \times 10^{-3} & \cdots & -3.90625 \times 10^{-3} \\ \cdots & \cdots & \cdots & & \cdots \\ -4.00000 \times 10 & -1.60000 \times 10^1 & -2.40000 \times 10^1 & \cdots & 0.0 \\ -2.00000 \times 10^0 & -2.00000 \times 10^0 & 2.00000 \times 10^0 & \cdots & 7.00000 \times 10^{-1} \end{bmatrix},$$

which differs from the identity matrix by an average magnitude error of only 2.835.

At first, one might think that the exact Hilbert inverse obtained from Eq. 1 would yield a better identity matrix. But when the multiplication is carried out with 7090 arithmetic of eight significant figures,

$$H^{-1}_{8\ \mathrm{figs}} H = \begin{bmatrix} 9.97071 \times 10^{-1} & 1.26953 \times 10^{-2} & -5.85938 \times 10^{-3} & \cdots & 6.34766 \times 10^{-3} \\ 8.12500 \times 10^{-1} & -5.62500 \times 10^{-1} & -1.06250 \times 10^0 & \cdots & -1.37500 \times 10^0 \\ \cdots & \cdots & \cdots & & \cdots \\ -1.53600 \times 10^3 & 4.60800 \times 10^3 & 1.15200 \times 10^4 & \cdots & 2.17600 \times 10^3 \\ -1.28000 \times 10^2 & -8.32000 \times 10^2 & -9.60000 \times 10^2 & \cdots & -7.04000 \times 10^2 \end{bmatrix},$$

which has an average magnitude discrepancy from the identity matrix of 1.224×10^3. The reason for this behavior is not hard to see. Because of the large magnitude of the elements of the exact Hilbert inverse, the elements of the product $H^{-1} H$ are computed as the difference between a large positive number and a large negative number. If the two numbers are of the order of 10^{12} but their difference is of the order of 1, then the difference will be in error by the order of 10^4, if only eight significant figures are carried in the computation.

Evidently, we must abandon our hope that the exact inverse times the original matrix yields a good identity matrix. Yet it is just this property which determines the validity of the solution of a system of linear equations, $Ax = b$, because of the identity:

$$x_{\mathrm{exact}} - x_{\mathrm{calculated}} = (I - A^{-1}_{\mathrm{calculated}} A) x_{\mathrm{exact}} . \quad (2)$$

It happens that the Gauss-Jordan method yielded a much smaller average absolute error; thus the matrix H^{-1}_{Gauss} would be much more preferable to the matrix

$H^{-1}_{8\,\mathrm{figs}}$ if the objective were to solve a system of linear equations. It is, however, more or less accidental that the Gauss-Jordan routine yielded such a small average absolute error. The 10 by 10 section of the Hilbert matrix is nearly singular in the sense that the ratio of the minimum eigenvalue to the maximum eigenvalue is equal to 6.040×10^{-14}. This means that the matrix is essentially numerically singular to a computer giving eight significant figures, and therefore the inverse is not defined. Thus one finds that slight coding changes which have no substantial effect on a well-conditioned matrix cause a large change in H^{-1}_{Gauss}.

Clearly, the property $A^{-1}A = I$ may be more important in some applications than having a matrix such as $H^{-1}_{8\,\mathrm{figs}}$, which is close to the exact inverse. Thus we are motivated to make a definition of a "working inverse":

Definition

The working inverse A^W *of a matrix* A *is that matrix for which the rms value of* $[I - A^W A]$ *is a minimum, when the computation is carried out on a real computer with specified precision.*

Obviously, the working inverse approaches the usual inverse when the matrix A is well conditioned, or when the precision of the machine is increased without limit. An important point is that the working inverse differs with the use of computers that have a different amount of precision and treat rounding differently (e.g., the IBM 7090 and the CDC 1604). A second point is that the number of rows of A need not equal the number of columns in order for the working inverse to exist. In this last respect, the working inverse bears a close resemblance to the generalized inverse introduced by Moore[2] and popularized by Penrose.[3]

We have written a very simple algorithm in FORTRAN which computes a close approximation to the working inverse. The amount of computation required is approximately $^{19}/_{6}$ that of ordinary matrix inversion, but may be reduced substantially at the expense of additional storage. For the 10 by 10 section of the Hilbert matrix,

$$H^W = \begin{bmatrix} 3.21317 \times 10^1 & -5.12071 \times 10^2 & 2.39302 \times 10^3 & \cdots & 1.71302 \times 10^4 \\ -5.12158 \times 10^2 & 1.13256 \times 10^4 & -6.18671 \times 10^4 & \cdots & -5.67897 \times 10^5 \\ \cdots & \cdots & \cdots & & \cdots \\ -1.85300 \times 10^3 & 5.74279 \times 10^4 & -3.94165 \times 10^5 & \cdots & -6.12190 \times 10^5 \\ 1.71410 \times 10^3 & -5.67995 \times 10^4 & 4.11301 \times 10^5 & \cdots & 7.10825 \times 10^5 \end{bmatrix},$$

and

$$H^W H = \begin{bmatrix} 1.00004 \times 10^0 & 4.76837 \times 10^{-4} & -1.31607 \times 10^{-4} & \cdots & -1.26839 \times 10^{-4} \\ -4.88281 \times 10^{-4} & 9.71825 \times 10^{-1} & 4.08936 \times 10^{-2} & \cdots & 3.29590 \times 10^{-3} \\ \cdots & \cdots & \cdots & & \cdots \\ -5.85938 \times 10^{-3} & -8.78906 \times 10^{-3} & -7.32422 \times 10^{-2} & \cdots & 2.79785 \times 10^{-1} \\ 6.83594 \times 10^{-3} & 9.76563 \times 10^{-3} & -1.26953 \times 10^{-2} & \cdots & 8.45215 \times 10^{-1} \end{bmatrix}.$$

The average element of $[I - H^W H]$ is 0.0974, which is a substantial but not spectacular improvement over H^{-1}_{Gauss}. The real importance of the idea of the working inverse is, however, that the result is achieved by design instead of by accident.

A report[4] on the algorithm has been prepared and will be submitted for publication as soon as the program has been completely checked out.

References

[1]Central Data Processing Facility, Oak Ridge Gaseous Diffusion Plant.

[2]E. H. Moore, *Mem. Am. Phil. Soc.* **1**, 197–209 (1935).

[3]R. A. Penrose, *Proc. Cambridge Phil. Soc.* **51**, 406–13 (1955).

[4]C. Schneeberger and W. R. Burrus, *Application of an Algorithm for the Generalized Inverse to Linear Equations* (in preparation).

5.11. THE UTILIZATION OF *A PRIORI* INFORMATION BY MEANS OF MATHEMATICAL PROGRAMMING IN THE STATISTICAL INTERPRETATION OF MEASURED DISTRIBUTIONS[1]

W. R. Burrus

A statistical approach has been developed for unfolding instrument measurements which are related to an unknown function by a linear integral transformation. If statistical uncertainties are present in the measured function and in the kernel of the transformation, then the use of *a priori* information is shown to be necessary for a nontrivial solution. Without such information, an infinite-width confidence interval can be found for any nontrivial function of the unknown function. Suitable *a priori* information, however, nearly always exists in physically motivated problems. The weakest form of *a priori* information considered is simple nonnegativity. Stronger *a priori* information, such as smooth or monotonic behavior, can be put in the same form as simple nonnegativity by suitable transformation. The unfolding problem requires two steps: selecting a set of functions of the unknown function to adequately describe the function and then numerically obtaining the width of the confidence interval for each function. Several computational techniques based on linear and quadratic programming are described. Finally, the method is illustrated by unfolding gamma-ray and neutron spectra from pulse-height distributions obtained with scintillation spectrometers and by solving a poorly conditioned set of equations.

References

[1]Abstract of ORNL-3743 (to be published).

5.12. A GENERALIZED ONE-CONSTRAINT LAGRANGE MULTIPLIER NUMERICAL FORMULATION[1]

F. S. Clark F. B. K. Kam

The one-constraint LaGrange multiplier problem has been written for the CDC-1604 in a FORTRAN program called "MAX." The program can deal with a combination of any varied function and any constraining function that depend on no more than 18 independent variables and for which all second derivatives exist throughout the domain. The user is required to write two subroutines: one defines the varied function, the other the constraining function. The computational method used is absolutely nondivergent, but for some starting values in some problems it will stop in the neighborhood of an extraneous point and require a restart at a different point. A test problem is included.

References

[1]Abstract of ORNL-3742 (to be published).

6. Radiation Detector Studies (I)

6.1. RECENT DEVELOPMENTS IN THE PROTON-RECOIL SCINTILLATION NEUTRON SPECTROMETER

W. R. Burrus V. V. Verbinski

The proton-recoil scintillator technique for measuring neutron spectra has been used with larger scintillators than was possible previously by taking into account multiple scattering, charged-particle reactions, and carbon recoils. Also, pulse-shape gamma rejection is utilized. The main features are high efficiency, good resolution, and simple circuitry. The recently developed SLOP code[1] was used to analyze the data. This code requires accurate responses of the scintillator to monoenergetic neutrons, which were obtained by a combination of calculations and experimental measurements described elsewhere (see Sect. 6.2). The code forms combinations of the counting efficiency functions for each channel of the analyzer, such that the resulting combinations approximate an "idealized" spectrometer with the desired response function. The code is based on "quadratic programming" and utilizes the known nonnegativity of the neutron spectrum.

Two examples of discrete line spectra from the $^{9}Be(\alpha,n)^{12}C$ reaction are shown in Fig. 6.1.1. These were obtained with a 2- by 2-in.-diam NE-213 liquid scintillator and a Forte-type gamma rejection circuit.[2] The ground level and several excited levels are obtained with about 15% resolution. A neutron spectrum from a water-moderated reactor is also shown to illustrate the feasibility of using the same technique on nondiscrete spectra.

In Fig. 6.1.2 pulse-height distributions are shown with and without a gamma rejection circuit using a 1- by 2-cm-diam stilbene crystal in a gamma background of 20 mr/hr from a ^{60}Co source. The counting rate from the gamma source would have been 20 times higher than the desired neutron pulses without the circuit, as is shown in the top curve. A 2- by 2-in.-diam NE-213 scintillator can tolerate 2 to 3 mr/hr equally well. The capabilities of the method have been demonstrated.

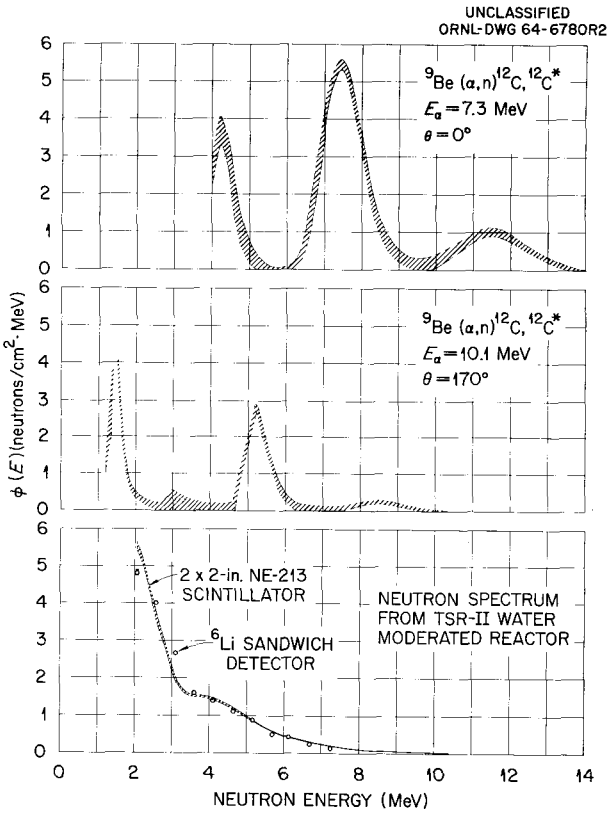

Fig. 6.1.1. Examples of Differential Neutron Spectra Obtained with a 2- by 2-in.-diam NE-213 Scintillator. The lowest curve represents the neutron spectrum emerging from a beam hole through the shield of the water-moderated Tower Shielding Reactor II; the point of measurement was 142 in. from the core surface.

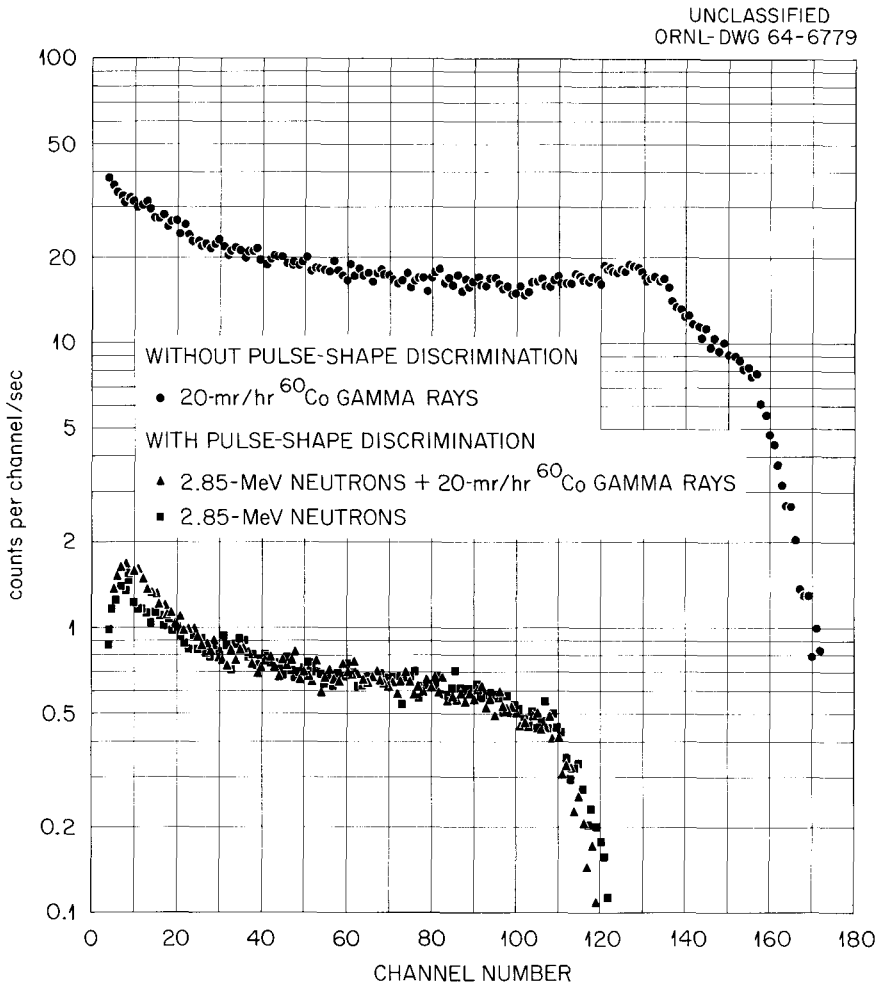

Fig. 6.1.2. Pulse-Height Distributions Obtained in 5-min Runs with a 1- by 2-cm-diam Cylindrical Stilbene Scintillator.

References

[1]W. R. Burrus, *Neutron Phys. Div. Ann. Progr. Rept. Aug. 1, 1963,* ORNL-3499, Vol. II, pp. 120–24.

[2]V. V. Verbinski *et al., Neutron Phys. Div. Ann. Progr. Rept. Sept. 1, 1962,* ORNL-3360, p. 107.

6.2. RESPONSE FUNCTIONS OF AN ORGANIC SCINTILLATOR TO FAST NEUTRONS[1]

V. V. Verbinski W. R. Burrus
J. C. Courtney[2] T. A. Love
J. G. Sullivan[3]

Knowledge of the neutron response of organic scintillators over a wide range of energies and scintillator sizes would yield the response functions required for unfolding measured neutron pulse-height distributions obtained with such detectors, and also facilitate determination of the efficiencies of organic detectors used in time-of-flight spectrometry. A method for obtaining the response function of organic scintillators using experimental calibrations and Monte Carlo calculations has been devised and applied to a 2- by 2-in.-diam NE-213 scintillator.[4] Good accuracy has been achieved over a wider range of pulse heights than was heretofore possible.

First, light output vs recoil-proton energy was measured with the largest pulses induced by a set of monoenergetic neutron exposures. This relationship was then used in a Monte Carlo calculation to obtain whole response functions, including

efficiencies, for monoenergetic neutrons. These were smeared and adjusted to fit the measured responses in shape and maximum light pulse size. Iteration gives the best light output function, which was fit to Birks' formula,[5] $dL = A[1 + B(dE/dx)]^{-1}\, dE$, after carefully deriving dE/dx for the NE-213 ($CH_{1.2}$) from published data.[6–9] The final Monte Carlo calculations utilized the corrected $L(E_p)$ curves, as well as light functions for alpha particles and recoil ^{12}C nuclei similarly calculated with Birks' formula and checked experimentally.

Figure 6.2.1*a* presents sample calculated distributions normalized to one incident neutron. The detector efficiency is the integral of the corresponding curve from the highest pulse height down to the bias setting. The "zero bias" efficiency of each function agrees with an exact analytic calculation within the 0.6% Monte Carlo statistics.

Figure 6.2.1*b* shows the measured response for 14.45-Mev neutrons from the $^3H(d,n)^4He$ reaction.

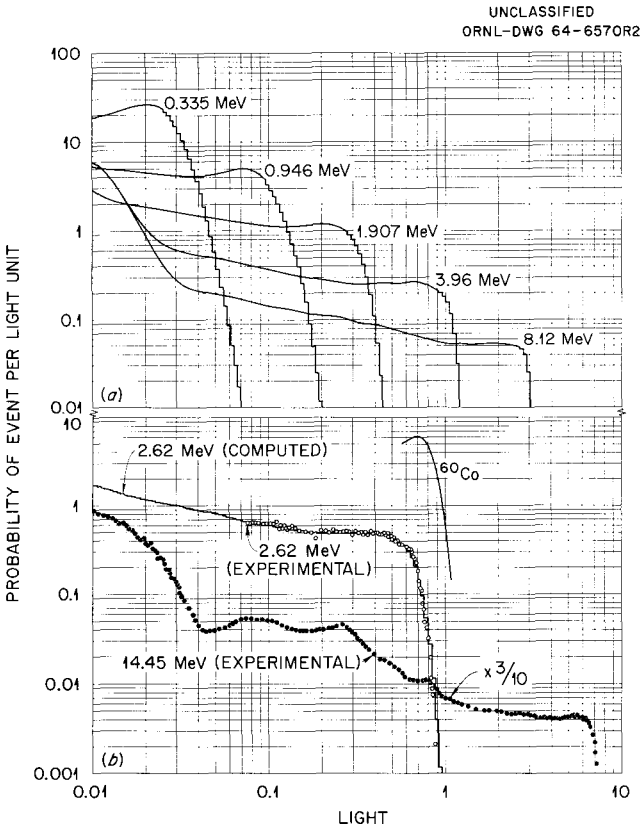

Fig. 6.2.1. Neutron Pulse-Height Responses of an NE-213 Scintillator. (*a*) Calculated values, (*b*) experimental values.

These results are reliable even for low pulse heights because coincidences with the associated ^4He nuclei were demanded. The irregularities of the curve represent, from left to right, carbon recoils (at a value of about 0.4 on the abscissa), $^{12}C(n,n')3\alpha$ via the 9.6-Mev excited state of ^{12}C, $^{12}C(n,n')3\alpha$ via the 10.8-Mev excited state of ^{12}C, $^{12}C(n,\alpha)^9Be$, and proton recoils. Also shown in Fig. 6.2.1*b* is a comparison of a computation for a 2- by 2-in.-diam scintillator to an associated-particle experiment with 2.62-Mev neutrons irradiating the center of the flat surface of a 1- by 5-in.-diam scintillator. The shape is seen to be relatively insensitive to geometric change.

All responses are normalized horizontally to the ^{60}Co calibration curve shown, which removes ambiguity relating to light units.

References

[1]Work partially funded by U.S. Army Nuclear Defense Laboratory, Edgewood Arsenal, Md., under Order NDL-23-63.

[2]Catholic University, Washington, D.C.; Graduate Fellow, Oak Ridge Institute of Nuclear Studies.

[3]Mathematics Division.

[4]Nuclear Enterprises, Ltd., Winnepeg, Manitoba, Canada.

[5]J. B. Birks, *Proc. Phys. Soc.* **A64**, 874 (1951).

[6]Ward Whaling, *Handbuch der Physik*, Vol. XXXIV, p. 193, Springer, Berlin, Germany, 1958.

[7]P. E. Schambra, A. M. Rauth, and L. C. Northcliffe, *Phys. Rev.* **120**, 1758 (1963).

[8]P. G. Roll and F. E. Steigert, *Nucl. Phys.* **17**, 54 (1960).

[9]M. S. Livingston and H. A. Bethe, *Rev. Mod. Phys.* **9**, 246 (1937).

6.3. MODIFICATIONS OF BONNER SPHERE SPECTROMETER TO MEASURE SPECTRA OF LOW-ENERGY NEUTRONS FROM (α,*n*) SOURCES

S. K. Mehta[1]

The so-called "Bonner sphere" neutron spectrometer, intended for the measurement of neutron spectra in the energy range below 15 Mev, has been described previously.[2] This instrument is currently being modified so that its resolution in

the energy range 0.01–1 Mev will be good enough for measurements of the spectra of low-energy neutrons from various (α,n) sources.

The spectrometer consists essentially of a thermal-neutron detector [a 4-mm-diam by 4-mm-thick LiI(Eu) (96.1% ^{6}Li) crystal] successively centered in polyethylene-moderating spheres having diameters 2, 3, 5, 8, and 12 in. Since Bonner's specifications[3] were followed closely in constructing the spectrometer, the response curves determined by him were accepted for the six channels given by the five sphere diameters plus the bare detector. These curves are shown in Figs. 6.3.1 and 6.3.2. In order to improve the resolution at low energies, ten more channels are being added by constructing B_4C shells of various thicknesses around the 2- and 3-in.-diam spheres. The modified spectrometer with a surrounding B_4C shell is shown in Fig. 6.3.3. The thicknesses of ^{10}B (based on its natural abundance in B_4C) have been chosen, on the basis of calculations which considered neutron absorption, so that the resulting response curves will have peaks equally spaced over the energy range from 0.01 to 10^5 ev as shown in Figs. 6.3.1 and 6.3.2. Additional calculations, which will be performed with the DSN transport code,[4] will evaluate the effect of neutron scattering on the response curves.

Preliminary experiments have been carried out with an Am-Be source and the original six-channel spectrometer. The SLOP code[5] was used to calculate the spectrum and the dose from the counts in the thermal peaks for the six channels, the response curves of Fig. 6.3.1, and published RBE dose curves.[6]

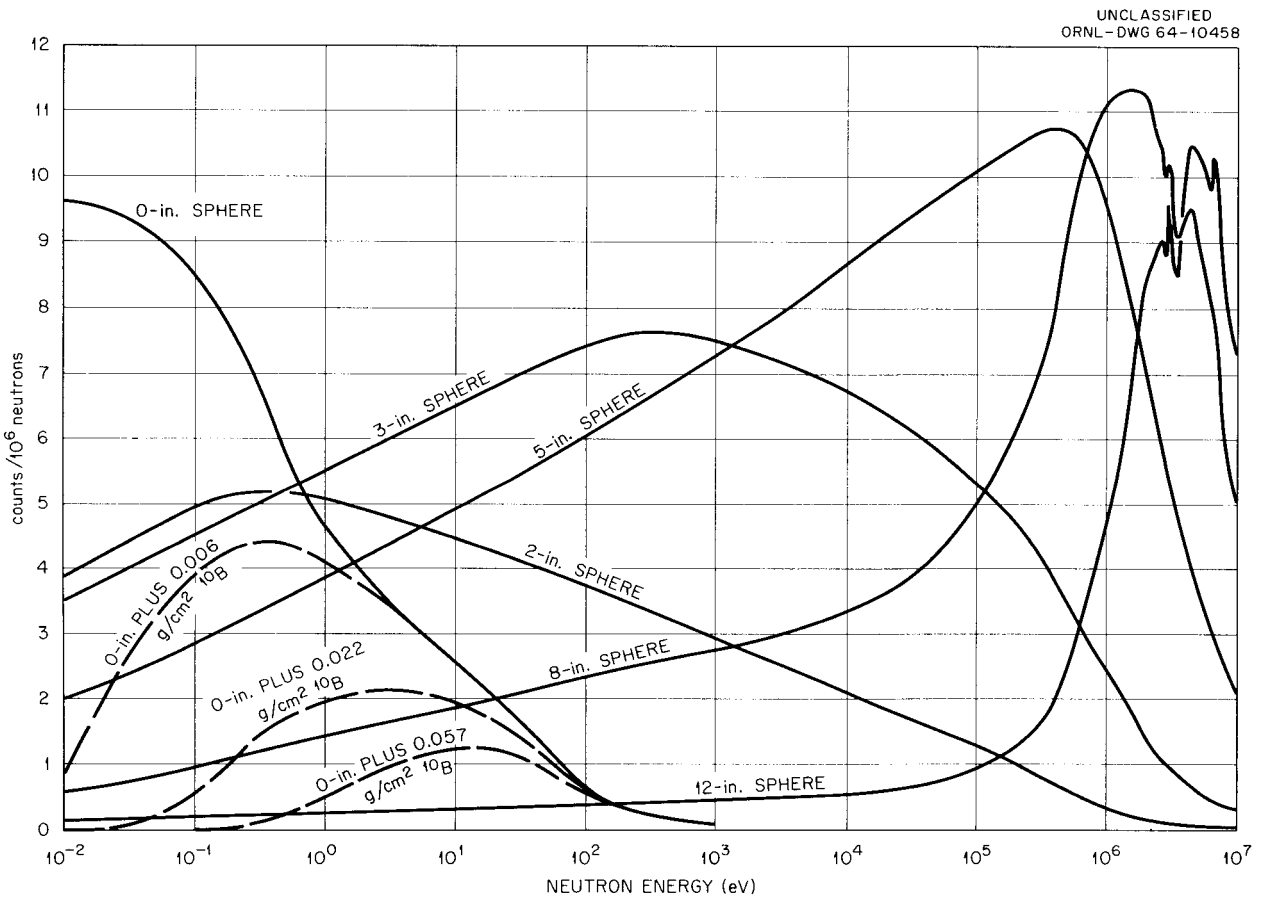

Fig. 6.3.1. Tentative Counting Efficiency (Nine Channels) for the Bonner Sphere Neutron Detector. Data are for an isotropic point source 40 cm from the detector.

References

[1]Atomic Energy Establishment Trombay, Bombay, India.

[2]W. R. Burrus, *Neutron Phys. Div. Ann. Progr. Rept. Sept. 1, 1962*, ORNL-3360, p. 296.

[3]R. L. Bramblett, R. I. Ewing, and T. W. Bonner, *Nucl. Instr. Methods* **9**, 1 (1960).

[4]B. Carlson, C. F. Lee, and J. Worlton, *The DSN and TDC Neutron Transport Codes*, LAMS-2346 (1960).

[5]V. D. Bogert and W. R. Burrus, *Neutron Phys. Div. Ann. Progr. Rept. Sept. 1, 1962*, ORNL-3360, p. 22.

[6]*National Bureau of Standards Handbook 63*, U.S. Dept. of Commerce, USGPO, Washington, D.C., 1957.

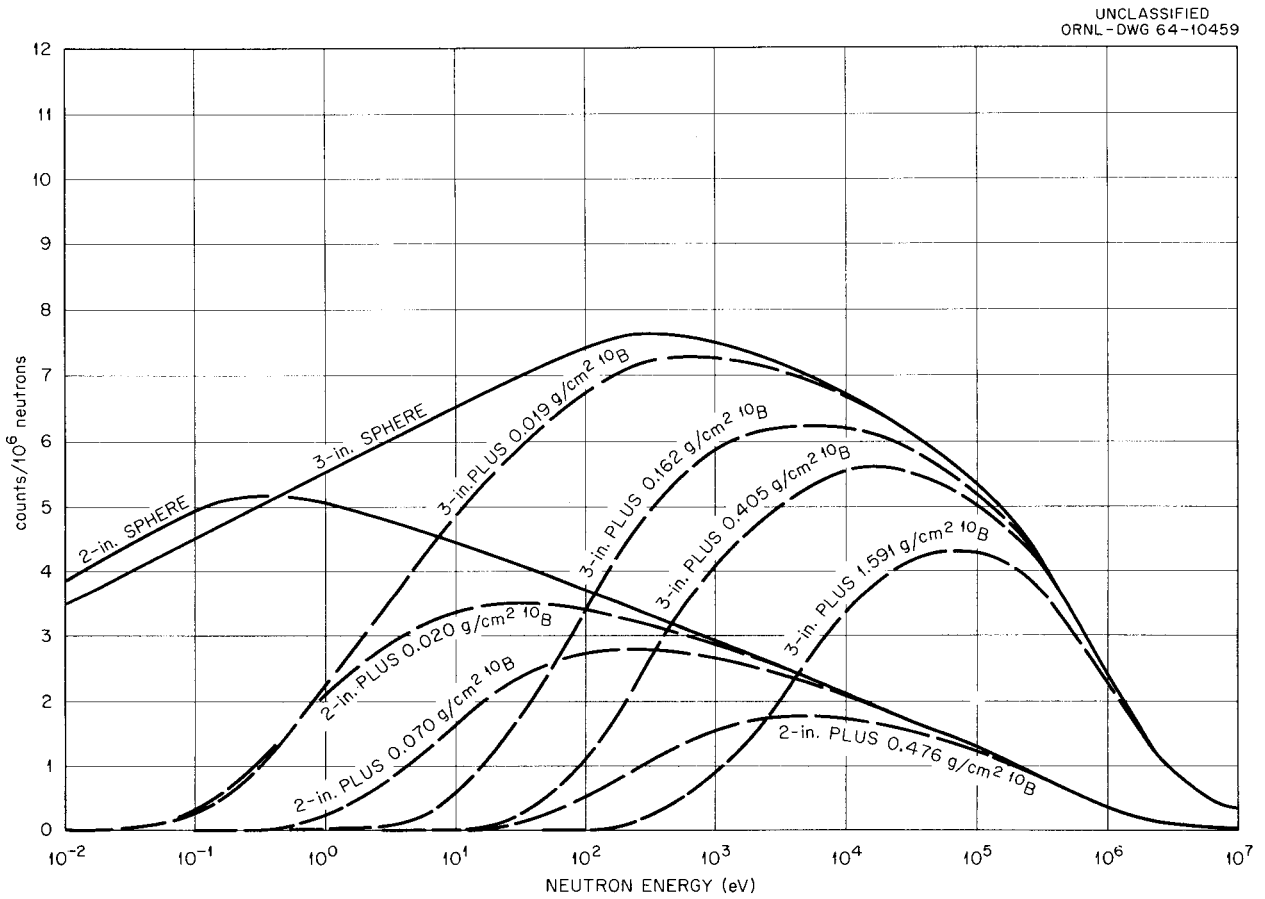

Fig. 6.3.2. Tentative Counting Efficiency (Seven Additional Channels) for the Bonner Sphere Neutron Detector. Data are for an isotropic point source 40 cm from the detector.

UNCLASSIFIED
ORNL-DWG 64-10460

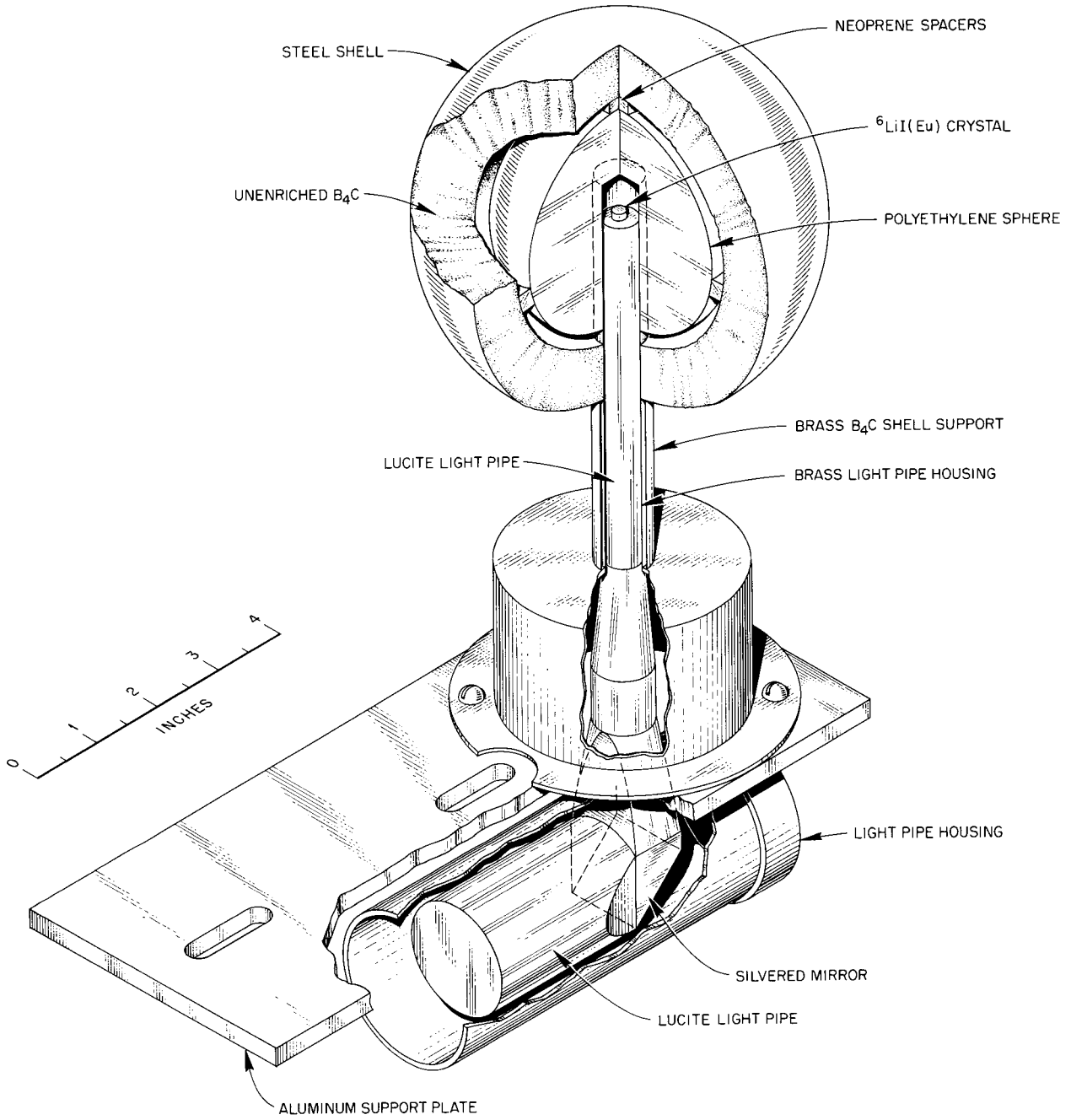

Fig. 6.3.3. The Bonner Sphere Neutron Detector, Showing Removable B_4C Shell.

6.4. DESIGN OF TWO NEUTRON-RESPONDING INSTRUMENTS: AN ISOTROPICALLY RESPONDING FAST-NEUTRON DOSIMETER AND A SPECTROMETER FOR THE ENERGY RANGE FROM THERMAL TO 10 kev[1]

T. V. Blosser

Fast-Neutron Dosimeter

The characteristic directionality inherent in existing instruments for measuring fast-neutron dose rates has long been a source of difficulty when measurements are made in isotropic neutron fluxes. Such fluxes exist in some shielding geometries and at large distances from unmoderated and unreflected critical assemblies such as the ORNL Health Physics Research Reactor. Concomitant with this difficulty has been the continuing lack of knowledge of the contribution made to the physical dose rate by low-energy neutrons, since conventional dosimeters must be biased to refuse pulses representing energies below a relatively high level, say 0.2 Mev. In an attempt to alleviate both these difficulties, the development of a sensitive, isotropically responding fast-neutron dosimeter whose lower limit of sensitivity will be 0.01–0.02 millirad/hr is under way. Its response in terms of dose rate will be matched to the multicollision neutron dose curve computed by Snyder and Neufeld,[2] and its lower limit in terms of energy response is expected to extend into the epithermal range.

The dosimeter consists essentially of a small spherical BF_3 counter enclosed in a cadmium-covered spherical shell of polyethylene. The outside diameter of the shell will be between 8 and 12 in., depending upon the results of experimental tests. Somewhat inconclusive Monte Carlo calculations suggest that the optimum diameter will be about 10 in. Spherical BF_3 detectors consisting of a 16-mil-thick copper shell filled with BF_3 gas (enriched to 96% in the ^{10}B isotope) to a pressure of 1 atm have been made in several diameters and with various sizes and types of collector wires. Experiments indicate that a 2-in.-diam counter having a 2-mil-diam tungsten collecting wire will be most suitable. The collecting wire is formed as a circular loop concentric with the sphere, with a short straight radial extension for connection to a preamplifier. End effects (essentially the variation in collection efficiency observed along the length of a straight collector) are effectively minimized with this arrangement. A transistorized preamplifier feeding a conventional linear amplifier is used with this dosimeter.

Thus far, the development of the dosimeter is basically empirical. Calibration in the energy range from 0.03 to 14 Mev will be made with monoenergetic neutrons obtained from targets bombarded at an accelerator. At lower energies, from 0.03 Mev to cadmium cutoff energy, no readily available monoenergetic neutron sources exist. In this region, therefore, calibration will be made against a beam of reactor neutrons filtered by various thicknesses of ^{10}B absorbers to produce neutrons within controlled energy intervals. This procedure should eliminate the usual dependence of the calibration upon calculated responses in this energy region.

The construction of the dosimeter has been completed, and preliminary calibrations with 14- and ~3-Mev neutrons have been performed. In the course of these calibrations, detailed comparisons have been made of the response of the new instrument with the responses of a conventional Hurst-type fast-neutron dosimeter and of the modified long counter[3] developed for the examination of the shield of the NS "Savannah." These data are in the process of reduction and analysis.

Low-Energy Neutron Spectrometer

Simultaneously with the dosimeter development, a neutron spectrometer is being constructed which is designed to measure neutron spectra from thermal to ~10 kev. This device will enable a more accurate assessment of the contribution low-energy neutrons make to the overall dose, and, in addition, it will be useful in a wide range of shielding experiments, particularly in the correlation of capture gamma-ray production with the low-energy neutron spectrum.

As shown in Fig. 6.4.1, the spectrometer consists of a 3-in.-diam spherical BF_3 counter, much like the counter described above, within a spherical annulus of powdered boron. The boron is contained between two concentric, spherical aluminum shells. The maximum particle size of the boron

is 70 μ, and it is enriched to about 92% in ^{10}B. Attached to the spectrometer is a conical annulus of boron surrounding an air collimator. In front of the collimator a carefully graded (in thickness) series of ^{10}B filters are positioned in succession. The principle of operation of the spectrometer is essentially the inverse of the method described by Newson and Gibbons[4] for the measurement of neutron cross sections. Depending upon the mass of ^{10}B contained in the filter, approximately 99% of the neutrons below a given energy will be absorbed in a filter of a given thickness, with those of higher energy being transmitted. Thus, by successive substitution of thicker filters, an unknown neutron spectrum can be "chopped" into a step function relating the neutron flux to energy. It is planned to use 29 steps with this spectrometer.

The design of the mounting for the spectrometer provides for rotation about an axis coincident with the face of the filter, remote control of all movements, and a compactness which will permit the use of the device within cubical shields as small as about 30 in. on a side.

Some difficulties have been encountered in obtaining satisfactory compaction of the boron.

UNCLASSIFIED
ORNL-DWG 64-10250

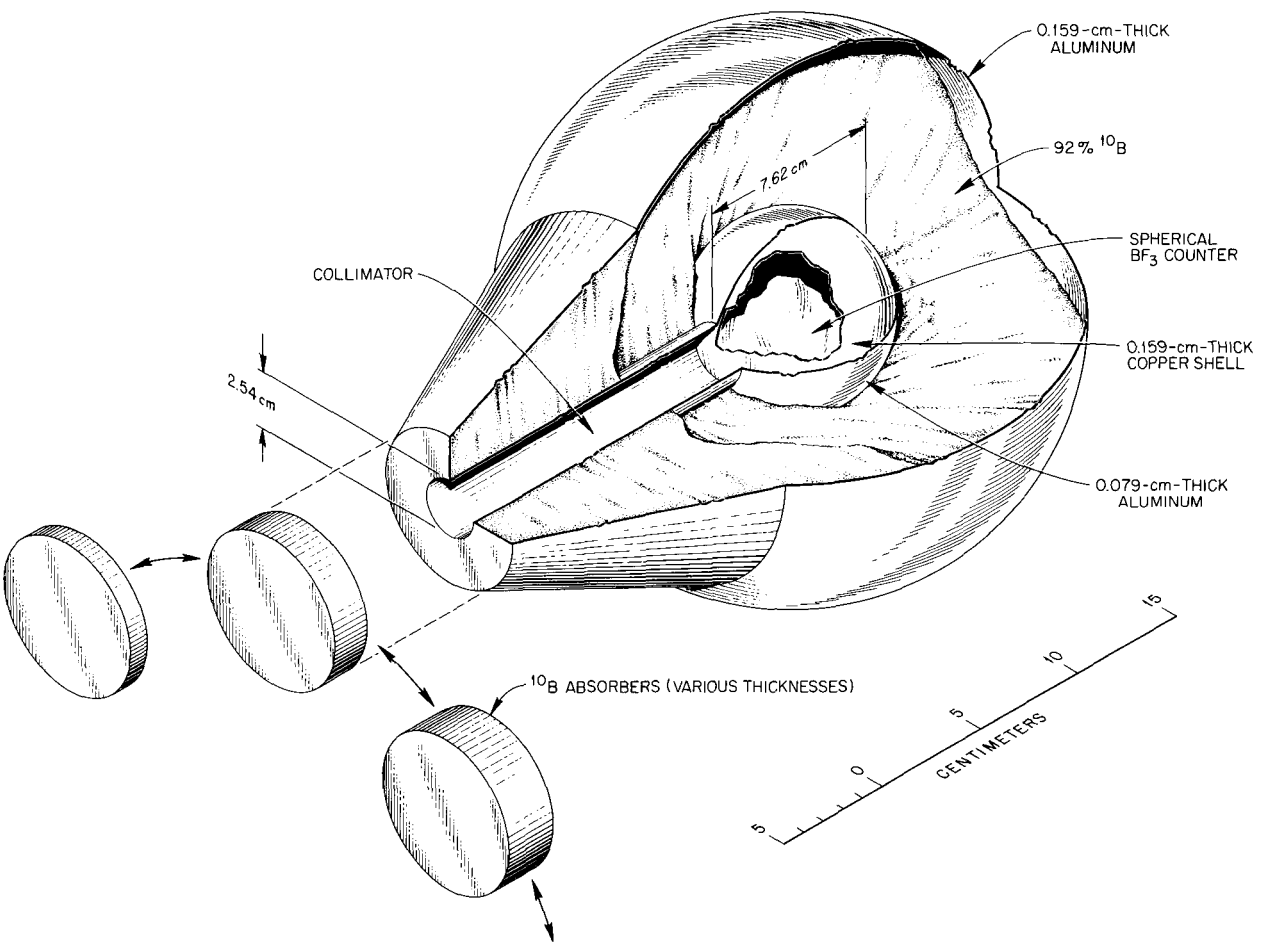

Fig. 6.4.1. Schematic Design of Neutron Spectrometer for Energy Range from Thermal to ~10 kev.

At present it appears that a boron density of ~ 1.4 g/cm^3 may be the greatest that can be attained even though a mixture of particles with a wide range of sizes is used. This value may be compared with the literature value of 2.45 g/cm^3 for crystalline boron.

Most of the ^{10}B filters have been delivered, and the calibration of their transmission, using the time-of-flight neutrons from the ORNL Neutron Chopper Facility, was begun in mid-October. Most of the components of the neutron spectrometer are still under construction or assembly.

References

[1]Work funded by Defense Atomic Support Agency under DASA Order EO-851-64.

[2]W. S. Snyder and C. Neufeld, *Radiation Res.* **6**(1), 67 (1957).

[3]E. P. Blizard, T. V. Blosser, and R. M. Freestone, Jr., *The Radiation Leakage Survey of the Shield of the Nuclear Ship Savannah,* ORNL-3336 (1962).

[4]H. W. Newson and J. H. Gibbons, chap. VL, p. 1601, in *Fast Neutron Physics, Part II,* ed. by J. B. Marion and J. L. Fowler, Interscience, New York, 1963.

7. Water Desalination Studies — Theoretical*

7.1. BOUNDARY LAYER BUILDUP IN THE DEMINERALIZATION OF SALT WATER BY REVERSE OSMOSIS[1]

L. Dresner

The buildup of saline boundary layers adjacent to permselective membranes has been studied. Two situations have been considered. In the first, water is forced by a piston through a semipermeable membrane; there is no lateral flow of the water over the face of the membrane. The salt concentration at the surface of the membrane increases monotonically with time and is asymptotically linear in time. In the second situation, the pressurized feed solution flows continuously through a channel whose walls are made of the semipermeable membrane. The flow may be either laminar or turbulent. In the laminar case, formulas for the salt concentration at the wall in both the asymptotic region ("well-developed" concentration profile) and the entrance region (boundary-layer region) have been derived. In the turbulent case, a simple formula for the salt concentration at the wall has been derived from the Chilton-Colburn analogy.

References

[1]Abstract of ORNL-3621 (May 1964).

7.2. SALT CONCENTRATION AT PHASE BOUNDARIES IN DESALINATION PROCESSES[1]

T. K. Sherwood[2] R. E. Fisher[2]
P. L. T. Brian[2] L. Dresner

Water removal from saline solutions by freezing or reverse osmosis causes the salt concentration at the phase boundary to be increased over that in the bulk solution, thus decreasing the freezing point or increasing the effective osmotic pressure. The magnitude of this effect is investigated for both turbulent and laminar flow in round tubes, and for laminar flow in a two-dimensional channel. It is concluded that the salt buildup effect may become a serious problem as better membranes for reverse osmosis are developed.

References

[1]Abstract of paper submitted to *Industrial and Engineering Chemistry, Fundamentals.*

[2]Massachusetts Institute of Technology, Cambridge.

7.3. A CONCENTRATION POLARIZATION METHOD FOR DETERMINING SALT REJECTION BY HYPERFILTRATION MEMBRANES

K. A. Kraus[1] R. J. Raridon[1]
L. Dresner

Certain membranes, notably those of cellulose acetate, have the ability to hold back dissolved

*The work reported in this section was performed for the Office of Saline Water, U.S. Department of the Interior.

salts when saline water is passed through them under pressure. Hyperfiltration is the process of purifying water with such membranes. In the course of hyperfiltration, unless the feed liquid is vigorously stirred, the salt held back by the membrane will accumulate in a thin boundary layer adjacent to the membrane. This phenomenon is called the concentration polarization of the membrane.

The salt-rejecting ability of a membrane is one of its most important properties. It is quantitatively defined as the ratio of the salt concentration of the effluent liquid to the salt concentration of the feed liquid that prevails in the absence of concentration polarization. To measure it directly requires that concentration polarization of the membrane be suppressed either by vigorous stirring or by maintaining a sufficiently high flow rate of feed liquid over the surface of the membrane.

In the method described in this summary, concentration polarization of the membrane is allowed to occur but is accounted for theoretically. The end of an ordinary tuberculin syringe is closed by a small piece of the membrane under investigation. Feed solution is added to the syringe and compressed. Liquid passes through the membrane and into a very fine capillary attached to the syringe. A pair of fine wires embedded in the capillary as close as possible to the membrane monitor the conductivity of the effluent liquid.

As the experiment proceeds, salt accumulates at the feed side of the membrane, causing the concentration and thus the conductivity of the effluent liquid to increase with time. If the flow rate through the membrane is constant, the time dependence of the concentration of the effluent liquid may be calculated as a function of the salt-rejecting ability of the membrane. Shown in Fig. 7.3.1 is a family of such calculated curves. Comparison of the measured time dependence of the salt concentration of the effluent liquid with this family of curves immediately gives the value of the salt-rejecting ability of the membrane.

The advantages of this method are threefold: (1) No special precautions have to be taken to eliminate concentration polarization of the membrane. (2) The method is very rapid, the time

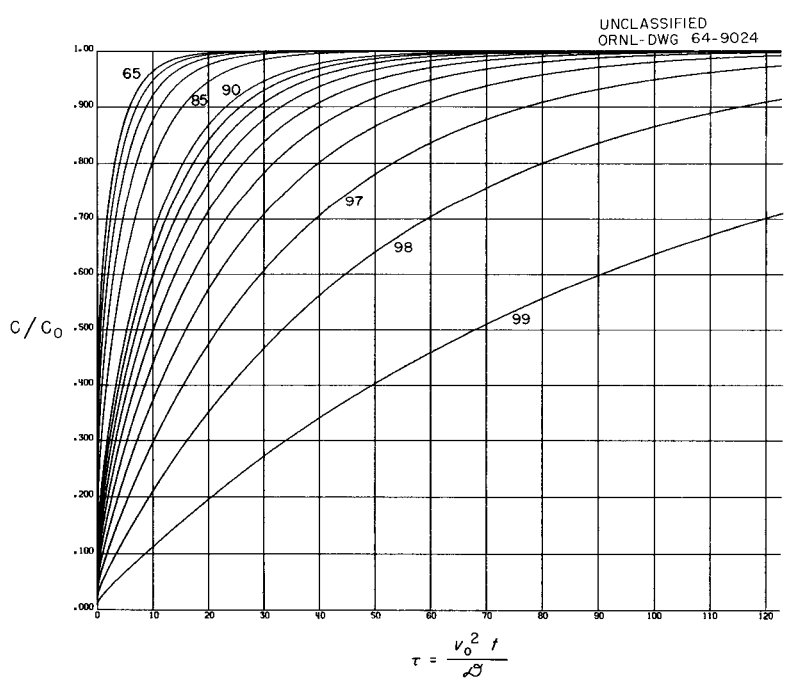

Fig. 7.3.1. The Time Dependence of the Salt Concentration of the Effluent Liquid. c is the salt concentration of the effluent liquid, c_0 is the salt concentration of the feed liquid, v is the flow velocity through the membrane, t is the time, D is the diffusivity of the salt, and the values on the curves indicate the salt-rejecting ability of the membrane.

involved in an individual experiment being approximately 1 hr. (3) The method gives the highest accuracy for membranes with very high salt-rejecting abilities, in contrast to the direct method, which for these cases requires the collection of relatively large samples of effluent for analysis.

References

[1]Chemistry Division.

Publications

ALSMILLER, R. G., JR.

"A Note on Importance Functions for the Shielding of Manned Space Vehicles," ORNL-3583 (March 1964).

"A Solution to the Nucleon-Meson Cascade Equations Under Very Special Conditions," ORNL-3570 (March 1964).

ALSMILLER, R.G., JR., AND J. E. MURPHY*

"Space Vehicle Shielding Studies. Part II. The Attenuation of Solar Flares by Aluminum Shields," ORNL-3520 (Jan. 10, 1964).

"Space Vehicle Shielding Studies. Part III. The Attenuation of a Particular Solar Flare by an Aluminum Shield," ORNL-3549 (Feb. 6, 1964).

ALSMILLER, R. G., JR., J. E. MURPHY,* AND J. BARISH*

"Numerical Solution of the One-Dimensional Nucleon-Meson Cascade Equations," ORNL-TM-951 (Sept. 19, 1964).

ARMSTRONG, T. W., AND S. K. PENNY

"OGREISH-P1 – A Monte Carlo Code Utilizing Importance Sampling for the Computation of Gamma-Ray Transmission Through Laminated Slabs," ORNL-TM-953 (October 1964).

BLIZARD, E. P., A. D. CALLIHAN, AND F. C. MAIENSCHEIN

"Neutron Physics Division Annual Progress Report for Period Ending August 1, 1963," Vols. I and II, ORNL-3499.

BLOSSER, T. V., AND R. M. FREESTONE

"A Study of the Shield of the University of Virginia Nuclear Research Reactor," ORNL-TM-662 (Nov. 25, 1963).

"A Study of the Shield of the Virginia Polytechnic Institute UTR-10 Reactor," ORNL-TM-290 (Dec. 11, 1963).

"A Radiation Study of the Westinghouse Testing Reactor," ORNL-TM-332 (Dec. 11, 1963).

BLOSSER, T. V., F. C. MAIENSCHEIN, AND R. M. FREESTONE

"The Energy Deposition in a Water-Filled Spherical Phantom by Secondaries from High-Energy Protons and by Neutrons," *Health Phys.* **10**, 743–50 (1964).

CAIN, V. R.

"A Study of the Radiation Shielding Characteristics of Basic Concrete Structures at the Tower Shielding Facility," ORNL-3464 (Jan. 21, 1964).

"Calculations of Thermal-Neutron Flux Distributions in Concrete-Walled Ducts Using an Albedo Model with Monte Carlo Techniques," ORNL-3507 (Jan. 21, 1964).

---

*Non-Division personnel.

CAIN, V. R., C. E. CLIFFORD, L. B. HOLLAND, AND TSF STAFF
"Measurements of Radiation Intensities in Vertical Concrete-Lined Holes and an Adjoining Tunnel at the Tower Shielding Facility," ORNL-3513 (March 1964).

CALLIHAN, A. D.
"Safety Standard for Operations with Fissionable Materials Outside Reactors, ASA N6.1-1964," *Mech. Eng.* **86**, 92 (1964).

CLARK, F. H. S., F. B. K. KAM, AND N. A. BETZ*
"Monte Carlo Calculations of Fast-Neutron Penetration in Lithium Hydride," *Trans. Am. Nucl. Soc.* **6**(2), 426 (1963).

DICKENS, J. K.
"Kinematics Nomogram for Low-Energy Nuclear Reactions," ORNL-3636 (June 1964).

DICKENS, J. K., AND F. G. PEREY
"Elastic and Inelastic Scattering of 5- to 13.5-Mev Deuterons from Ni^{60}: Tabulated Differential Cross Sections," ORNL-3637 (June 1964).

DICKENS, J. K., F. G. PEREY, AND R. J. SILVA*
"Level Structure of Ni^{64}," *Phys. Rev.* **132**, 1190 (1963).

DICKENS, J. K., F. G. PEREY, R. J. SILVA,* AND T. TAMURA*
"Proton Excitation of Two-Phonon Levels," *Phys. Letters* **6**(1), 53 (1963).

DRESNER, L.
"Boundary Layer Buildup in the Demineralization of Salt Water by Reverse Osmosis," ORNL-3621 (May 1964).

EMMETT, M. B.**
"INTRIGUE, An IBM-7090 Subroutine Package for Making Linear, Logarithmic, and Semilogarithmic Graphs Using the CALCOMP Plotter," ORNL-3581 (March 1964).

FREESTONE, R. M., JR.
"Fast-Neutron Dose Rates Behind Slabs of Water and of Concrete: Comparison of ORNL TSF Experimental Results with Calculations," ORNL-TM-646 (Sept. 9, 1963).

FRENCH, R. L.**
"A First-Last Collision Model of the Air-Ground Interface Effect on Fission Neutron Distributions," *Trans. Am. Nucl. Soc.* **6**(2), 435 (1963).

"A First-Last Collision Model of the Air/Ground Interface Effects on Fission Neutron Distributions," Radiation Research Associates Report RRA-M32 (November 1963).

FRENCH, R. L.,** AND M. B. WELLS**
"An Angle-Dependent Albedo for Fast-Neutron-Reflection Calculations," *Trans. Am. Nucl. Soc.* **6**(2), 435 (1963); also *Nucl. Sci. Eng.* **19**(4), 441 (1964).

GIBSON, W. A.
"Curled Light Pipes for Thin Organic Scintillators," *Rev. Sci. Instr.* **35**(8), 1021–23 (1964).

GILLEY, L. W.
"Effects of Various Reflectors on the Reactivity of the Health Physics Research Reactor," ORNL-TM-710 (February 1964).

GILLEY, L. W., AND L. B. HOLLAND
"Procedures Manual for the Health Physics Research Reactor (Including High-Level Gamma Facility)," ORNL-3519 (Oct. 24, 1963).

*Non-Division personnel.

**Non-Division personnel, reporting on work funded by Neutron Physics Division.

HILL, N. W.,** R. J. SCROGGS,** J. W. McCONNELL,** AND J. M. MADISON**
"Performance Characteristics of Modular Nanosecond Circuitry Employing Tunnel Diodes," ORNL-3687 (October 1964).

IIJIMA, S.
"Resonance Absorption and the Resonance Disadvantage Factor," *Nucl. Sci. Eng.* **17**(1), 42 (1964).

JARRARD, J. D.
"ADJUST," *Nucl. Sci. Eng.* **17**(1), 174 (1963).

JARRARD, J. D., AND G. T. CHAPMAN
"Some FORTRAN Codes Used in the Initial Reduction of Data Taken with Multichannel Pulse-Height Analyzers," ORNL-TM-659 (Feb. 10, 1964).

KAM, F. B. K., R. S. HUBNER,* F. H. S. CLARK, AND J. G. LaTORRE*
"Monte Carlo Calculations of Neutron Scattering from Cylinders of Be, C, Al, and Fe," *Trans. Am. Nucl. Soc.* **6**(2), 424 (1963).

KINGTON, J. D.,*** AND J. M. MILLER
"A Feasibility Study of Operating the BSR-I at 1 MW on a 16-hr-Day Schedule," ORNL-TM-810 (May 25, 1964).

KINNEY, W. E.
"Radiation Hazards in Space," *Nucl. Safety* **5**(1), 15 (1963).

"The Nucleon Transport Code, NTC," ORNL-3610 (August 1964).

"Program STATEST, An Application of the Method of Statistical Estimation to the Calculation of Neutron Flux in Anisotropically Scattering Media by Monte Carlo," ORNL-3715 (November 1964).

LAWSON, J. D.
"Differential Bremsstrahlung Cross Sections for Low-Energy Electrons," ORNL-TM-790 (February 1964).

MIHALCZO, J. T.
"Critical Experiments and Calculations with Annular Cylinders of U(93.2) Metal," *Trans. Am. Nucl. Soc.* **6**(2), 217 (1963).

ORNL-TM-655 (Sept. 23, 1963) (classified).

"Prompt-Neutron Lifetime in Critical Enriched-Uranium Metal Cylinders and Annuli," *Nucl. Sci. Eng.* **20**, 60–65 (1964).

MUCKENTHALER, F. J., K. M. HENRY, V. V. VERBINSKI, M. S. BOKHARI, J. J. MANNING, AND J. L. HULL
"Measurements of Scattered Neutron Intensities from Cylinders of C, Al, Fe, and Be in a Collimated Beam of Neutrons from the TSR-II," *Trans. Am. Nucl. Soc.* **6**(2), 424 (1963).

PAXTON, H. C.,* J. T. THOMAS, A. D. CALLIHAN, AND E. B. JOHNSON
"Critical Dimensions of Systems Containing U^{235}, Pu^{239}, and U^{233}," TID-7028 (June 1964).

PEELLE, R. W.
"Statistical Fluctuations in the Output of an Intranuclear Cascade Monte Carlo Computation," ORNL-TM-771 (January 1964).

PENNY, S. K.
"Derivation of First- and Last-Flight Estimators for Monte Carlo Computations of Scattered Particle Fluxes in Attenuating Media with Spherical or Plane Symmetry," ORNL-TM-974 (November 1964).

*Non-Division personnel.

**Non-Division personnel, reporting on work funded by Neutron Physics Division.

***Deceased.

PENNY, S. K., AND G. R. SATCHLER*
"Inelastic Effects in Stripping and Other Direct Reactions," *Nucl. Phys.* **53**, 145 (1964).

PENNY, S. K., D. K. TRUBEY, L. JUNG, AND M. B. EMMETT*
"Cumulative Bibliography of Literature Examined by the Radiation Shielding Information Center (September 1963)," RSIC-2 (Jan. 3, 1964).

PEREY, C. M., AND F. G. PEREY
"Deuteron Optical-Model Analysis in the Range of 11 to 27 MeV," *Phys. Rev.* **132**, 755 (1963).

"Optical-Model Analysis of 15-MeV Deuteron Elastic Scattering," *Phys. Rev.* **134**, B-353 (1964).

PEREY, F. G., AND D. S. SAXON*
"The Local Energy Approximation to Nonlocality and Finite Range Effects," *Phys. Letters* **10**, 107 (1964).

PEREY, F. G., AND A. M. SARUIS
"Effects of Nonlocality in Off-Diagonal Potentials," ORNL-TM-967 (October 1964).

PEREZ, R. B., G. de SAUSSURE, AND E. G. SILVER
"Use of the Neutron Die-Away Technique to Test Control Rod Effectiveness Theories," p. 241 in *Exponential and Critical Experiments,* Proceedings of the Symposium on Exponential and Critical Experiments Held by the International Atomic Energy Agency in Amsterdam, Netherlands, 2–6 September 1963, Vol. III, International Atomic Energy Agency, Vienna, 1964.

SANTORO, R. T., AND R. W. PEELLE
"Measurement of the Intensity of the Proton Beam of the Harvard University Synchrocyclotron for Energy-Spectral Measurements of Nuclear Secondaries," ORNL-3505 (March 1964).

SILVER, E. G.
"SPERT Program Status Report," *Nucl. Safety* **5**(2), 151–55 (1964).

SMITH, W. R.
"Hauser-Feshbach Computer Program for Spin-1/2 Particles," ORNL-TM-875 (May 25, 1964).

"The Use of Elastic-Scattering Parameters in (d,p) Stripping Calculations," ORNL-TM-966 (October 1964).

"A Computer Program for Obtaining Neutron and Proton Elastic-Scattering Angular Distributions Using the Hauser-Feshbach Theory," ORNL-TM-930 (August 1964).

THOMAS, J. T.
"Critical Three-Dimensional Arrays of Neutron-Interacting Units," ORNL-TM-719 (Oct. 1, 1963).

"Critical Three-Dimensional Arrays of Neutron-Interacting Units, Part II. U(93.2) Metal," ORNL-TM-868 (July 1964).

TRUBEY, D. K.
"Calculation of Fission-Source Thermal-Neutron Distribution in Water by the Transfusion Method," ORNL-3487 (August 1964).

TURNER, J. E.,* C. D. ZERBY, R. L. WOODYARD,* H. A. WRIGHT,* W. E. KINNEY, W. S. SNYDER,* AND J. NEUFELD*
"Calculation of Radiation Dose from Protons to 400 MeV," *Health Phys.* **10**, 783 (1964).

WELLS, M. B.**
"Angular Distribution of the Air-Scattered Fast Neutron Dose Rate at the Air-Ground Interface," *Trans. Am. Nucl. Soc.* **6**(2), 436 (1963).

*Non-Division personnel.

**Non-Division personnel, reporting on work funded by Neutron Physics Division.

"Reflection of Thermal Neutrons and Neutron-Capture Gamma Rays from Concrete," Radiation Research Associates Report RRA-M44 (June 1964).

"Angular Distribution of the Air-Scattered Fast-Neutron Dose Rate at the Air-Ground Interface," Radiation Research Associates Report RRA-M33 (November 1963).

WESTON, L. W., G. de SAUSSURE, AND R. GWIN

"Neutron Capture in U^{238} and the Ratio of Capture to Fission in U^{235}," in *Symposium on the Absolute Determination of Neutron Flux in the Energy Range 1–100 keV, Held at St. John's College, Oxford, September 10–13, 1963,* EANDC-33. United Kingdom Atomic Energy Authority, Aldermaston, England, 1963.

"Ratio of Capture to Fission in U^{235} at keV Neutron Energies," *Nucl. Sci. Eng.* **20,** 80–87 (1964).

ORNL-3714, Vol. I
UC-34 – Physics
TID-4500 (35th ed.)

INTERNAL DISTRIBUTION

1. L. S. Abbott
2. F. S. Alsmiller
3. R. G. Alsmiller, Jr.
4. J. Barish (K-25)
5. H. W. Bertini
6. N. A. Betz
7-46. E. P. Blizard
47. T. V. Blosser
48. M. S. Bokhari
49. W. R. Burrus
50. V. R. Cain
51. A. D. Callihan
52. G. T. Chapman
53. H. C. Claiborne
54. F. H. Clark
55. C. E. Clifford
56. W. Coleman
57. J. C. Courtney
58. R. R. Coveyou
59. G. deSaussure
60. J. K. Dickens
61. L. Dresner
62. M. B. Emmett
63. K. Franz (K-25)
64. R. M. Freestone, Jr.
65. J. Gibbons
66. W. A. Gibson
67. F. E. Gillespie
68. J. H. Gillette
69. M. Guthrie
70. R. Gwin
71. V. M. Hamrick
72. J. A. Harvey
73. R. M. Haybron
74. K. M. Henry, Jr.
75. N. W. Hill
76. B. D. Holcomb (K-25)
77. L. B. Holland
78. J. L. Hull
79. D. Irving
80. E. B. Johnson
81. W. H. Jordan
82. L. Jung
83. F. B. K. Kam
84. M. M. Kedle
85. W. E. Kinney
86. K. A. Kraus
87. C. E. Larson
88. M. Leimdorfer
89. J. Lewin
90. T. A. Love
91. R. L. Macklin
92. J. M. Madison
93. R. E. Maerker
94. D. W. Magnuson
95. F. C. Maienschein
96. J. J. Manning
97. B. F. Maskewitz
98. J. W. McConnell
99. B. McGill
100. C. O. McNew
101. S. K. Mehta
102. J. T. Mihalczo
103. J. M. Miller
104. H. S. Moran
105. F. J. Muckenthaler
106-107. R. B. Parker
108. R. W. Peelle
109. S. K. Penny
110. C. M. Perey
111. F. J. Perey
112. S. J. Rafferty
113. R. J. Raridon
114. J. Repolgle (K-25)
115. B. Rust (K-25)
116. G. R. Satchler
117. R. T. Santoro
118. R. J. Scroggs
119. R. J. Silva
120. E. G. Silver
121. M. J. Skinner
122. G. G. Slaughter
123. R. D. Smiddie
124. W. R. Smith
125. J. G. Sullivan
126. J. A. Swartout
127. T. Tamura
128. J. T. Thomas
129. H. A. Todd
130. D. K. Trubey
131. V. V. Verbinski
132. J. Wachter

133. D. R. Ward
134. J. W. Webster
135. A. M. Weinberg
136. L. W. Weston
137. E. P. Wigner
138. G. C. Williams
139. Gale Young
140. W. Zobel
141. R. A. Charpie (consultant)
142. R. F. Taschek (consultant)
143. G. Dessauer (consultant)
144. M. L. Goldberger (consultant)
145. Radiation Shielding Information Center
146. Biology Library
147-149. Central Research Library
150. Reactor Division Library
151-152. ORNL-Y-12 Technical Library, Document Reference Section
153-334. Laboratory Records Department
335. Laboratory Records, ORNL R.C.

EXTERNAL DISTRIBUTION

336. Research and Development Division, AEC, ORO
337-982. Given distribution as shown in TID-4500 (35th ed.) under Physics Category (75 copies – CFSTI)